The mechanistic action of Silver (I) thiocyanate 4-methoxyphenyl phosphine promoting apoptosis in MCF-7 and MDA-MB-231 breast cancer cell lines.

by

Alisha Badal

(1102823)

Dissertation

Submitted in fulfilment of the requirements for the degree

Master of Science

in

Molecular and Cell Biology

in the Faculty of Science, University of the Witwatersrand, Johannesburg, South Africa

Supervisor: Prof. Marianne J. Cronjé

Co-supervisor: Dr. Zelinda Engelbrecht

12/2022

Declaration

I, **Alisha Badal** (**1102823**), am a student registered for the degree of _MSc Dissertation___ in the academic year __2022____.

I hereby declare the following:

- I am aware that plagiarism (the use of someone else's work without their permission and/or without acknowledging the original source) is wrong.
- I confirm that the research proposal submitted for assessment for the above degree is my own unaided work except where explicitly indicated otherwise and acknowledged.
- I have followed the required conventions in referencing the thoughts and ideas of others.
- I understand that the University of the Witwatersrand may take disciplinary action against me if there is a belief that this is not my own unaided work or that I have failed to acknowledge the source of the ideas or words in my writing.

Signature  _ _5th___ day of __12/2022_____ **YEAR**

Dedication

I dedicate this dissertation to my parents Narisha and Anesh Badal. Thank you for all your love, support and encouragement. I am forever grateful.

In loving memory:

My grandmother: Mrs. Sushila Singh

(Battled against Non-Hodgkin's lymphoma)

My grandfather: Mr. Naar Singh

(Battled against carcinoma of the colon)

I also dedicate this dissertation to anyone who has lost a loved one during their fight against cancer.

“Service to humanity is service to God’’ - Abdu'l-Bahá

Acknowledgments

- Prof. Marianne J. Cronjé for her constant guidance, expert supervision and support throughout this research project. I am truly honored to have had the opportunity to study anti-cancer research under your supervision.

- Dr. Zelinda Engelbrecht for her continuous guidance, expert supervision and motivation throughout this project. Her scientific mind and contribution to anti-cancer research is inspirational.

- The University of the Witwatersrand and the School of Molecular and Cell Biology for enabling the completion of this study.

- The National Research Foundation (NRF) for awarding a Masters scholarship to complete this study. I am truly grateful for this award.

- Miss Kim Roberts, Miss Mizan Ferreira and Miss Zami Ntshingila for their assistance in the lab, support and friendship.

- My dear parents and brother Kashvir Badal for all your love.

Table of contents

List of Abbreviations

A

AAD - aminoactinomycin D

AIF - apoptosis-inducing factor

AJCC - American joint committee on cancer

APAF-1 - adaptor protein called apoptosis protease–activating factor 1

APS - Ammonium persulfate

ATP - adenosine triphosphate

B

Bcl-2 - B-cell lymphoma 2

BRCA1 - breast cancer gene 1

BRCA2 - breast cancer gene 2

BSA - bovine serum albumin

C

CAD - caspase-activated deoxyribonuclease

CAM - cell adhesion molecules

CARD - caspase recruitment domain

CDDP - Cisplatin

CHEK2 - checkpoint kinase 2

CICD - caspase-independent cell death

D

DAMPs - damage-associated molecular patterns

DALYs - disability-adjusted life years

DCIS - ductal carcinoma *in situ*

DED - death effector domain

DISC - death-inducing signaling complex

DMSO - dimethyl sulfoxide

DPPE - diphenylphosphine

DR3 - death receptor type 3

E

ECM - extracellular matrix

EF-2 - elongation factor-2

EGFR - epidermal growth factor receptor

EndoG - endonuclease G

ER - endoplasmic reticulum

ER - estrogen receptor

ETC - electron transport chain

F

FADD - fas-associated death domain

FADH2 - reduced flavin adenine dinucleotide

FAK - focal adhesion kinase

FasL - fas Ligand

H

HDGF - hepatoma-derived growth factor cytokines

HER-2 - human epithelial receptor 2

HMGB1 - high-mobility group box 1 protein

Htra2/Omi - high-temperature requirement protein A

I

IAPs - inhibitors of apoptosis proteins

ICAD - inhibitor of caspase-activated deoxyribonuclease

L

LCIS - lobular carcinoma *in situ*

M

MDR - multi-drug resistance

MEKK-1 - mitogen-activated protein kinase kinase kinase 1

MLKL - mixed lineage kinase domain-like proteins

MOMP - mitochondrial outer membrane permeabilization

N

NADPH - nicotinamide adenine dinucleotide phosphate

NCCD- national committee on cell death

NETs - neutrophil extracellular trap

NHC - N-heterocyclic carbenes

NuMa - nuclear mitotic apparatus protein

P

PAK2 - P21 (RAC1) Activated Kinase 2

PALB2 - partner and localizer of BRCA2

PARP - poly-(ADP-ribose) polymerase

PCD - programmed cell death

P-gp - p-glycoprotein

PKD - protein kinase D

PLA2 - phospholipase A2

PR - progesterone receptor

PS - phosphatidylserines

PTEN - phosphatase and tensin homolog

PTP - permeability transition pore

PVDF - polyvinylidene difluoride

R

RIPK-1 - receptor-interacting protein kinase-1

ROS - reactive oxygen species

RT - room temperature

S

SASP - senescence-associated secretory phenotype

SDS - Sodium dodecyl sulfate

SEM - selective estrogen-receptor modulator

SEM - standard error of the mean

Smac/DIABLO - second mitochondria-derived activator of caspase

SOD - superoxide dismutase

STK11 - serine / threonine kinase 11

STS - Staurosporine

T

tBid - truncated Bid

TEMED - N,N,N′,N′-Tetramethylethylenediamine

TME - tumor microenvironment

TNBC - triple-negative breast cancer

TNF - tumor necrosis factor

TNFR1 - tumor necrosis factor receptor 1

TP53 - tumor protein 53 gene

TPP^+ - triphenylphosphine groups

TRADD - TNFR-associated death domain

TRAF2 - TNF receptor-associated factor 2

TRAIL-R1 - TNF -related apoptosis-inducing ligand receptors- 1

TRAIL-R2 - TNF -related apoptosis-inducing ligand receptors- 2

TrxR - thioredoxin reductase

U

UJ3 – Silver (I) thiocyanate 4-methoxyphenyl phosphine

V

VEGF - vascular endothelial growth factor

VEGF-A - vascular endothelial growth factor-A

List of symbols

µM - micromolar

µm - micrometer

mM - millimolar

nM - nanomolar

% - percent

hrs - hours

mins - minutes

°C - Celsius

g - gram

µg - microgram

µg/ml - microgram per millilitre

ml - milliliter

l - liter

1° - primary

2° - secondary

kDa - kilodalton

x*g* - centrifugal force

List of Figures

List of Tables

Abstract

Breast cancer is at the forefront of the most frequently diagnosed cancer globally. The available multidisciplinary treatments succumb to adverse toxicity and drug resistance. Anti-cancer metallodrugs with apoptosis potential have been adopted in systemic cancer therapeutics. The quest for effective metal coordination complexes with improved pharmacological profiles are on the rise in the current cancer metallotherapy era. Herein, we aim to report the apoptosis-inducing potential and mechanistic action of UJ3 on *in vitro* MCF-7 and MDA-MB-231 breast cancer cell lines. A cytotoxicity assessment involving dose-response and viability studies was undertaken to evaluate the pharmacological profile of UJ3. In the MCF-7, UJ3 operated as a pharmacological anti-cancer agent, exhibiting malignant selectivity and sustained potency. In the MDA-MB-231, UJ3 proved selective and cytotoxic; however, cell recovery impeded the drugs profile. The Annexin V and 7-AAD assay, MitoPotential assay, oxidative stress assay, MitoTracker Orange dye and Hoechst 33258 dye were used to determine the cell death modality. UJ3 elicited mitochondrial-mediated apoptosis in both malignant cell lines, made evident via reduced mitochondrial membrane potential, disrupted bioenergetics, phosphatidylserine exposure, oxidative stress, cellular morphology and nuclear apoptotic morphology. Pro-apoptotic caspases and poly-(ADP-ribose) polymerase (PARP) were studied via western blots to gain insight into the apoptosis pathway. In the MCF-7, UJ3 activated the intrinsic apoptosis pathway via cytochrome *c* expulsion, caspase-7 activity and PARP cleavage. In the MDA-MB-231, UJ3 activated a caspase-independent cell death pathway which led to the study of the apoptosis-inducing factor (AIF) via fluorescent tracking. UJ3 induced an AIF-mediated apoptosis pathway in MDA-MB-231. This study highlights UJ3 as an apoptosis-inducing agent that executes selective malignant death via mitochondrial targeting in MCF-7 and MDA-MB-231 cell lines. UJ3 demonstrates promising activity in MCF-7 cells that warrant further investigation. Future studies are required to further clarify and validate UJ3s mechanistic action.

Introduction to the relevance of this study

Cancer is consistently ranked as one of the leading diseases that execute death and despair to humanity (Sung *et al*., 2021). According to WHO (2022), cancer was responsible for 1 in 6 deaths in 2020, with approximately 10 million lives lost. The most dominant cancer diagnosis globally is breast cancer. Breast cancer accounted for 2.3 million cases in 2020 and the COVID-19 pandemic had largely impaired screening, diagnosis and treatment leading to an underestimate of case reports (Figueroa *et al*., 2021). South African women suffer a great ordeal due to disadvantaged socioeconomic status and limited treatment options compared to highly developed countries. The lack of awareness and screening is an additional disadvantage to South Africans because breast cancer is often detected in advanced stages, further narrowing treatment options (Lambert *et al*., 2020). Globally, Africa is recorded as one of the continents with the highest mortality in breast cancer patients (Azubuike *et al*., 2018). Breast cancer outcompetes any other cancer with respect to the loss of disability-adjusted life years (DALYs) (WHO, 2022). In support of this finding, Lambert *et al*. (2020), reported the severe physical and emotional distress South Africans face in their breast cancer battle. Moreover, the available conventional treatment options are prone to malignant resistance and high toxicity, stimulating severe side effects (Smoot *et al*., 2009). Breast cancer patients with advanced cancer stages are presented with limited treatment options that are unable to adequately prolong their lifespan. The cancer burden will continue to proliferate without further interventions from improved treatments or novel anti-cancer drugs (Lambert *et al*., 2020).

Cancer therapeutics often aim to elicit an apoptosis cell death modality in malignant cells since apoptosis is intrinsically wired to inhibit carcinogenesis from initiation to the final oncogenic transformation (Goldberg, 2019). A repertoire of metal anti-cancer complexes is emerging in the medical field, demonstrating apoptosis induction and improved potency compared to the current chemotherapeutic drug, Cisplatin (Canudo-Barreras *et al*., 2021; Harurluoglu *et al*., 2021; Raju *et al*., 2022). Silver metals offer advantageous low toxicity and appear to exhibit selective malignant mitochondrial targeting based on the addition of phosphine ligands with a selective lipophilic character (Engelbrecht *et al*., 2018; Berners-Price and Sadler, 1988; Medici *et al*., 2016). Selective malignant targeting is an attribute of successful pharmacological anti-cancer drugs and is associated with reduced toxicity (Chatelut *et al*., 2003).

The Silver (I) thiocyanate complexes represent a novel class of complexes with anti-cancer potential (Meijboom *et al*., 2009). The silver (I) thiocyanate 4-methoxyphenyl phosphine complex (UJ3) was reported to elicit apoptosis in malignant SNO oesophageal cells with greater efficacy than Cisplatin and minimal toxicity due to malignant mitochondrial targeting (Engelbrecht *et al*., 2018).

The reported anti-cancer potential of UJ3 has steered this study to evaluate UJ3 anti-cancer efficacy in malignant MCF-7 and MDA-MB-231 breast cancer cell lines. The outcome of this *in vitro* study will shed light on the pharmacodynamic profile of UJ3 and aid in understanding its anti-cancer mechanistic action in two vastly distinct breast cancer cell lines. Promising results from this research contribute to the body of literature on silver metal complexes in cancer therapeutics. More specifically, it re-enforces the efficacy of silver (I) thiocyanate phosphine complexes as a promising apoptosis inducer against commonly diagnosed breast cancer. Therefore, this *in vitro* study will shape future studies of UJ3 in the drug discovery process and pave the future for *in vivo* and potential clinical trials of UJ3 in MCF-7 and MDA-MB-231 cell lines. Moreover, Africa is at a major disadvantage as advanced targeted and hormonal therapy drugs are unavailable to patients due to low income or other accessibility issues (Vanderpuye *et al*., 2017). Therefore, if UJ3 continues to exhibit promising results in future studies throughout the discovery process, this will aid the ongoing cancer battle.

Chapter 1 : Literature Review

1. Defiance of cellular regulation

1.1 Carcinogenesis

The cell has several independent mechanisms to regulate cellular turnover, ensuring healthy cellular division, differentiation, and programmed suicide. Cancer is a multistage process influenced by malfunctions in the genetic and epigenetic expression of crucial regulatory genes or intracellular circuits that manage cell proliferation and tissue homeostasis. A collection of independent aberrant regulatory events and mutational acquisitions promotes the phenotype and genotype characteristic of malignant neoplasms. During carcinogenesis, cells deviate from normality into pre-neoplastic cells and towards an invasive malignant neoplasm through three stages: initiation, promotion, and progression (Compton, 2021; Karakosta *et al*., 2005; Weinstein *et al*., 1984).

In the initiation stage, the cell may undergo DNA alterations that produce mutations that occur spontaneously or upon exposure to a genotoxic carcinogen called the initiator. The initiated cell is not considered a neoplastic cell but has taken its first initiative toward this state. The carcinogenic dose directly affects the number of possible neoplasia. The initiated cell may undergo different cell fates. It may reside in a static or latent non-dividing state or gather mutations that dysregulate cellular functions, in which case the cell may be removed by apoptotic cellular suicide (Klaunig, 2020; Oliveira *et al*., 2017). However, if mutations are present in ‘’driver’’ genes (proto-oncogenes or tumor suppressor genes) and the mutated cell has the capacity to proliferate, this may drive the initiated cell towards carcinogenesis (Compton, 2021). With the lack of functional regulatory control and repair machinery, errors in the DNA sequence will result in a fixed heritable mutation within the initiated cell (McKinnell *et al*., 2006) (Figure 1.1).

Endogenous or exogenous agents that act on the initiated cells during the second stage of carcinogenesis are referred to as promoters. Tumor promoters are non-genotoxic and mutagenic but can disrupt gene expression levels and increase proliferation by altering epigenetic mechanisms. During the promotion stage, a pre-neoplastic lesion is developed by clonal expansion of the initiated cells due to promoters that stimulate mitogenesis and apoptosis circumvention. The development of a focal lesion from the initiated cells relies on the sustained application of the tumor promoter agent. The clonal expansion induced by tumor promoters is reversible and dosage-dependent (Klaunig, 2020; McKinnell *et al*., 2006; Siddiqui *et al*., 2015) (Figure 1.1).

The transformation of a pre-neoplastic lesion to a neoplasm occurs in the last stage of carcinogenesis, referred to as the progression stage. Progression is an irreversible process influenced by accelerated genetic instability and assorted mutations contributing to invasive and metastatic potential. As clonal expansion proceeds, the resultant daughter cells generate subclones with uniquely assorted mutations, subsequently giving rise to the heterogeneity typical of neoplasms (Compton, 2021; Oliveira *et al.*, 2017) (Figure 1.1).

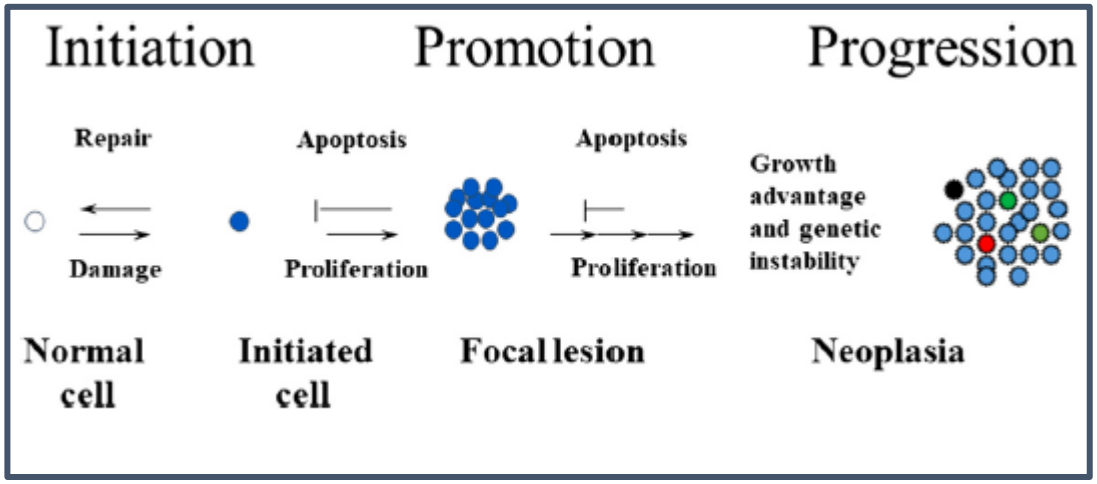

Figure 1.1: Stages of carcinogenesis. An initiated damaged cell may be dormant, repaired, removed by apoptosis, or may proceed to the promotion stage of carcinogenesis depending on the location of the mutation on the gene and the cellular type. In the promotion stage, a pre-neoplastic lesion is developed by clonal expansion of the initiated cells due to promoters that stimulate proliferation and inhibit apoptosis. In the progression stage, a pre-neoplastic lesion is transformed into a neoplasm by enhanced genetic instability, fostering invasive and metastatic potential (Adapted from Klaunig, 2020).

1.1.1 Genetic instability as a key player in carcinogenesis

Mutations are inevitable in the evolution of biological species; germline mutations are inherited from parent to offspring, and various somatic mutations occur throughout one's lifetime. Passenger mutations, common during cell division, are somatic mutations that are biologically inert and do not directly contribute to carcinogenesis. However, these mutations may be present in a cell with a mutated ''driver gene'' causally incorporating the passenger mutation into the clonal expansion of a developing neoplasm. Most mutations that nurture carcinogenesis development occur in "driver genes." Cells with mutated ''driver genes'' have beneficial evolutionary selectivity to survive, outperforming non-mutated cells (Burkard and Jallepalli, 2015; Compton, 2021; Stratton *et al.*, 2009).

Mutations range from minor to major DNA modifications. Minor modifications encompass point mutations, insertions or deletions of nucleotides that influence gene length, or a frameshift mutation involving the addition or subtraction of nucleotides in a DNA sequence. Major DNA modifications include changes in the number of gene copies, chromosomal breakage followed

by an incorrect chromosomal insertion, translocation of chromosomal segments, or a varying number of whole chromosomes (Burkard and Jallepalli, 2015; Compton, 2021). Alternatively, DNA modifications may be obtained exogenously from viruses such as the Epstein Barr virus and the human papillomavirus. Cancer genomes may also accumulate epigenetic alterations influencing the methylation of cysteine residues in the DNA sequence and expression of genes (Stratton *et al*., 2009).

Experimental research carried out on healthy human cells proposed that the modification of a minimum of five to six functional genes is required to convert a cell towards carcinogenesis. In epithelial cancers, such as breast cancer, at least 5-7 mutational events, with most of the events prompted by ‘’driver genes’’ were necessary for cancer transformation (Stratton *et al*., 2009). “Driver genes” include mutations in proto-oncogenes or tumor suppressor genes; their mutations may drive a cell towards cancer progression through a gain of function frequently detected in proto-oncogenes and a loss of function in tumor suppressor genes (Lee and Muller, 2010).

Proto-oncogenes include genes associated with growth factors, cytokines, transcription factors involved in DNA replication, cyclins controlling the cell cycle and division, signal transduction, and their regulatory mechanisms. Therefore, proto-oncogenes oversee cell proliferation. Mutated proto-oncogenes are called oncogenes as they lack negative feedback regulation and function autonomously to expedite cell proliferation. Since mutated oncogenes are dominant in nature, a mutational event by major DNA modifications in one allele can easily convert a proto-oncogene to an oncogene. Subsequently promoting structural alteration of the gene product or aberrant protein expression (Compton, 2021; Kontomanolis *et al*., 2020; Martínez-Jiménez *et al.,* 2020). Gene amplification mutations in the human epithelial receptor 2 (*HER-2*), involved in cell division and repair account for 20% of breast cancers and result in amplified expression of the oncogene product (Osborne *et al*., 2004).

Tumor suppressor genes inhibit abnormal proliferation and defend against neoplasm development. The two main types of tumor suppressor genes are caretaker genes and gatekeeper genes. Caretaker genes orchestrate DNA repair, detect mutations, and correct or eliminate mutated genes. Gatekeeper genes monitor checkpoint activity in the cell cycle and cellular suicide, thus maintaining healthy cellular turnover (Compton, 2021; Lee and Muller, 2010). Unlike proto-oncogenes, mutated tumor suppressor genes lose their tumor inhibition properties by two mutational events (heterozygosity loss) since their genes are recessive in nature (Compton, 2021; Martínez-Jiménez *et al*., 2020). Non-mutational alterations of tumor suppressor genes include accelerated proteasomal degradation and methylation of the gene promoter such that transcriptional activity is inhibited. Mutations in tumor suppressor breast

cancer gene 1 *(BRCA1*) and breast cancer gene 2 (*BRCA2*) promote autonomous cell division and DNA damage and may occur in 90% of hereditary-related cancers (Osborne *et al*., 2004; Sun *et al*., 2017). The tumor protein 53 gene (*TP53*) is a gatekeeper gene with additional caretaker functions and is involved in several pathways; therefore, *p53* mutants are expected in 50% of human cancers (Harris *et al*., 2017; Osborne *et al*., 2004). Genomic instability nurtures the evolution and complexity of malignancy by facilitating the development of various traits associated with neoplasia (Andor *et al*., 2017).

1.1.2 Physiological traits that characterize malignancy

When a defective cell progresses towards malignancy, acquired traits enable it to override regulatory control and thrive in a tumor microenvironment with a characteristic phenotype. The following traits are a brief summary of the widespread literature published by Hanahan and Weinberg (2000), Hanahan and Weinberg (2011), and Hanahan (2022).

1. *Dysregulation of proliferation*

   Malignant cells self-produce growth ligands to which their receptors respond via autocrine stimulation. Alternatively, transformed cells signal and employ healthy cells in the stroma of the tumor to produce growth factors for their benefit. Malignant cells may increase their number of surface receptor proteins to enhance their sensitivity to growth factors in the vicinity. Receptors may also undergo structural modification to support ligand-independent firing ensuing sustained proliferation (Hanahan and Weinberg, 2000).

2. *Suppression of anti-growth signals*

   Healthy tissue adheres to signals received via growth inhibitors, including those in the extracellular matrix. Consequently, holding the cell in a quiescent, terminal, or post-mitotic state of differentiation. Malignant cells disregard signals that order the cell cycle by disrupting pathways such as the pRb pathway and stimulating *c-myc* growth factors rendering the transformed cells insensitive to contact inhibition (Hanahan and Weinberg, 2000).

3. *Apoptosis evasion*

   The apoptotic cell death program is an innate barrier to defending against malignancy. However, malignant cells inhibit many apoptotic signals and circuits (detailed in section 2). Other cell-death modes, such as necrosis and autophagy, are also corrupted to facilitate cell survival (Hanahan and Weinberg, 2000).

4. *Infinite replication*

   Healthy cells possess a finite replicative potential and follow senescence after several doublings. However, corruption of the pRb and p53 tumor suppressor proteins permits cells to undergo further replication to enter a state of crisis. Telomeres located at the

end of chromosomes undergo shortening (50 -100 bp) upon completion of the cell cycle. Continuous degradation of telomeres during replication results in unprotected chromosomal DNA that marks an end to a cell's lifetime. Malignant cells up-regulate telomerase to add hexanucleotides onto telomere DNA. Alternatively, an ALT mechanism may be employed involving the recombination-based inter-chromosomal exchange of sequence data. Either mechanism permits transformed cells to pursue immortality (Hanahan and Weinberg, 2000).

5. *Angiogenesis maintenance*

   Cell survival is dependent on oxygen and nutrients supplied via blood vessels. Angiogenesis is the genesis of new blood vessels. Malignant cells exploit an "angiogenic switch" by activating stimulators of angiogenesis such as vascular endothelial growth factor (VEGF) and blocking angiogenesis inhibitors (β-interferon) (Hanahan and Weinberg, 2000).

6. *Tissue invasion and metastasis*

   The migration of tumor masses to distant regions refers to metastasis and is associated with higher-grade tumors. Invasion and metastasis are often achieved by previously mentioned acquired capabilities (1 – 5). Under physiological conditions, cell adhesion molecules (CAMs) govern cells to the extracellular matrix. In malignant cells, the regulatory mechanism of CAMs is lost. Moreover, E-cadherin cell-cell interaction molecules are mutated in many cancers such that their regulatory anti-growth function between adjacent cells is also lost. Malignant cells follow an invasion-metastasis cascade that begins with local invasion followed by migration in blood and lymph vessels termed intravasation. The following migratory route is directed to the parenchyma of distant sites termed extravasation. Subsequently, promoting nodule formation termed micrometastases. Enhanced nodular growth encourages the development of a macroscopic tumor referred to as "colonization" (Hanahan and Weinberg, 2000; Hanahan and Weinberg, 2011).

7. *Rewiring energy metabolism*

   Malignant cells select glycolysis for energy metabolism despite the presence of oxygen. The preferential adenosine triphosphate (ATP) production via aerobic glycolysis in malignant cells is known as the Warburg effect. However, such a preference generates lower ATP compared to oxidative phosphorylation. Malignant cells employ glucose receptors (GLUT1) to increase glucose levels in the cytoplasm to keep up with the high proliferative demands of malignant cells. Moreover, increased glucose plays a role in the oncogenic capabilities of *RAS*, *MYC,* and mutated tumor suppressor genes. Hypoxic tumor conditions further enhance glycolysis by up-regulating glucose transporters and glycolytic enzymes. The resultant glycolytic

intermediates then play a role in the biosynthesis of amino acids, nucleotides, large molecules, and organelles necessary for new malignant cell development (Hanahan and Weinberg, 2011).

8. *Escaping immune eradication*

   Innate and adaptive immunity, such as protection via cytotoxic T lymphocytes and natural killer cells, contribute to malignant eradiation. Hosts with strong immunity facilitate the elimination of strong immunogenic malignant clones with only the variants of weak immunogenicity left behind that develop into tumors. However, immunogenic malignant cells in immunocompromised hosts thrive (Hanahan and Weinberg, 2011).

9. *Phenotypic plasticity (emerging trait)*

   Refers to changes in malignant cell differentiation that promote a phenotype more inclined to proliferate. A malignant cell developing towards complete differentiation may de-differentiate to take on a progenitor state. An undifferentiated malignant cell may remain in a progenitor-like state or transdifferentiate between programs to acquire traits that inhibit terminal differentiation (Hanahan, 2022).

10. *Non-mutational epigenetic rewiring (emerging trait)*

    Epigenetic variations to genes or histones and expression “switches” with their respective feedback loops are corrupted in malignant cells. For example, the hypoxic condition of a tumor microenvironment results in the weakened activity of TET demethylases facilitating hypermethylation. Furthermore, limited vascularization promotes alterations to translational control and reinforces breast cancer phenotypes (Hanahan, 2022).

11. *Polymorphic microbiomes (emerging trait)*

    New evidence via next-generation sequencing and bioinformatics highlight that microbiome ecosystems may stimulate or inhibit acquired traits of malignant cells. For example, bacteria in the gut microbiome may release mutagenic toxins weakening the genomic stability and disrupting DNA replication and repair. Moreover, bacteria may generate mimetics of ligands that activate proliferative signals (Hanahan, 2022).

12. *Senescent cells (emerging trait)*

    Cell senescence is essential to maintaining homeostasis, and its anti-cancer defense mechanisms have been well documented. However, emerging research suggests that senescence induces modifications to metabolism and morphology with the stimulation of (SASP) senescence-associated secretory phenotype. SASP is associated with expulsing proteases, chemokines, and cytokines to healthy cells and cells in the tumor microenvironment. As such, apoptosis evasion and other acquired malignant traits are promoted (Hanahan, 2022)

1.1.3 Breast cancer

1.1.3.1 Prevalence

Breast cancer is at the forefront of the most frequently diagnosed cancer in the world (Sung *et al*., 2021). According to WHO (2020), breast cancer accounted for 2.3 million cases in 2020. The COVID-19 pandemic has largely delayed screening, diagnosis, and treatment such that many cases go unreported, leading to an underestimate. Breast cancer prognosis is often improved with early detection; delayed detection is associated with more intense treatments and higher mortality (Figueroa *et al*., 2021). According to Lambert *et al*. (2020), South African women encountering socioeconomic challenges detect their cancer at advanced stages and are offered limited treatment options. Moreover, the available conventional treatments caused significant physical and emotional distress (Lambert *et al*., 2020). Globally, Africa is one of the continents to record the highest breast cancer mortality rates (Azubuike *et al*., 2018). The burden is expected to rise without further intervention via improved treatment options, safer anti-cancer drugs, and better awareness (Lambert *et al*., 2020).

1.1.3.2 Pathogenesis

Breast neoplasms present wide-ranging heterogeneity with complex variability in phenotypes and genotypes that guide prognosis and treatments. The breast contains lobules (milk production) and ducts (milk transportation) located in glandular tissue, thus forming a tubuloalveolar gland. Within the breast are luminal and basal epithelium (myoepithelium) coupled via CAMs confined to a basement membrane (Bahcecioglu *et al*., 2020; Bosch *et al*., 2010). The basement membrane is an epithelium barrier to the stromal adipose or fibrous tissue (Figure 1.2 (A)). During carcinogenesis, stringent cell adhesion is lost, facilitating epithelium detachment, proliferative capacity, and tumor mass confined to the lumen, referred to as ductal carcinoma *in situ* (DCIS). If the transformed cells are within lobules and have not bypassed the basement membrane, it is referred to as lobular carcinoma *in situ.* As such, both DCIS and LCIS are non-invasive, as only once transformed cells have migrated past the basement membrane do they pose a metastatic threat. Cells within the neoplasm experience variable nutrient and oxygen supply, promoting further cellular heterogeneity. Cytokines and other factors released by tumor and stromal cells influence the extracellular matrix (ECM) and epithelial integrity. Within the tumor microenvironment (TME) are many cell-cell and ECM cross-talk to facilitate the release of immunosuppressive factors and are capable of fostering cell migration, proliferation, differentiation, and degradation of the ECM. The deterioration of the ECM and basement membrane enables tumor metastasis and invasive neoplasia development (Figure 1.2 (c)) (Bahcecioglu *et al*., 2020).

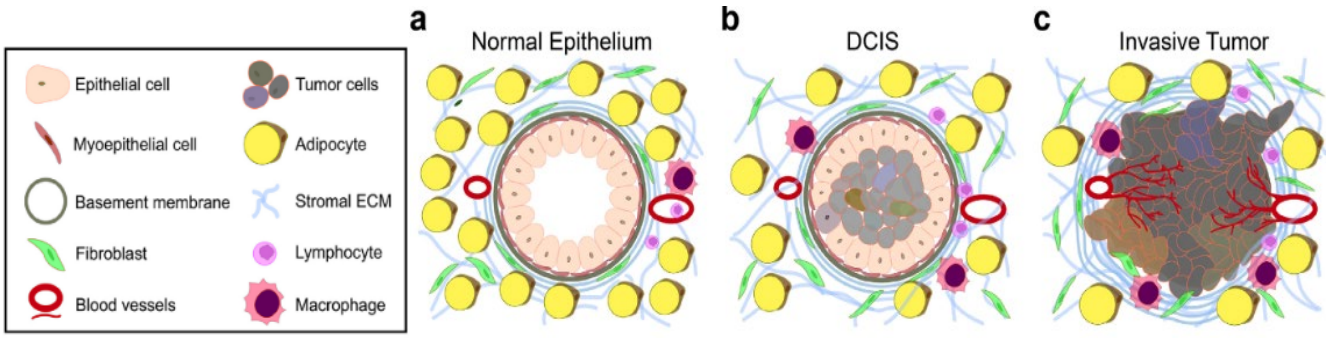

Figure 1.2: Breast cancer development. Healthy luminal and basal epithelium of breast tissue (A) transformed cells confined to the basement membrane (DCIS), restricting blood flow and supporting hypoxic conditions (B) acquired cancer hallmarks and deterioration of the ECM promote metastatic neoplasia (C). Adapted from (Bahcecioglu *et al*., 2020).

1.1.3.3 Risk Factors

Non – modifiable risk factors

Women have a 100 x greater chance of developing breast cancer than men due to higher endogenous levels of estrogen and progesterone (Feng *et al*., 2018). Estrogens have many important physiological roles in sexual development, metabolism, stress feedback, and mineral balance. However, elevated estrogen levels contribute to tumorigenesis (Figure 1.3) and may regulate pro-apoptotic and anti-apoptotic genes. Changes in endogenous hormones in premenopausal and postmenopausal women may influence tumorigenesis (Bhardwaj *et al*., 2019). Increased age is a risk factor since carcinogenesis develops over time. Women with inherited high penetrance genes such as mutated *BRCA1* and *BRCA2* are at higher risk. Although any individual may have the *BRCA* mutations, it is most frequently detected in Ashkenazi Jews. Women with either of the *BRCA* mutations are at risk (60 – 85%) of developing breast cancer before the age of 80. Moreover, a *BRCA* mutation carrier may develop bilateral breast cancer at a young age and risk developing ovarian cancer (15 – 40%) (Bosch *et al*., 2010; Feng *et al*., 2018; Sharma *et al*., 2010). Carriers of the caretaker *BRCA* mutation often have mutated *p53* gatekeeper mutations, as cells with impaired DNA were permitted clearance by corrupted cell cycle checkpoints (Bosch *et al*., 2010). Additional mutations that increase the risk of breast cancer include phosphatase and tensin homolog (*PTEN*), checkpoint kinase 2 (*CHEK2*), serine / threonine kinase 11 (*STK11*) and partner and localizer of BRCA2 (*PALB2*). Women with dense breasts and proliferative lesions such as atypia or non-proliferative lesions such as fibrosis or cysts are also at risk (Feng *et al*., 2018).

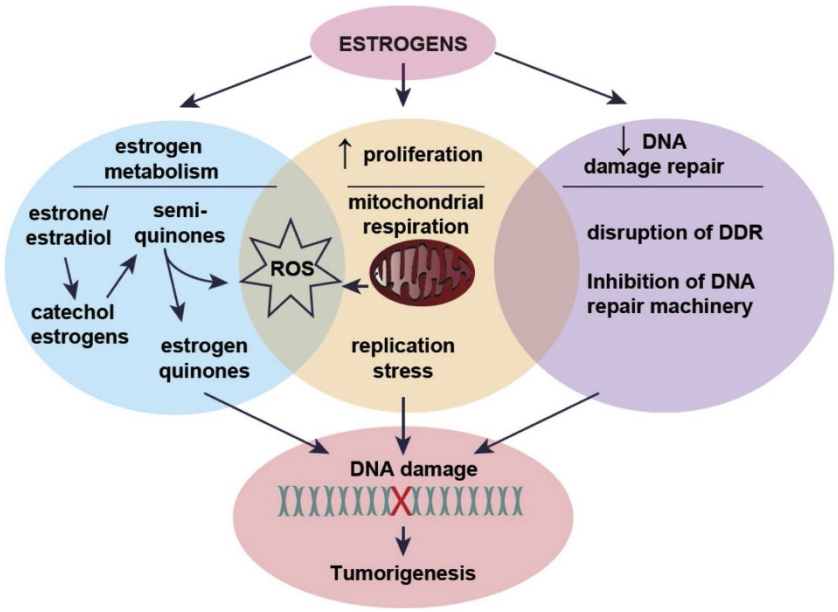

Figure 1.3: Role of estrogen in tumorigenesis. Estrogens stimulate high cellular proliferation promoting replication errors and mutations. Proliferating cells require enhanced cellular respiration producing greater reactive oxygen species (ROS) that promote oxidative stress. Estrogen metabolism results in ROS production and mutagenic quinone production. In addition, estrogen increases tumorigenesis in breast cancers that are negative for its receptor due to metabolites (quinones) that directly damage DNA. Furthermore, estrogens may stress DNA repair machinery and DNA damage responses (DDR). (Adapted from Bhardwaj *et al*., 2019).

Modifiable risk factors

Obesity poses a risk factor since the aromatase enzyme in breast adipose tissue conveys the rate-limiting step of estrogen production. High expression of aromatase, mainly in obese postmenopausal women, is associated with higher breast cancer risks. Furthermore, high alcohol intake increases estrogen levels, and smoking increases carcinogenic events in tumor suppressor genes or oncogenes. Thus, a healthy BMI, regular exercise, and a balanced diet with limited processed food consumption may modify risk factors (Łukasiewicz *et al*., 2021). Pregnancy and lactation may decrease a mother's risk by reducing menstrual cycles that influence hormonal changes associated with breast cancer. Another proposed mechanism is that lactation facilitates mammary cell differentiation, thereby decreasing malignant transformation. Moreover, lactation removes damaged cells from breast tissue via apoptosis (Anstey *et al*., 2017).

1.1.3.4 Molecular classification of breast cancer

Histologically breast cancer is divided into either ductal or lobular carcinomas. The modern genomics era allows breast cancer to be molecularly classified according to receptor expression status into subtypes. Luminal breast cancer can differentiate into invasive ductal/lobular, micropapillary carcinoma, cribriform or mucinous invasive types (Łukasiewicz

et al., 2021). Luminal A sub-types are positive for estrogen receptor (ER +), progesterone (PR +), and negative for human epidermal growth factor receptor 2 (HER2 -). Clinically, luminal A subtypes have a lower proliferation marker (Ki67) and grade with a better prognosis. Conversely, luminal B is of higher grade and Ki67 index with poor prognosis. Luminal B subtypes are (ER +), possibly (PR -) and / or (HER2 +/-) with intermediate prognosis. The HER2 subtype is (ER -), (PR -), and (HER2 +) and has an intermediate prognosis. HER2 types have a higher Ki67 index than luminal subtypes. HER2 subtypes have a high grade and are aggressive, but targeted therapies have improved clinical outcomes (Harbeck *et al*., 2019; Łukasiewicz *et al*., 2021). Triple-negative breast cancer (TNBC) is exceptionally heterogeneous in nature and offers the worse prognosis. TNBC is (ER -), (PR -) a, and (HER2 -). Moreover, TNBC often nurtures mutated *BRCA1* and *BRCA2* and has a high Ki67 index and grade with no response to endocrine therapy. TNBC has no special type of histology. Histological forms include medullary like, secretory, lymphocytic infiltrate, cystic and metaplastic (Feng *et al*., 2018; Harbeck *et al*., 2019; Łukasiewicz *et al*., 2021).

1.1.3.5 Staging

Staging guides prognosis and the treatment paradigm. The American Joint Committee on Cancer (AJCC), the 7th edition, stages cancer-based on Tumor size (T), the status of lymph nodes (N), and distant metastases (M). The stage increases as the tumor size and nodal involvement increase (Figure 1.4). Tumors that have invaded the basement membrane have their sizes grouped as T1 (2 cm or <), T2 (2-5 cm), T3 (> 5 cm), and T4 (tumor developing into chest wall). Lymph nodes may be N1 (1-3 nodes involved), N2 (4-9 nodes), and N3 (10 or > nodes). If cancer has metastasized, this will be M1 (Figure 1.4). Surgery may be used from stages 0 – 3, radiation and endocrine therapy from stages 0 – 4, and chemotherapy from stages 1 – 4 (Alkabban and Ferguson, 2022; Edge and Compton, 2010; Koh and Kim, 2019).

Developed countries make use of an updated staging system. The AJCC (8th edition) has made use of prognostic staging that includes grade (degree of differentiation), receptor status (ER, PR, HER2) and genomic status (Oncotype Dx or mammaprint genomic tests) together with the TNM staging. *LCIS* is no longer classified as *in situ* but rather as a marker of high risk, multiple synchronous (m) tumors are now classified in 1 biological specimen, and T and N deposits are measured. The use of genomic markers and grades facilitates personalized therapy with a revised prognosis. Understanding the mutated genes, receptor status, biological differentiation of the tumor, and anatomical features allow a better response to available treatments (Amin *et al*., 2017; Giuliano *et al*., 2017; Koh and Kim, 2019; Weiss *et al*., 2018).

ANATOMIC STAGE/PROGNOSTIC GROUPS			
Stage 0	Tis	N0	M0
Stage IA	T1*	N0	M0
Stage IB	T0	N1mi	M0
	T1*	N1mi	M0
Stage IIA	T0	N1**	M0
	T1*	N1**	M0
	T2	N0	M0
Stage IIB	T2	N1	M0
	T3	N0	M0
Stage IIIA	T0	N2	M0
	T1*	N2	M0
	T2	N2	M0
	T3	N1	M0
	T3	N2	M0
Stage IIIB	T4	N0	M0
	T4	N1	M0
	T4	N2	M0
Stage IIIC	Any T	N3	M0
Stage IV	Any T	Any N	M1

Figure 1.4: Breast cancer anatomic staging. The AJCC 7th edition stages carcinoma based on tumor size (T), nodal involvement (N), and Metastasis (M) (Tis = *in situ*, mi = microscopic deposits/micrometastasis) (Edge and Compton, 2010).

1.1.3.6 Treatment paradigm

Breast cancer involves a series of treatments, the most common are surgery, radiation, and systemic therapy.

Surgery

Surgery is a mainstay of cancer treatment. The type of surgery performed is dependent on the number of tumors, grade, and stage. Surgery aims to remove the tumor and detect the presence of invasive lymph nodes. Patients may undergo a total mastectomy (removal of entire breasts) and skin-sparing mastectomy with delayed or immediate reconstruction. A patient may have the option of partial mastectomy or lumpectomy to remove the part of the breast with the localized tumor; this is a form of breast-conserving surgery (Leclerc *et al*., 2016; Sutter *et al*., 2016). According to Sutter (2016), many African patients are offered total mastectomy rather than breast-conserving surgery because their cancer was detected at advanced stages, and neoadjuvant (pre-surgery) therapies are limited in certain regions. Following surgery, chemotherapy or radiation is often employed to prevent a recurrence. However, surgery has severe side effects (Figure 1.5) (Smoot *et al*., 2009).

Radiation

Transformed cells are targeted with x-rays / gamma rays to disrupt cellular DNA, thereby triggering apoptosis. Patients undergoing breast-conserving surgery are often treated with radiation to provide similar efficacy as a total mastectomy. Post-surgery radiation may eradicate cells that may remain or to prevent recurrence (Sharma *et al.*, 2010; Smoot *et al*., 2009). However, radiation is toxic to non-malignant cells and associated with adverse side effects (Figure 1.5) (Smoot *et al*., 2009).

Chemotherapy

Chemotherapy may be administered prior to surgery to reduce tumor size, permitting breast-conserving surgery, or administered post-surgery. Chemotherapy aims to inhibit cell proliferation, invasion, and metastasis by damaging DNA, RNA, and protein synthesis or disrupting the cell cycle of neoplastic cells and stimulating apoptotic mechanisms (Muhammad *et al*., 2022; Sharma *et al.*, 2010). Combination chemotherapy includes various anti-cancer drugs with multiple mechanisms of action to form a potent treatment regimen with reduced drug resistance. Types of chemotherapeutic drugs include alkylating agents (Cisplatin) and antimetabolites (Azacitidine) that halt DNA replication and transcription. Antimicrotubular agents (Doxorubicin) are topoisomerase II inhibitors that prevent DNA repair and nucleic acid synthesis. Antibiotics (Actinomycin D) are inhibitors of nucleic acid synthesis, and Miscellaneous (Hydroxyurea) is an inhibitor of ribonucleoside diphosphate reductase. Chemotherapy may be administered orally, intravenously, subcutaneously (injections), or intrathecally (into the cerebrospinal fluid) (Muhammad *et al*., 2022). Chemotherapy also affects non-malignant cells, resulting in adverse side effects and possible drug resistance (Figure 1.5) (Smoot *et al*., 2009).

Endocrine therapy

Endocrine therapy has positively impacted therapeutic outcomes in carcinomas that express estrogen and progesterone receptors. Tamoxifen, a selective estrogen-receptor modulator (SEM), functions as an estrogen antagonist by competitively binding to the ER, decelerating estrogen pro-tumorigenic effects (Smoot *et al*., 2009). Tamoxifen has potent efficacy but is associated with the development of uterine or endometrial cancers and reduced blood flow to the brain. Fulvestrant degrades ER and decreases systemic estrogen levels much quicker than tamoxifen and is used to treat post-menopausal patients (Bhardwaj *et al*., 2019). Aromatase inhibitors such as exemestane prevent the conversion of testosterone to estrogen resulting in a decline of systemic estrogen. Herceptin, in HER2-positive breast cancers, attaches to HER2 proteins and inhibits cell division. However, malignant cells may become

unresponsive and resistant to endocrine therapy over time, especially in advanced stages, and adverse side effects remain (Bhardwaj *et al*., 2019; Smoot *et al*., 2009).

Targeted therapy

Targeted therapy aims to inhibit biochemical pathways and mutated proteins that promote tumorigenesis. Further advancements in targeted therapy target mutated proteins specific to an individual's tumor, enabling "personalized'' therapy. Small molecule inhibitors are a class of targeted therapy that block kinase activity by competitive binding to the ATP site of tyrosine kinases to prevent the action of dysregulated pathways via inhibition of downstream signaling. The small molecule Gefitinib affects the epidermal growth factor receptor (EGFR) in lung cancer, and Gleevec targets a proto-oncogene in chronic myeloid leukemia (Baudino, 2015; Meattini *et al*., 2022). The second class of targeted therapy utilizes monoclonal antibodies by activating an immune response or blocking ligand and receptor associations required for cell proliferation. Monoclonal antibodies may be raised against vascular endothelial growth factor-A (VEGF-A) involved in cancer angiogenesis; this promotes T cell activity and counteracts VEGF activity (Vanneman and Dranoff, 2012). Immunotoxins are another class of targeted therapy generated by utilizing recombinant DNA to form a fusion protein with a toxin attached to a domain on a growth factor or antibody. The resultant immunotoxin attaches to a cell via surface proteins and is allowed entry via clathrins. Thereafter the immunotoxin triggers apoptosis. Ontak is an immunotoxin that targets the interleukin-2 receptor in T-cell lymphoma and has shown effectivity in phase III clinical trials. Ontak contains a bacterial toxin called DT that inactivates elongation factor-2 (EF-2) to inhibit protein biosynthesis. Many side effects are still reported on targeted therapy. Various targeted therapeutic drugs are combined with conventional treatments to enhance efficacy (Baudino, 2015).

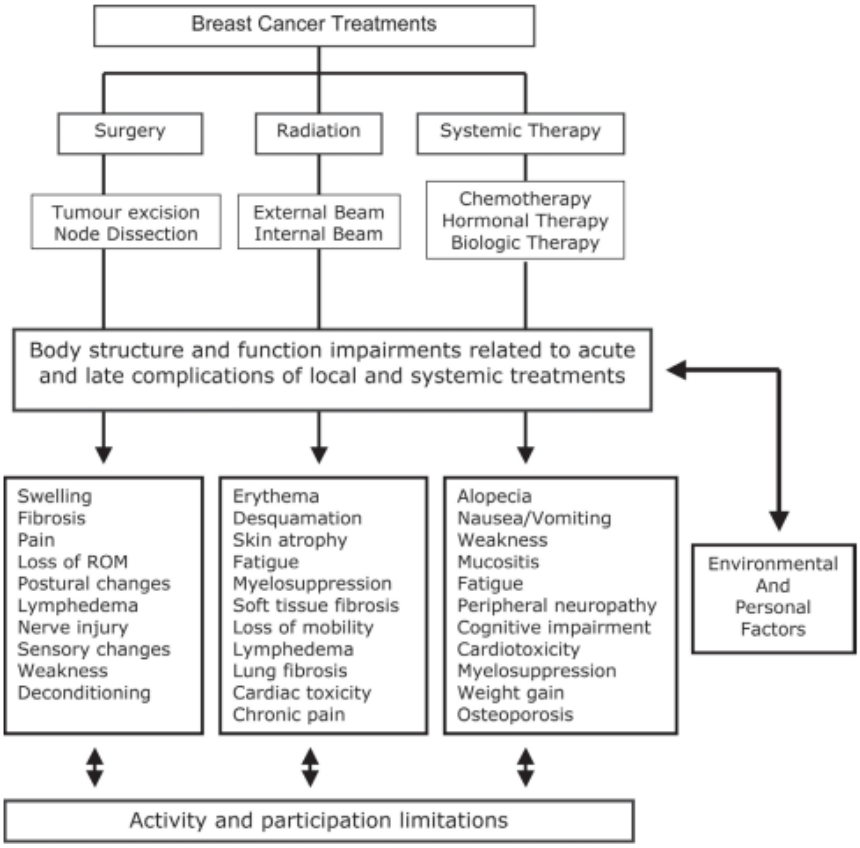

Figure 1.5: Mainstay breast cancer treatment paradigms. All paradigms accompany adverse toxic side effects (Adapted from Smoot *et al*., 2009).

1.2 Modes of cell death

The human body replaces over fifty billion cells daily, using many cell death modalities to maintain homeostasis (Compton, 2021). Cell death modes were previously divided into apoptosis, necrosis, and autophagy. With evolving research, new modalities have been discovered and classified according to the death signal received, the mechanism of action, and its associated morphology (Figure 1.6) (Yan *et al*., 2020). Cancer therapeutics may employ many cell death modalities. However, apoptosis is the most frequently harnessed mode to battle cancer. Apoptosis cell death is intrinsically wired to inhibit carcinogenesis from initiation to the final oncogenic transformation (Figure 1.1) (Goldberg, 2019). Therefore, this sub-chapter will focus on the apoptosis modality, and other cell death modalities will be briefly discussed.

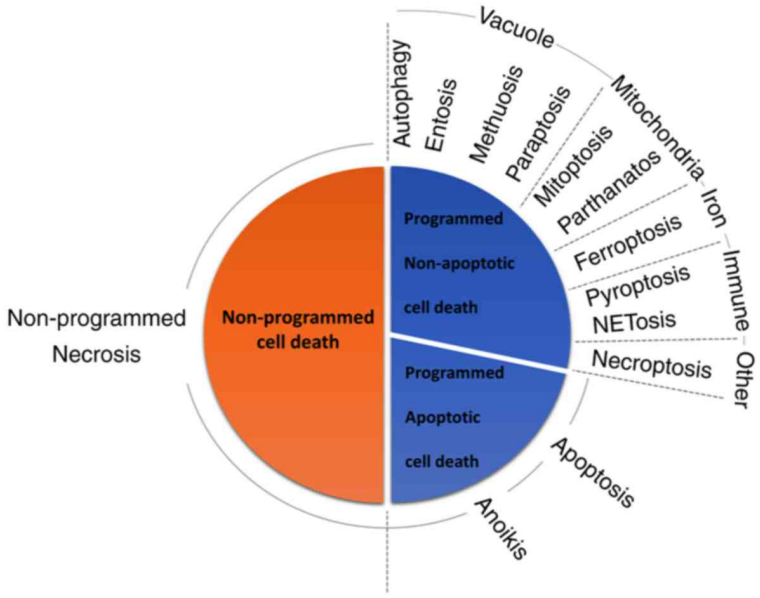

Figure 1.6: The various cell death modalities. Cell death modalities can be classified based on signal transduction, mechanical action, and resultant morphology. Moreover, they can be classified into un-regulated necrosis or regulated cell death modalities, further sub-divided into apoptotic and non-apoptotic cell death modes (Adapted from Yan *et al*., 2020).

1.2.1 Apoptosis

Apoptosis is an ATP-dependent death modality that conducts essential duties in embryonic development, cellular differentiation, development, and homeostasis throughout a human's lifespan. After a cell has completed its physiological obligations or undergone damage, it will commit cell suicide in a programmed, ordered manner (programmed cell death (PCD)), referred to as apoptosis. Various defects along the apoptosis pathways contribute to carcinogenesis or drug resistance. As such, apoptosis evasion is a significant cancer hallmark.

The classical apoptotic pathways include the intrinsic (mitochondrial) and extrinsic pathways. Both pathways converge to a common path to carry out the execution phase of apoptosis (Wong, 2011).

1.2.1.1 Apoptosis Morphology and biochemical changes

The term 'apoptosis' was coined based on the unique morphology of apoptotic cells observed under an electron microscope (Kerr *et al*., 1972). Apoptotic morphology includes cell rounding, reduction of cell volume (pyknosis), and chromatin condensation along the nuclear periphery. An increase in condensation promotes intracellular chromatin fragmentation (karyorrhexis) within an intact nuclear membrane. Later in the degradation phase of apoptosis, membrane integrity is weakened, membrane blebbing occurs, apoptotic bodies are formed, and cytoplasmic organelles are modified (Wong, 2011). Small apoptotic bodies may consist of cellular fragments and organelles. In contrast, the larger apoptotic bodies may consist of significant cellular components such as nuclear fragments, while the mitochondria may remain intact (Saraste and Pulkki, 2000). The movement of phosphatidylserines from the interior to the exterior of the cell membrane signals macrophages or phagocytes to engulf apoptotic bodies (Fadok *et al*., 1998). Apoptotic bodies then undergo degradation by lysosomes in a neat and ordered manner without the spillage of inflammatory reactions by reducing the production of damage-associated molecular patterns (DAMPs). If apoptotic cells are not engulfed, they undergo secondary necrosis deterioration while still inhibiting inflammatory responses. Studies proposed that this was due to the inactivation of DAMPs by caspase cleavage during the apoptosis cascade (Tait *et al*., 2014; Vénéreau *et al*., 2015).

1.2.1.2 Caspases as classical apoptosis machinery

The link between apoptosis and caspases was first published in 1993 when the *ced-3* gene was linked to apoptosis in the nematode *Caenorhabditis elegans*. Thereafter, the role of caspases in mammalian apoptosis was progressively explored. Caspases are endonucleases or cysteine proteases that hydrolyze peptide bonds and cleave after aspartic residues of cellular proteins critical to maintaining the DNA network and cytoskeleton (Li and Yuan, 2008). Caspases are produced as monomeric inactive zymogens (pro-caspases), and only when dimerized or cleaved will they be activated to promote a caspase cascade. The zymogen contains an N-terminal domain, a p20 subunit, and a smaller p10 subunit. Initiator caspases may undergo activation by means of protein interactions. The binding of adaptor proteins to the caspase recruitment domain (CARD) or death effector domain (DED) of pro-caspases allows activated dimers to form. After receiving an apoptotic signal in the initiation phase of apoptosis, caspases manage the activation or inhibition of the apoptosis pathway (McIlwain *et al*., 2013). Initiator caspases involved in the early phases of apoptosis include caspase-2, -8, -9, and -10. In the executioner phase of apoptosis, the effector caspase-3, -6, and -7 depend

on initiator caspases for activation following cleavage. Many effector caspases undergo activation via proteolysis among the p20 and p10 subunits or in the middle of the prodomain and the p20 subunit (Cohen, 1997). Another subfamily of caspases exists, caspases-1, -4, -5, -11, and -12 mediate cytokines and inflammatory responses. The activated effector caspases involved in apoptosis activate DNAse and cleave many structural proteins within the cell that initiate the morphology characteristic of apoptosis in the degradation phase (Juan *et al*., 2006; McIlwain *et al*., 2013). For example, caspases cleave actin, spectrin, gelsolin, and Gas2 involved in microfilament formation and cytoskeleton preservation. Proteins associated with cell-cell adhesion or junctions (Mitogen-activated protein kinase kinase kinase 1 (MEKK-1) and focal adhesion kinase (FAK)) and kinase activity that regulates the cytoskeleton (P21 (RAC1) Activated Kinase 2 (PAK2)) undergo caspase cleavage. Proteins that generate the nucleus laminar, regulate chromatin and matrix (nuclear mitotic apparatus protein (NuMa)), and are involved in DNA replication and repair, such as poly-(ADP-ribose) polymerase (PARP), also undergo cleavage. Thus, caspases cleave proteins essential to cell integrity to induce apoptotic morphology (Saraste and Pulkki, 2000).

1.2.1.3 Apoptosis pathways

The Extrinsic pathway

The extrinsic pathway relies on ligands that bind to death receptor domains to initiate signal transduction. There are many death receptor domains, such as Tumor necrosis factor receptor 1 (TNFR1), Death receptor type 3 (DR3), TNF -related apoptosis-inducing ligand receptors- 1 and 2 (TRAIL-R1 and TRAIL-R2). The most common death receptor is the TNF type 1 receptor which binds the tumor necrosis factor (TNF) ligand, and a protein referred to as Fas which binds the FAS ligand (FasL). Within the transmembrane death receptor lies a death domain that facilitates the recruitment of adaptor molecules such as the TNFR-associated death domain (TRADD) and FAS-associated death domain (FADD). Once the ligand attaches to the receptor, a conformational alteration promotes a binding position for an adaptor protein. This complex consisting of the ligand, receptor, and adaptor protein is called the death-inducing signaling complex (DISC). DISC then activates pro-caspase-8, which activates pro-caspase-3 (McIlwain *et al*., 2013; Wong, 2011) (Figure 1.7). Caspase-8 may also promote crosstalk between apoptosis pathways by initiating the intrinsic pathway of apoptosis through cleavage of Bid to form truncated Bid (tBid), which regulates pro-apoptotic effector Bax and Bak to permeabilize the mitochondrial membrane and expel pro-apoptotic proteins that facilitate activation of executioner caspases (Elmore, 2007).

The Intrinsic (mitochondrial) pathway

Initiation of the intrinsic pathway occurs when stress stimuli are received internally via hypoxia, genetic stress, elevated oxidative stress, excessive cytosol calcium influx, irregular oncogene expression, and toxic compounds (Saraste and Pulkki, 2000; Wong, 2011). In response to the apoptotic stress stimuli, the mitochondrion increases its membrane permeability, also known as mitochondrial outer membrane permeabilization (MOMP), to facilitate the expulsion of pro-apoptotic proteins such as cytochrome *c*, AIF (Apoptosis-inducing factor), second mitochondria-derived activator of caspase (Smac/DIABLO), and high-temperature requirement protein A (Htra2/Omi) from the intermembrane space of the mitochondria to the cytosol (Lopez and Tait, 2015; Wong, 2011).

Cytochrome *c* is an electron transporter facilitating the generation of ATP in the mitochondria. However, once expelled from the intermembrane space, it serves as an apoptosis assistant by promoting caspase activation. Cytochrome *c* reacts with an adaptor protein called apoptosis protease–activating factor 1 (APAF-1) and ATP; such interaction conformationally alters APAF-1 into a heptameric structure referred to as an apoptosome that binds and cleaves pro-caspase-9. Initiator caspase-9 catalyzes the activation of caspase-3 and caspase-7 effector caspases. Inhibitors of apoptosis proteins (IAPs) inhibit the activity of caspase-3 and caspase-9 by preventing the caspases from interacting with their substrate or facilitating the degeneration of caspases. Therefore, the pro-apoptotic proteins Smac/DIABLO and Omi bind to IAPs, enabling executioner caspase activation. Both intrinsic and extrinsic pathways lead to a common pathway that activates caspase-3 (Figure 1.7). Caspase-3 cleaves the inhibitor of caspase-activated deoxyribonuclease (ICAD) to activate caspase-activated deoxyribonuclease (CAD) to embark on nuclear apoptosis and promote its characteristic morphology. Activated downstream caspases cleave proteins associated with the cell cycle, DNA integrity, cytoskeleton preservation, kinases, and signaling cascades (Wong, 2011).

The B-cell lymphoma 2 (BCL-2) family controls irreversible MOMP generated by the intrinsic pathway. This family comprises the pro-apoptotic Bax and Bak effector proteins, BH-3 pro-apoptotic proteins (such as BID, BAD, and PUMA), and the anti-apoptotic BCL-2 proteins (BCL-xL). Bax and Bak effector proteins interact with a BH3-only protein to partake in conformational adjustments and oligomerization in the mitochondrial external membrane. Subsequently, leading to MOMP due to the oligomerized effector proteins initiating lipid pores indirectly or creating pores directly in the membrane. BH3-only proteins serve as stress indicators that pass on apoptotic signals to the mitochondria by activating effector proteins (Adams *et al*., 2019; Lopez and Tait, 2015; Wong, 2011). BH3-only proteins can activate the effector Bax or Bak and counteract the anti-apoptotic BCL-2 proteins. BCL-2 proteins inhibit MOMP through attaching to BH-3 only proteins averting their association with the effector

proteins, alternatively, by linking directly to the activated effector proteins. BH3 domains (present in activated effector and BH3-only proteins) and the BH3 binding site in BCL-2 anti-apoptotic proteins are the primary mediators of MOMP via competitive interruption of protein interactions. The level of pro and anti-apoptotic proteins controls MOMP initiation. The pro-apoptotic proteins stimulate the expulsion of cytochrome *c* from the mitochondria by increasing MOMP, whereas anti-apoptotic proteins prevent MOMP (Figure 1.8) (Adams *et al*., 2019; Lopez and Tait, 2015; Wong, 2011).

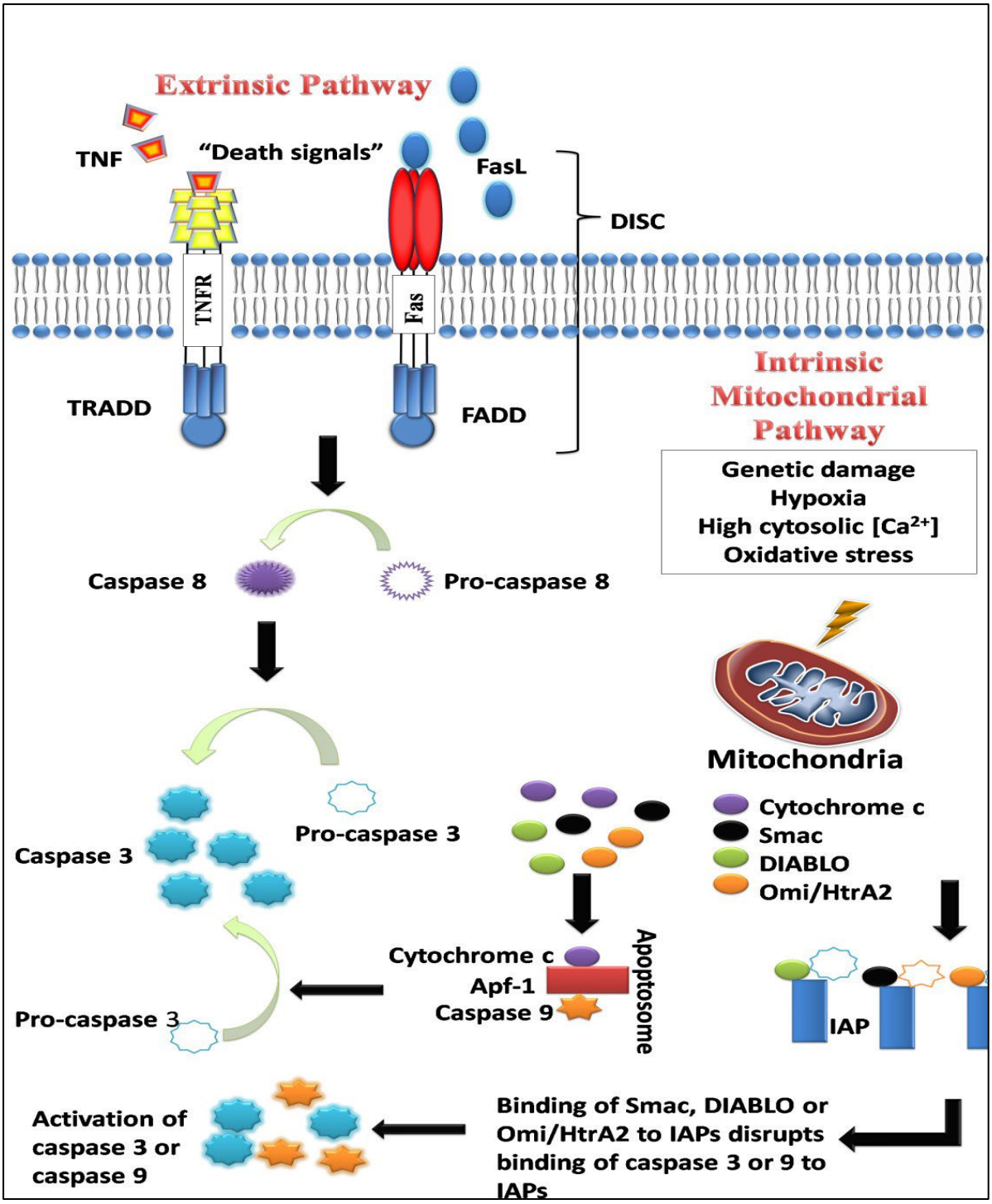

Figure 1.7: The classical apoptosis pathways. The classical extrinsic (receptor-dependent) and intrinsic (MOMP-dependent) pathways rely on caspase machinery to signal apoptosis cell death and its characteristic morphology. The initiator caspase-8 is a key player of the extrinsic pathway, whereas initiator caspase-9 functions in the intrinsic pathway. In the intrinsic pathway, MOMP aids the expulsion of pro-apoptotic proteins to permit apoptosome formation and downstream effector caspase-3 and caspase-7 activation. In the extrinsic pathway, caspase-3 effector caspase is also activated and promotes the characteristic apoptotic morphology (Adapted from Wong, 2011).

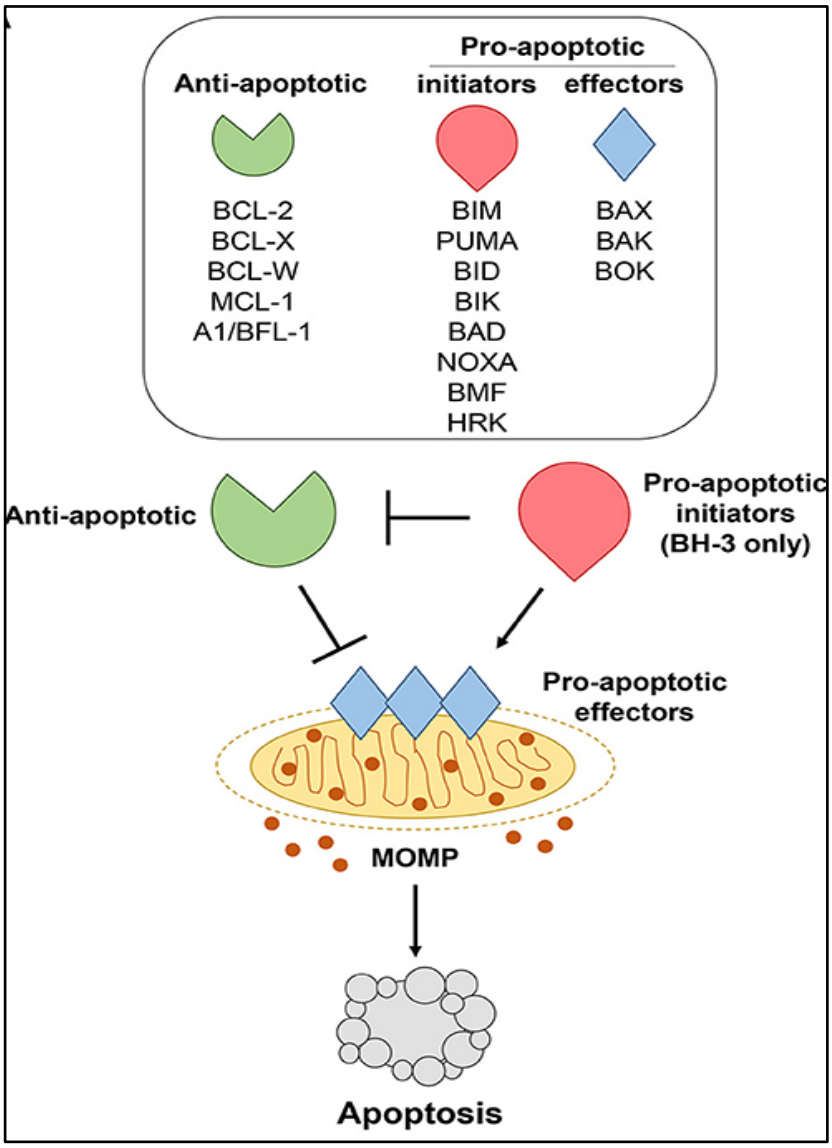

Figure 1.8: The BCL-2 family regulates MOMP. Apoptotic stimuli activate BH3-only proteins (red) and prevent anti-apoptotic protein (green) activity, permitting the oligomerization of the effector proteins (blue) to initiate MOMP to proceed with apoptosis. Effector proteins (blue) interact with BH3-only proteins (red) for their activation and oligomerization in the mitochondrial membrane that generates pores facilitating MOMP. Anti-apoptotic proteins BCL-2 (green) bind BH3-only proteins (red) or effector proteins (blue) to obstruct MOMP activation. The level of pro and anti-apoptotic proteins controls MOMP and consequently intrinsic apoptosis (Adapted from Adams *et al*., 2019).

The intrinsic endoplasmic reticulum pathway

This pathway can initiate apoptosis independently of the mitochondria and is stimulated by strain on the endoplasmic reticulum (ER). The strain may be caused by hypoxia, glucose depletion, free radicals, incorrect protein folding, or aberrant protein translation within the cell. The strain elicits the disassociation of TNF receptor-associated factor 2 (TRAF2) from pro-

caspase-12, and caspase-12 will serve as the initiator of apoptosis (Winter *et al*.,2014; Wong, 2011).

1.2.1.4 Caspase-Independent cell death (CICD)

When apoptotic cues are signaled, and caspase activation is inhibited, this is called caspase-independent cell death (CICD). CICD often shares some common features with apoptosis, such as MOMP and chromatin condensation. However, the type of CICD induced will be the determinant factor for its corresponding morphology and biochemical markers (Tait and Green, 2008). CICD may be activated via death receptors in the plasma membrane or DNA impairment stimuli managed at the outer mitochondrial membrane. Thereafter, non-caspase proteolytic enzymes facilitate the death process. The endoplasmic reticulum and lysosomes serve as stress sensors and may activate various proteases to proceed with cell death (Jäättelä and Tschopp, 2003).

MOMP may induce apoptosis independent of caspases via the release of AIF from the mitochondrial intermembrane space to the cytosol. AIF undergoes proteolysis and migrates to the cytosol, where it interacts directly with nuclei to facilitate chromatin condensation and extensive DNA fragmentation (Barbosa *et al*., 2016; Loane *et al*., 2015). Besides conducting CICD, AIF monitors redox metabolism and regulation of oxidative phosphorylation (Sevrioukova, 2011). Post-MOMP, Omi, and endonuclease G (endoG) release further facilitate CICD as the serine protease activity of Omi provokes PCD while endoG promotes DNA-fragmentation. Therefore, AIF, Omi, and endoG serve as apoptogenic molecules dependent on MOMP for their release and cell death execution (Guerin *et al*., 2006; Jäättelä and Tschopp, 2003) (Figure 1.9)

Necroptosis is another form of CICD. Necroptosis death may be initiated via cell stress, damage, or infections that often involve extrinsic death receptor ligations. In the absence of active caspases, death receptors such as toll-like receptors may provoke necroptosis via phospholipase A2 (PLA2) activity which generates high levels of ROS activity (Tait and Green, 2008). Studies indicated that the tumor necrosis factor (TNF) in the absence of caspases inhibited by the z-VAD-fmk or CrmA promoted necroptosis cell death (Hirsch *et al*., 1997; Okuno *et al*., 1998). The oligomerization of FADD adaptor protein (as mentioned in the extrinsic pathway) may also promote necroptosis (Kawahara *et al*., 1998). The receptor-interacting protein kinase-1 (RIPK-1) is an adaptor protein with kinase activity and critical involvement in the necroptosis pathway via nuclear factor-kB activation. A proposed mechanism for RIPK-1 participation in necroptosis is inhibition of adenine nucleotide translocase with cyclophilin D, provoking mitochondrial impairment (Tait and Green, 2008). Further studies revealed that RIPK-1 and RIPK-3 are required in forming a necrosome. RIPK-1 may auto phosphorylate in the absence of caspase-8 and recruit RIPK-3. RIPK-3

phosphorylates mixed lineage kinase domain-like proteins (MLKL), facilitating their oligomerization to puncture the cell membrane and destabilize it, leading to cell death. Subsequent morphological changes include intracellular organelle swelling, ruptured membrane, and expulsion of pro-inflammatory molecules (Koren and Fuchs, 2021).

Lysosomal proteases such as cathepsins may function with or without caspase activity and are initiated via stimuli such as retinoids, TNFR or B cell receptors, oxidants, or the p53 protein to promote lysosomal dependent cell death. Cathepsins leak out of lysosomes and migrate to the cytosol or nucleus. The change from an acidic to a neutral environment upon leakage was proposed as the activator of cathepsins' enzymatic activity. Moreover, these proteases cleave similar substrates as caspases such as PARP, Bid, and cytosolic PLA2 and share common apoptotic morphological characteristics such as PS exposure, chromatin condensation, and membrane blebs. Cathepsins may activate Bid prompting cathepsin-mediated MOMP (Figures 1.9 and 1.10) (Jäättelä and Tschopp, 2003).

An alternative CICD is the autophagy modality. During macro-autophagy, the cytosol and its organelles are sequestered into an autophagosome separated from the remainder of the cell components via a double membrane. Fusion of the autophagosome with lysosomes leads to degradation of the sequestered components and the inner membrane. However, autophagy does not always lead to cell death and can suffice as a cell renewal system. Autophagy can rid the cell of damaged organelles or recycle it to provide amino acids. A slow metabolic death may be triggered by apoptotic stimuli that result in mitochondrial removal via autophagy in CICD. Studies propose that cathepsins may promote autophagic cell death independent of caspase. However, the precise mechanism has not been clarified. Autophagic morphology is characterized by cytosolic vacuole presence, organelle swelling, membrane blebs, and no chromatin condensation or inflammatory reactions (Figure 1.9) (Jäättelä and Tschopp, 2003; Kroemer and Martin, 2005; Koren and Fuchs, 2021).

The endoplasmic reticulum guards cell stress and triggers MOMP PCD when aberrantly high calcium levels prevail and misfolded proteins are abundant. Stimuli from neurotoxins, etoposide, and irradiation activate high calcium levels, which in turn stimulate the activity of proteases harbored in the cytosol called calpains. Calpains can trigger caspase activity. However, they can also elicit cell death independent of caspases via mitochondrial impairment or Bax activation via calpain-mediated cleavage (Figure 1.10) (Jäättelä and Tschopp, 2003; Kroemer and Martin, 2005).

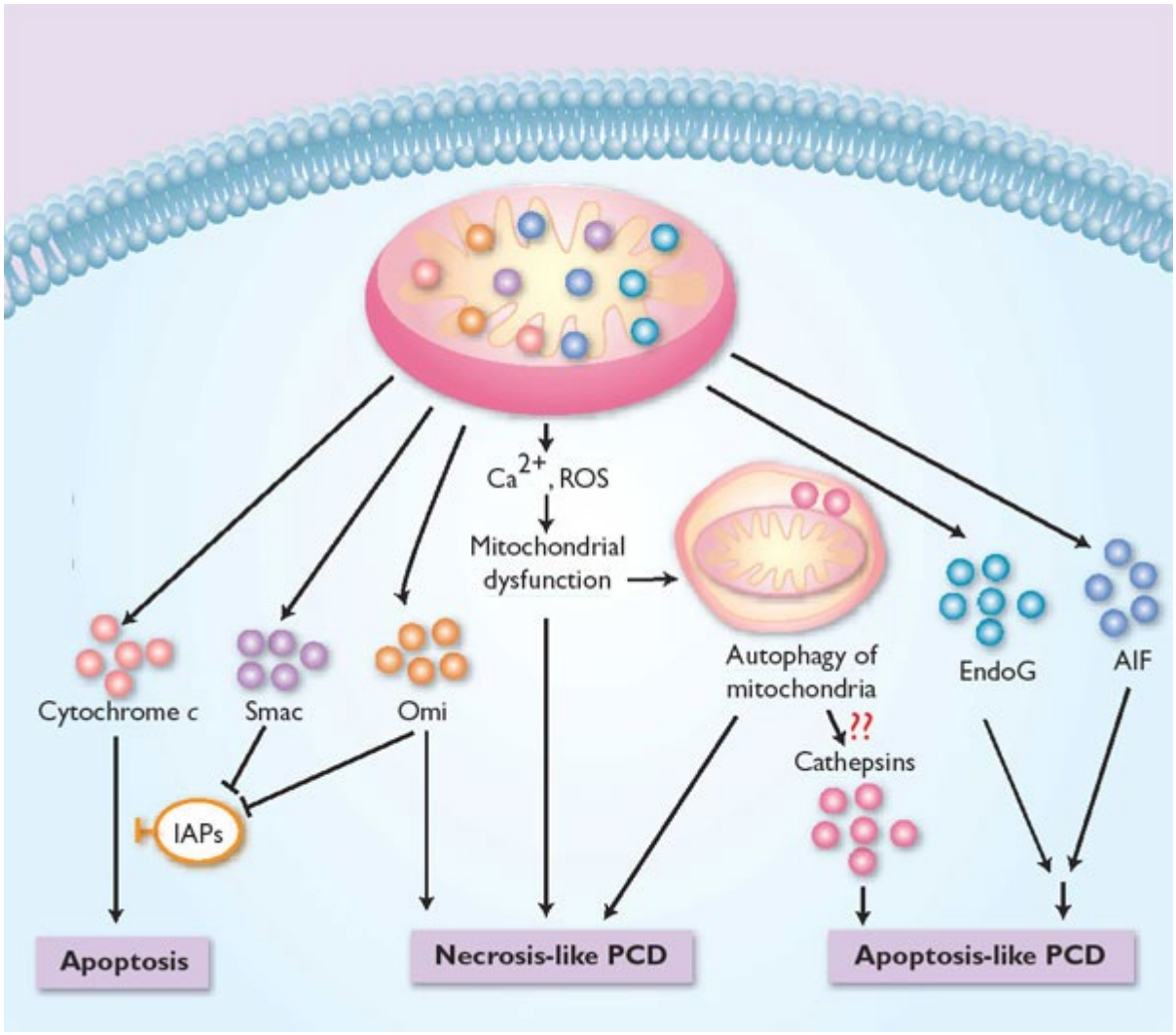

Figure 1.9: MOMP may promote caspase-dependent or independent cell death. MOMP may expel cytochrome *c* to promote the formation of the apoptosome whereases Smac and Omi inhibit the activity of IAPs to trigger caspase-dependent apoptosis. AIF triggers apoptotic-like death without caspase activity, producing DNA fragmentation and chromatin condensation morphological characteristics. EndoG further promotes DNA fragmentation. The serine proteolytic activity of omi does not change nuclear morphology but promotes necrotic-like cell death. High ROS and calcium activity may directly impair the mitochondria resulting in necrotic-like death, or it may indirectly promote autophagy of the mitochondria. Moreover, studies propose that autophagy may be enabled via cathepsin activation (Adapted from Jäättelä and Tschopp, 2003).

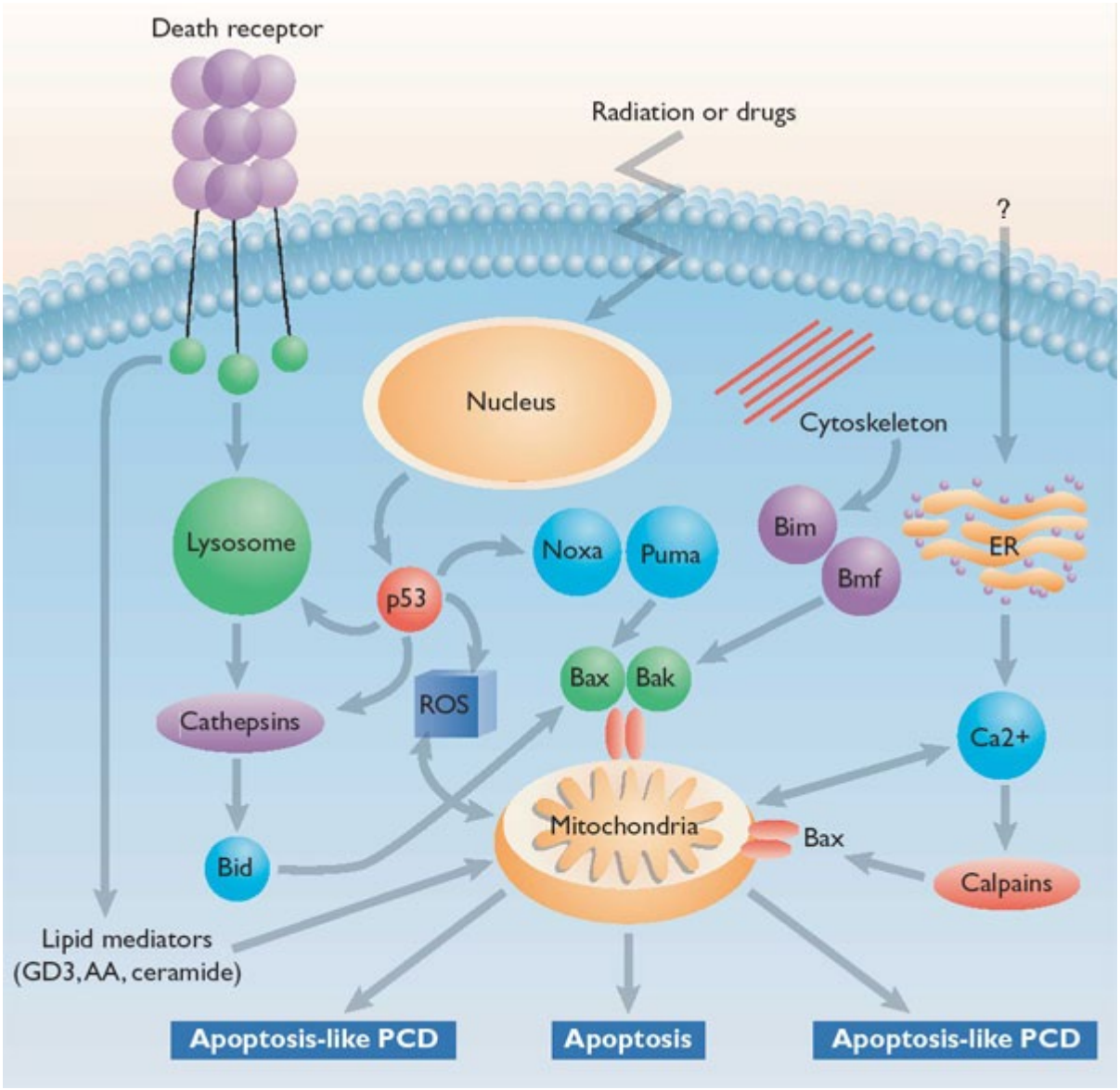

Figure 1.10: CICD pathways that activate MOMP. Death receptors, chemotherapeutic agents, and oxidants facilitate the expulsion of cathepsins from lysosomes into the cytosol or nucleus. Cathepsins cleave many substrates, including Bid, which promote MOMP activation. Impairments to the cytoskeleton provoke the release of BH3-only proteins Bim and Bmf, which activate effector proteins. DNA alteration via chemotherapeutic drugs / radiation initiates *p53* transcription of Noxa and Puma BH3-only proteins, which initiate the effector Bax and Bak to promote MOMP. High cytosolic calcium generated due to ER stress may activate Bax activity via calpain-mediated cleavage. Moreover, death receptor stimuli may produce lipid mediators that influence the mitochondria to initiate CICD (Adapted from Jäättelä and Tschopp, 2003).

1.2.2 Routes cancer use to escape apoptosis

Cancer avoids the intrinsic pathway of apoptosis by using routes that prevent MOMP or caspase activation. Several malignancies up-regulate the expression of BCL-2 anti-apoptotic proteins and down-regulate their inhibitors by means of oncogenic signals, which inhibit MOMP and cytochrome *c* release from the mitochondria. Malignant cells may have dysfunctional p53 tumor suppressor proteins and apoptotic proteins (Bax or Bak). Pro-apoptotic proteins (BH3 and PUMA) may lose their function by transcriptional silencing or sequence deletions in tumors inhibiting apoptosis induction (Lopez and Tait, 2015). Death receptors and their ligands may be down-regulated or impaired, preventing extrinsic pathway stimulation (Wong, 2011). Various mechanisms inactivate caspases, including epigenetic silencing of the apoptosome or prevention of APAF-1 activation. Post-MOMP, cytochrome *c* may be tagged for ubiquitination preventing apoptosome formation. Caspases can be inhibited by XIAP or c-IAP1 since they may inactive Smac and Omi, which bind to the receptors that inhibit apoptosis (Lopez and Tait, 2015).

1.2.3 Exploiting dysregulated apoptotic events in cancer therapeutics

Enhanced activity of anti-apoptotic proteins and impaired regulation of the BCL-2 family can be exploited by BH3 mimetics which mimic binding to the hydrophobic groove of the anti-apoptotic BCL-2 proteins; therefore, serving as a BH3-only protein mimic. An alternative target to the BCL-2 family that prevents apoptosis is to silence their genes, thereby inhibiting their expression and promoting apoptosis (Lopez and Tait, 2015; Wong, 2011). Certain small molecule drugs such as PhiKan083 aim to restore wild-type p53 from their mutated forms. Targeting mutated p53 can occur through gene therapy, drug therapy, or immunotherapy (Boeckler *et al*., 2008). Targeting IAPs has shown high efficacy. For example, XIAP inhibits both intrinsic and extrinsic pathways by inhibiting initiator caspase-9, caspase-3 and caspase-7. Therefore, antisense tactics and siRNA molecules can inhibit XIAP activity and facilitate apoptosis. Moreover, IAP antagonist small molecules may be designed; for instance, Smac mimetics were designed to bind to XIAP to restore caspase-9, -3, and -7 functions in the classical apoptosis pathways (Dai *et al*., 2009). Many drugs also aim to target or awake caspase activation in malignant cells, and an example of such a drug is Apoptin (Rohn and Noteborn, 2004). Small molecule caspase activators may auto-activate pro-caspase-3 and initiate apoptosis directly (Lopez and Tait, 2015; Wong, 2011).

1.2.4 Other cell death modalities

Necrosis is a form of cell death that may occur in physiological and pathological conditions such as neurodegeneration, infections, cell injury, ischemia, and trauma. Necrosis is stimulated by aberrant calcium levels, ATP reduction, and elevated ROS generation (Ricci and Zong, 2006). Features of necrotic cells include an increase in cell size, ruptured plasma membrane, disrupted mitochondria, enlargement of the mitochondria, organelle clustering towards the nucleus, and cell lysis. In contrast to apoptosis, necrotic cells burst open, spraying their pro-inflammatory cellular contents into the ECM sending signals to induce an adaptive immune response that may aid tissue repair (Golstein and Kroemer, 2007; Rock and Kono, 2008). However, the inflammatory reaction may impair non-malignant cells and elicit the release of high-mobility group box 1 protein (HMGB1) and hepatoma-derived growth factor cytokines (HDGF). The cytokines can promote cell proliferation and metastasis, affecting the prognoses of anti-cancer treatments that promote necrotic cell death (Ricci and Zong, 2006). Furthermore, the inflammatory response may promote additional side effects in cancer patients (Rock and Kono, 2008).

Anoikis PCD has the common classical apoptotic pathways; however, it is triggered by stimuli such as insufficient cell-matrix association (Yan *et al*., 2020). Non-apoptotic death modalities include cells with vacuole formation, as previously discussed in macro-autophagy. When a cell has undergone irreversible stress, autophagy is induced as a protective or survival mechanism or PCD. Three levels of autophagy exist macro-autophagy (previously mentioned in CICD), micro-autophagy, and chaperone autophagy. Micro-autophagy involves the direct sequestration of cytoplasm elements into a lysosome via protrusion, septation, and invagination of the lysosomal membrane followed by acid hydrolases. Whereas, in macro-autophagy, the cytoplasm is sequestered in a double membraned autophagosome that undergoes fusion with a lysosome forming an autolysosome. Chaperone autophagy targets proteins with specific amino acids (KFERQ) recognized by chaperones. Thereafter, the target protein is captured and transported along the lysosomal membrane followed by its degradation, and macromolecules are transported to the cytosol via membrane permeases (Denton and Kumar, 2018; Koren and Fuchs, 2021). Particularly, when the mitochondrion is degraded, this is known as mitophagy. Apart from autophagy, other cell death modalities also present with vacuole formation, such as entosis, methuosis, and paroptosis (Yan *et al*., 2020).

Entosis modality involves a cell's entrance to its neighboring cell through cadherins. Instead of generating ‘’eat me’’ signals as in phagocytosis, entotic cells enter other cells via actomyosin contractions and are initiated due to loss of integrin ECM attachment (Yan *et al*., 2020). Methuosis involves huge fluid-filled vacuoles and is activated via the Ras family and involve the formation of macropinosomes. Methuosis has common morphological

characteristics as necrosis (Maltese and Overmeyer, 2014). Paraptosis modality is often used by immune cells that have undergone damage or have received pathogen signals. Paraptosis displays extensive vacuole formation in the cytoplasm due to dilation of the ER or mitochondria due to excessive ROS and calcium levels. Morphology includes membrane rupture and organelle swelling (Koren and Fuchs, 2021).

Mitochondrial cell death includes Mitoptosis and Parthanatos. Mitoptosis involves fusion and fission of the mitochondria and impairment of ATP that promotes mitochondrial suicide and is often linked to apoptosis and autophagy. The resultant impaired mitochondria can result in mitoptotic bodies or autophagosomes. Parthanatos is a CICD; however, it is characterized by heightened PARP activity, AIF involvement, and large-scale DNA fragmentation with non-apoptotic body formation (Yan *et al*., 2020). Ferroptosis is a cell death modality dependent on iron and is initiated via impairment of the glutathione antioxidant defense system. Free iron may interact with hydrogen peroxide and result in high oxidative stress and the destruction of lipids in the plasma membrane (Jiang *et al*., 2021; Yan *et al*., 2020).

Pyroptosis is a regulated form of the necrosis modality that provokes an inflammatory response and often involves crosstalk with other death modalities such as apoptosis. Immune cells that have undergone damage or received pathogen signals often employ pyroptosis. It involves activating the Gasdermin family, which creates plasma membrane pores upon oligomerization. This modality is mediated by caspase-1, -4, -5, and -11 (Koren and Fuchs, 2021; Yan *et al*., 2020). Netosis modality frequently occurs in neutrophil immune cells in the presence of pathogens. Contact with the neutrophil and pathogen results in histone modification and decondensation of chromatin that facilitates a neutrophil extracellular trap (NETs) which is often promoted by high ROS activity (Vorobjeva and Chernyak, 2020). Morphological characteristics of the various cell death modalities are depicted in Figure 1.11.

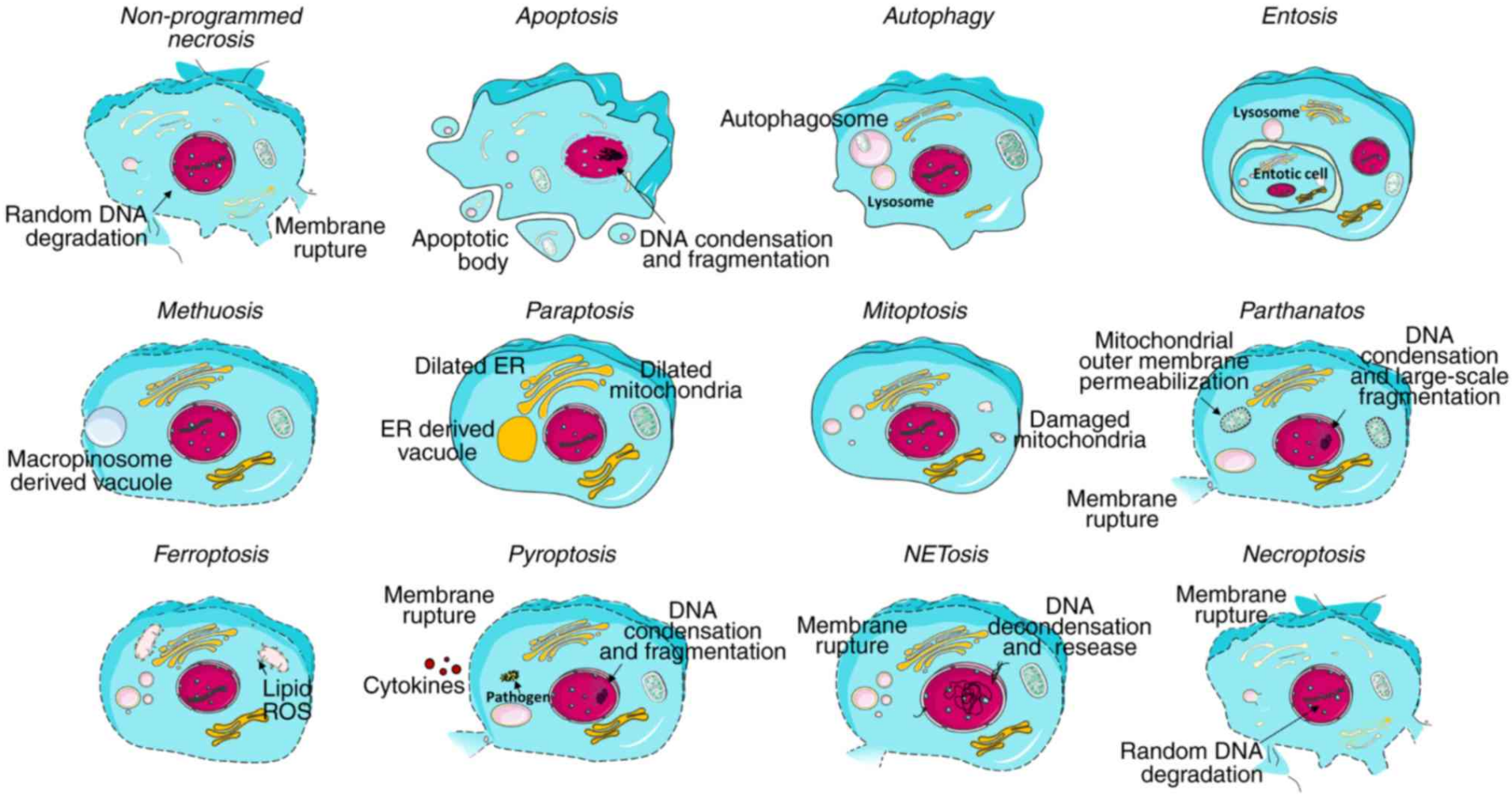

Figure 1.11: The various cell death modalities and their characteristic morphology with respect to their membrane, chromatin, and organelle integrity (Image adapted from Yan *et al*., 2020).

1.3 Metals in cancer

1.3.1 Transition metal complexes transitioning into cancer treatments

The human body requires stringent regulation of metals to maintain cellular homeostasis. Several metallodrugs drugs have been investigated to potentially restore metal imbalances in malignant cells (Jungwirth *et al*., 2011). Metal ions play significant roles in multiple biochemical reactions where they function as enzyme co-factors, bind receptors, and transcription factors, thus supporting many cellular structures and ensuring the stability of the genome (Serra *et al*., 2020). Metallodrugs, particularly transition metal complexes, display a wide array of therapeutic applications ranging from treating diabetes, inflammation, neurological illness, infections, and cancer. The incomplete d shell of transition metals facilitated the emergence of metal coordination complexes which consist of a central metal atom adjoined to a ligand or a wide variety of molecules (Rafique *et al*., 2010). Within the metal complex, the metal itself may act as the active component or a carrier of ligands that may hold biological activity (Trudu *et al*., 2015).

Although metallodrugs have been utilized for centuries for their therapeutic properties, such as the 18^{tth} century Arsenic trioxide used against leukemia, it was the discovery of Cisplatin (CDDP) by Rosenberg in the 1960s that marked a significant insight into metal-based anti-cancer drugs (Franz and Metzler-Nolte, 2019; Jungwirth *et al*., 2011). The platinum CDDP cross-links to DNA, forming DNA adducts in malignant cells, triggering cells to undergo apoptosis. CDDP was the first anti-cancer drug to receive FDA approval and is often used in first-line chemotherapy to treat several malignancies such as breast cancer, non-Hodgkin's lymphoma, and cervical and prostate cancers (Dasari and Tchounwou, 2014).

CDDP accompanied adverse side effects and drug relapses were a possibility due to the development of drug resistance. Consequently, directing an influx of research investigating transition metal complexes that are highly effective in malignant cells and less toxic to non-malignant cells. Researchers focused on metals such as gold, ruthenium, copper, silver, and various platinum metals such as FDA-approved Carboplatin and Oxaliplatin to build a biologically and chemically effective metal coordination complex (Trudu *et al.,* 2015). During this current cancer metallotherapy era, the quest for highly effective metal coordination complexes with accompanying low toxicity is still ongoing (Gianferrara *et al*., 2009; Zeng *et al*., 2017).

1.3.2 Properties of transition metals that facilitate therapeutic potential

Transition metals carry redox potentials that allow metals to shift between many oxidation states and target abnormal redox levels in malignant cells (Jungwirth *et al*., 2011). Transition metals carry charges that facilitate binding to biological molecules based on the charge of their surroundings. Metal ions that possess high affinities for electrons can supply a hydrolysis reaction to their coordinated counterpart. Metal complexes aid in targeting specific molecules in a biological system due to their 3-D configuration, a property not possessed by carbon-constructed compounds. Furthermore, metal complexes offer advantageous varieties of geometries and kinetic traits (Frezza *et al*., 2010; Jungwirth *et al*., 2011). Lastly, metals can undergo ligand exchange reactions permitting interactions with various biological molecules (Sodhi and Paul, 2019).

1.3.3 Modes of cytotoxicity induced by metal coordination complexes

Metal complexes may elicit PCD through apoptosis, autophagy, or necroptosis. The mechanism of PCD is often cell-specific and is influenced by hormone-sensitive cancers. Many metallodrugs aim to trigger apoptosis, but a drug may initiate more than one type of cell death, such as autophagy, to provoke a cytoprotective effect (Tan *et al*., 2014).

Metal coordination complexes may induce PCD in malignant cells by targeting the nucleus, the mitochondria, tumor suppressor proteins, pro-apoptotic proteins, ROS, the cell cycle, or other biochemical enzymatic pathways (Figure 1.12). Several platinum complexes directly cross-link to DNA to form mono or bi-functional adducts that activate the intrinsic/mitochondrial pathway of apoptosis (Trudu *et al.,* 2015). Metals such as copper and zinc influence the production of ROS, thus affecting metabolic reactions, proliferation, and viability of cells through signal transduction. Metal coordination complexes may target the mitochondria or peroxisome, which harbors ROS. Since elevated ROS levels are expected in malignant cells, due to their high proliferative rate, metal coordination complexes may disrupt the redox balance and employ oxidative stress. Subsequently, promoting lipid peroxidation, MOMP, which indirectly alters cellular DNA and protein structure to activate cell death (Pedrosa *et al.,* 2018).

Metal complexes may activate checkpoints in the cell cycle involved in DNA synthesis, repair, and mitosis (S or G1, G2, and M phases) and induce cell cycle arrest in any phase to initiate PCD. DNA damage by metal complexes may elicit cell cycle arrest at the S or M phase (Figure 1.13) (Gałczyńska *et al*., 2020). Metal complexes may also strain the endoplasmic reticulum and initiate the intrinsic endoplasmic reticulum pathway to promote apoptosis (Winter *et al*., 2014; Wong, 2011).

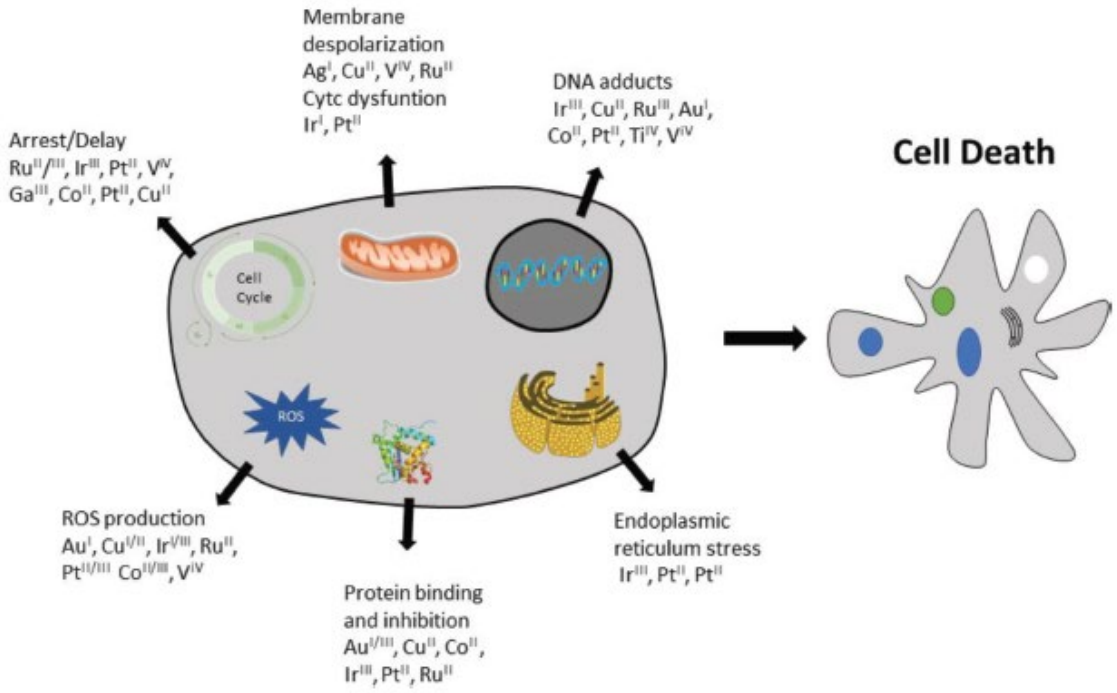

Figure 1.12: The various routes to cytotoxic activation in malignant cells by common metals used in metal coordination complexes. Complexes may act via either MOMP activation, DNA damage, ER strain, protein inhibition, increased ROS activity, or cell cycle arrest (Adapted from Pedrosa *et al.,* 2018).

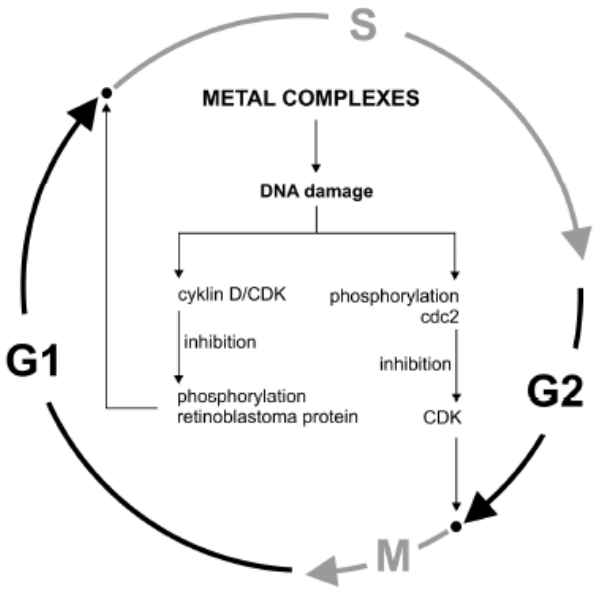

Figure 1.13: Metal complexes may activate cell cycle arrest. Metal complex-induced DNA impairment may prompt cell cycle arrest in the S phase (DNA synthesis) by inhibiting cyclin D/CDK from activating the retinoblastoma protein. DNA damage may also halt the M phase (Mitosis phase) by activating Cdc 2 tyrosine and avoiding CDK activity. Subsequently, promoting cell death or apoptosis due to cell cycle arrest (Adapted from Gałczyńska *et al*., 2020).

1.3.4 Spotlight on silver metal history

Silver is a transition metal with no known biological function in the human body, but its range of applications has been well established in the medical field. Since ancient civilization, silverware has been used to contain water, milk, and wine for preservation. Silver was recognized as a remedy for ulcers and wounds by the Greek physician Hippocrates. Silver has been used to prevent and manage infections since 4000 B.C.E. During the 1800s, silver wires were used to perform surgery on injured World War I soldiers (Medici *et al.,* 2019; Politano *et al*., 2013). Silver was used only traditionally until the Germ Theory of disease was established, which laid the scientific foundation of silver anti-microbial activity and prompted widespread research into the medicinal properties of silver (Melaiye and Youngs, 2005).

Silver salts were widely used to treat infections, namely gonorrhea, conjunctivitis, syphilis, mental diseases, and nicotine dependences. According to the Merck Index (1889), eighteen silver salts were employed in the pharmaceutical industry (Medici *et al.,* 2019). In the 1800s, Credé introduced silver nitrate to treat ophthalmia neonatorum. Silver nitrate decreased gonococcal ophthalmia incidents from 10% to 0.3%. However, the usage of silver nitrate for ophthalmia neonatorum was replaced by other antibiotics that demonstrated greater safety. Silver nitrate was still used in treating escharotics during the 20th century. Silver nitrate has been used as a wound treatment for over 150 years in the medical field. Von Naegeli (1895) observed and referred to the robust anti-bacterial activity of silver as 'oligodynamic' due to the low concentration of silver required to inhibit bacterial activity (Barillo and Marx, 2014).

Upon the introduction of antibiotics in the 20th century, there was a drop in the development of silver remedies. However, bacteria developed antibiotic resistance; researchers further explored the properties of silver. Silver sulphadiazine effectively impacted second and third-degree sepsis burn wounds and surgery, with applications extending to diagnostic pathology and medical devices. Combining silver nitrate with silver sulphadiazine to produce SSD cream was effective in burn treatments. Silver nitrate and silver sulphadiazine are considered necessary treatments for burn wounds today. Silver delivery technology successfully targeted certain antibiotic-resistant bacteria. Continuous release of silver ions from wound dressings enhanced healing (Lansdown *et al.,* 2006; Politano *et al*., 2013). Silver ion-coated catheters have decreased the risk of bloodstream infections, and silver-coated endotracheal tubes have reduced the number of patients with ventilator-associated pneumonia. Urinary catheters coated with silver have been commercially available for over 20 years (Barillo and Marx, 2014).

The extended repertoire of silver products is not limited to infectious diseases. Silver nanoparticles (size range 1 – 100 nm) vastly influenced many fields, including biomedical science, because of their typical physicochemical properties. Silver nanoparticles have been

effective in research areas, including anti-cancer treatments, anti-microbial drugs, wound, and bone healing, vaccine immunogenicity enrichment, and prevention of diabetes (Xu *et al*., 2020). Silver nanoparticles have shown *in vitro* antiviral activity in HIV-1 in early and late stages by preventing the association between gp120 and membrane receptor CD4, consequently preventing viral replication (Lara *et al*., 2010). Silver nanoparticles have been used *in vitro* and *in vivo* for their anti-cancer properties in breast, cervical, prostate, lung, colon, and nasopharyngeal cancer. The proposed mechanism of silver nanoparticle anti-cancer activity is attributed to apoptosis or necrosis induction and the inhibition of angiogenesis (Xu *et al*., 2020).

To the best of our knowledge, no evidence has been brought forward confirming that the accumulation of silver is toxic. However, lengthy exposure may bring about undesirable cosmetic effects such as argyria. Argyria is the accumulation of silver ions in the skin; silver can be reduced by sunlight or other reductants or precipitated as sulfides and selenides that could stain tissue. Silver can stimulate high production of melanin in the skin resulting in permanent discoloration of the skin due to silver accumulation in collagen bundles or the upper skin dermis. The blue-grey color may be localized upon external silver contact on the skin or generalized throughout the body when absorbed in the mucosa and could discolor organs when ingested at elevated concentrations over a lengthy period (Medici *et al*., 2019). Silver is ingested from food (10-100 µg /kg) and water (0.2 – 0.3 µg/l). Humans may ingest daily silver concentrations in a range of 20-80 µg which is dependent on the individual's diet (Kehoe *et al*., 1940). However, 90% of the silver is excreted by the intestine. Only 10% is absorbed based on a study administering radioactive silver to rats, mice, dogs, and monkeys via oral, intraperitoneal, and intravenous administration. The study found that the whole-body retention of silver in these animals was at a low level, less than 10% of the initial dose in dogs and less than 1% in rats, mice, and monkeys after a week (Furchner *et al*., 1971).

Today silver has been adopted in several personal hygiene products ranging from shavers to popular shower gels and dermatological products for their anti-microbial activity. Furthermore, silver has been included in a range of industrial, agricultural, and electrical items. Silver has gained interest in a variety of fields due to its properties. As such, the number of patent silver products is rising globally (Sim *et al*., 2018). The use of silver ions in medicine has been around for many millennia. It is regarded as one of a few metals in contemporary medicine with such an extensive medical history (Barillo and Marx, 2014). The birth of silver coordination complexes and their applications thereof continues to exhibit the medicinal properties of silver (Medici *et al*., 2016).

1.3.5 The Ag (I) coordination complexes

Ag (I) coordination complexes display a broad spectrum of therapeutic applications and contain several oligodynamic properties that have advanced the medical field. Ag (I) complexes have been documented to possess anti-cancer, anti-inflammatory, anti-bacterial, anti-fungal, anti-parasitic, anti-microbial, anti-malarial, and anti-septic properties (Medici *et al*., 2016; Medici *et al*., 2019). Silver ions have been exploited in coordination chemistry due to their acceptor characteristics and mainly their pliability of the coordination sphere. The pliability of the silver ion is a result of reduced stereochemical directionality induced by the d^{10} configuration. Thus, enabling the coordination of diverse ligands to the central silver ion, promoting a variety of geometries and topologies (Abul-Haj *et al*., 2013). The geometry of the Ag (I) complex is reliant on the stoichiometry of the ligand to silver ion. Possible geometries include the linear, trigonal planar or pyramidal, tetrahedral, and octahedral types (Meijboom *et al.*, 2009; Potgieter *et al*., 2017).

Ag (I) can be attached to ligands such as carboxylic acids, nitrogen, phosphorous or amino acids and some of these complexes display greater cytotoxicity *in vitro* than CDDP in cancer treatments (Banti and Hadjikakou, 2013; Biersack *et al*., 2012). The potency of silver anti-cancer complexes is dependent on characteristics such as redox reactivity, lipophilic activity, stabilization, the expulsion of silver ions, and water solubility. The ligand adjoined to the silver ion and its steric or electronic effects directly influence these characteristics. Ligands that commonly displayed therapeutic properties when coordinated to Ag (I) include phosphines, N-heterocycles, and N-heterocyclic carbenes (Medici *et al*., 2019). Ag (I) phosphine complexes have lipophilic characteristics, and the phosphine ligand cooperates with metal ions in various oxidation states (Medici *et al*., 2016). The assembled structure of Ag (I) complexes is influenced by the properties of the Ag and the ligand and its corresponding ratios, non-covalent associations between the solvent and counter anion, and the coordination geometry (Abul-Haj *et al*., 2013).

The synthesis of Ag (I) tertiary phosphine complexes was initially reported by Mann *et al*. (1937) according to the formula [AgXLn] (X = counter anion, L = ligand, and n = coordination number). Ag (I) can be adjoined to halides or pseudohalides such as CN- or SCN-. The resultant structure exhibits diversity induced by the geometry of the Ag (I), phosphine electronic characteristics, bite angle, and coordination number of the ligand in both aqueous and solid states. Anti-cancer activity of Ag (I) salts was limited to cationic lipophilic complexes that included a combination of silver, copper, and gold (‘’coinage’’) metals joined to bidentate phosphines in a tetrahedral shape. The association of Ag salts with bidentate phosphines or pyridylphosphines has sparked further studies due to their reported anti-tumor properties (Berners-Price and Sadler, 1996; Meijboom *et al.*, 2009). The conjugation of Ag (I) with

diphosphines without the cationic lipophilic ‘coinage’ metal combination has led to the foundation of a new class of selective anti-cancer agents (Meijboom *et al.*, 2009).

According to Ferreira *et al*. (2015), Ag (I) thiocyanate complexes conjugated to four different ligands with specific co-ordinations exhibited cytotoxicity to MCF-7 breast cancer *in vitro* via apoptosis induction. Moreover, the complexes displayed greater cytotoxicity to the malignant cell line than the non-malignant cell lines at the IC_{50} (50% cell inhibitory concentration). Moreover, the Ag (I) phosphine complexes exhibited greater cytotoxicity and selectivity than CDDP. Apoptotic cell death by these complexes was led via either cell cycle arrest or classical apoptosis pathway activation (Ferreira *et al*., 2015).

According to Engelbrecht *et al*. (2018), UJ3 elicited apoptosis in oesophageal cancer as UJ3 acted on the intrinsic pathway of apoptosis to promote MOMP, cytochrome *c* expulsion, aberrant ROS, ATP reduction, and caspase-9 activation. Moreover, UJ3 demonstrated high selective cytotoxicity for the malignant cell line than the non-malignant cell lines. Therefore, these *in vitro* studies re-enforce the efficacy so Ag (I) phosphine complexes as anti-cancer agents (Engelbrecht *et al*., 2018; Human-Engelbrecht *et al*., 2017).

1.4 Hypothesis

UJ3 exhibits cytotoxicity against the human MCF-7 and MDA-MB-231 malignant breast cell lines. The induced cytotoxicity is a result of apoptosis induction via mitochondrial targeting. In addition, UJ3 demonstrates significant pharmacological characteristics concerning inhibitory cell death concentrations, selectivity/toxicity and cell recovery.

1.5 Main Aim

To evaluate the apoptosis-inducing potential and the mechanism of action of silver (I) thiocyanate 4-methoxyphenyl phosphine (UJ3) on *in vitro* MCF-7 and MDA-MB-231 cell lines.

1.6 Aims and objectives

Aim 1

Assess the cytotoxicity of UJ3 on MCF-7 and MDA-MB-231 breast cancer cell lines.

Objectives

- Utilize alamar blue® proliferation assay to test the cytotoxicity of UJ3 on the malignant MCF-7 and MDA-MB-231 cell lines post-24 hr and 48 hr studies.
- Compare UJ3 cytotoxicity to the current chemotherapeutic drug CDDP.
- Determine the IC_{50} of UJ3 on both malignant cell lines.
- Determine the cytotoxicity of UJ3 on the HEK-293 and MRHF-1 non-malignant cell lines.
- Compare the IC_{50} of UJ3 on malignant and non-malignant cells to evaluate drug selectivity.
- Utilize CellTiter-Glo® Luminescent assay to investigate the impact of UJ3 on cellular respiration.
- Compare ATP cell viability to the mitochondrial activity levels obtained from alamar blue® proliferation assay.
- Visualize cellular morphology via light microscopy post-UJ3 treatment in all cell lines to determine whether it coincides with the biochemical assay viabilities.

Aim 2

Explore the preferred mode of cell death triggered in malignant cell lines post-UJ3 treatment.

Objectives

- Utilize the Muse cell analyzer with Annexin V and 7-AAD to differentiate cell death populations.
- Utilize the Muse MitoPotential kit to investigate cellular health and stress by studying alterations in the mitochondrial membrane potential.
- Utilize the Muse oxidative stress kit to measure intracellular superoxide radicles.

Aim 3

Fluorescently label intracellular organelles and pro-apoptotic proteins to detect apoptotic morphological features induced by UJ3.

Objectives

- Detect the presence of apoptotic nuclear morphology using Hoechst 33258 dye.
- Morphologically assess mitochondrial health status and membrane potential using MitoTracker orange dye.
- Detect the expulsion of cytochrome *c* using Alexa 488 dye.

Aim 4

Detect and analyze the activity of crucial pro-apoptotic proteins such as caspases and PARP associated with the classical apoptotic pathways.

Objectives

- Determine the activity of caspase-8, caspase-3 and caspase-7 essential to classical apoptosis. Thereafter, determine whether PARP, the effector caspase substrate, had undergone cleavage.

Aim 5

Investigate caspase-independent pathways induced by UJ3 via fluorescent detection of the AIF pro-apoptotic protein.

Objective

- Detect the presence and translocation of AIF to the nucleus via Alexa-488 tagged anti-AIF antibody.

Chapter 2: Methodology

Stringent cell culture aseptic techniques and conditions were followed throughout the experimental investigation. The malignant MCF-7 (Cellonex, SA) breast cell line is of the luminal A type, sensitive to CDDP and absent of caspase-3. The MDA-MB-231 breast cancer cell line was kindly gifted by Dr. Eloise van der Merwe at the University of the Witwatersrand. The MDA-MB-231 is of the TNBC type that demonstrates CDDP resistance and expresses caspase-3. The non-malignant human embryonic kidney cell line, HEK-293 was kindly gifted by Prof. Raymond Hewer from the University of Kwa-Zulu Natal. The non-malignant primary fibroblast cell line, MRHF-1 (Cellonex, SA) was also studied. All cell lines in this investigation were adherent. All reagents used to culture cells were warmed to 37°C in a water bath. All cell culture materials were wiped with 70% ethanol (Sigma-Aldrich, USA), glass apparatus was autoclaved and sterilized in the UV laminar flow hood (Nuve, Turkey).

2.1 Cell culture and sub-culturing

The respective cell lines were transferred from a stock solution to a T25 flask (Nest Biotechnology, China) containing cell culture growth media. The media consisted of 13.53 g/L of Dulbecco's Modified Eagle's medium (DMEM) (Sigma-Aldrich, USA), 3.7 g/L $NaHCO_3$ (Melford Biolaboratories, UK), 1% Penicillin / Fungizone / Streptomycin and 0.1% Gentamycin (Lonza, USA) and 10% heat deactivated Fetal Bovine Serum (FBS) (Capricorn Scientific, Germany) supplementation at pH 7.45. The conditions of the humidified NuveEC160™ incubator (Nuve, Turkey) were set at 37°C and 5% CO_2 to facilitate optimum growth. Sub-culturing of cells was dependent on confluency or growth rate. For sub-culturing purposes, the cells were rinsed in 10 ml Hanks balanced salt solution (HBSS) (Life Technologies, UK) consisting of 0.35 g/L $NaHCO_3$ (Melford Biolaboratories, UK). To detach adherent cells, 4 ml of 1% trypsin (Lonza, Belgium) was exposed to cells for 4 mins; the detached cells were transferred to 6 ml of supplemented media which prevented further trypsin activity (Lonza, Belgium). The cell suspension was centrifuged in the Nuve™ benchtop centrifuge (Nuve, Turkey) at 400 x*g* for 4 mins. Pelleted cells were resuspended in media and transferred appropriately to culture flasks with fresh media. Experiments were conducted once the cells had reached a passage number between P2 – P6 and the viability was greater than 90%.

2.2 Cell viability using Trypan Blue

To count the viability percentage of cells for experimentation, the pelleted cells (as mentioned in section 2.1) were resuspended in 5 ml media. Equal volumes (10 µl) of cell solution and Trypan blue (Sigma-Aldrich, USA) were added to an Eppendorf tube (Quality Scientific plastics, USA), from which 10 µl of the solution was placed in a counting slide. An automated

cell counter Countess™ Invitrogen™ (ThermoFisher Scientific, UK), was used to determine the viability, desired concentration and dilution volumes for cell seeding.

All assays involved a minimum of 3 biological repeats and were carried out for both the MCF-7 and MDA-MB-231 in triplicate. The non-malignant HEK-293 and MRHF-1 cell lines were included in the screening viability assay and light microscopy morphology studies.

2.3 Preparation of compounds and characterization of UJ3

UJ3 was characterized via many analytical methods. The Bruker Tensor 27 FTIR spectrophotometer (Bremen, Germany) and a PIKE miracle gate ATR accessory were used to record infrared spectra. 1 H NMR (400 MHz), 13C{H} NMR (101 MHz) and 31P{H} NMR (162 MHz) spectra were recorded by the Bruker Ultrashield Avance III 400 MHz spectrometer. TMS referenced peaks were possible via residual protio impurities in $CDCl_3$ / solvent signal. Melting points were recorded and microanalysis was completed using the Thermo Flash 2000 series CHNS/O (Waltham, MA, USA). AgCN salt (0.15 g, 1.12 mmol) was added to triphenylphosphine (0.6 g, 2.24 mmol) in acetonitrile (50 cm^3) followed by overnight heating under reflux. After solution filtration and evaporation (to ±10 cm^3), the solution was cooled at room temperature (RT) over 24 hrs. The cooling period facilitated UJ3 crystal formation (Engelbrecht *et al*., 2018; Human-Engelbrecht *et al*., 2017; Ferreira *et al*., 2015).

A UJ3 stock solution (2 mM) was made by dissolving 0.0034 g of UJ3 in 976 µl dimethyl sulfoxide (DMSO) (PanReac Applichem, Germany). Dissolution was facilitated at 70°C on an Accublock™ digital dry bath (Labnet Int., Taiwan). The stock solution was then kept in the dark at 4°C. The UJ3 stock solution was warmed to 70°C for 30 mins prior to use for cell treatment. CDDP was used as an apoptotic reference drug since it is the most prominent metal demonstrating high efficacy as a current metallodrug in anti-cancer treatment (Ghosh, 2019). The CDDP (Molekula, UK) stock solution (3.33 mM) was made by dissolution of 0.001 g of CDDP in a ml of filtered 0.9% saline solution (Sigma-Aldrich, USA). The solution was heated at 70°C for 15 mins prior to use for cell culture.

2.4 Cytotoxicity assessment of UJ3

2.4.1 Alamar blue® proliferation viability assay

A 96-well plate (Nest Biotechnology, China) was used to contain seeded cells, 100 µl of cell solution (2 x 10^5 cells/ml) was transferred to each well. After cell seeding, the plate was left in the incubator for 24 hrs. Cells were either left untreated (untreated control) or treated with 1% dimethyl sulfoxide (DMSO) (vehicle control) and a serial dilution of UJ3 or CDDP positive apoptosis control. A negative blank control (media only) was also included. For drug screening, a serial dilution of UJ3 (1.25 µM, 2.5 µM, 5 µM, 10 µM and 20 µM) and CDDP (12.5 µM, 25 µM, 50 µM, 100 µM and 200 µM) was made. Post-treatment, the cells were left in the

incubator for either a 24 hr or 48 hr study. The alamar blue® assay (BIO-RAD, USA) was conducted for all cell lines. Light micrographs of all controls and treatments were taken with the Invitrogen™ FLoid™ Cell Imaging Station (Thermo Fisher Scientific, UK) at 460x magnification, white light. Thereafter, 10 µl of alamar blue® reagent was pipetted per well and the plates were covered with foil (to prevent light sensitivity) and left in the incubator for 2 hrs. The fluorescence was recorded on the VICTOR® Nivo™ (PerkinElmer, USA) microplate reader with an excitation filter set at 530/30 nm and an emission filter at 580/20 nm. Fluorescent readings were input into Microsoft Excel™ to generate the respective IC_{50} of UJ3 or CDDP for all cell lines under 24 hr and 48 hr studies.

2.4.2 CellTiter-Glo® Luminescent ATP assay

After cell collection and counting (as in sections 2.1 and 2.2). Petri dishes (Nest Biotechnology, China) were used to contain seeded cells at 2 x 10^5 cells/ml and 3 ml of cell suspension was pipetted per dish [6 x 10^5 cells]. After a 24 hr incubation, cells were either left untreated or treated with either 1% DMSO, UJ3 (20 µM) and CDDP (200 µM). After 24 hrs, the media was collected and transferred to Eppendorf tubes; and 1 ml HBSS (Life Technologies, UK) was used to rinse cells. Thereafter, 600 µl of Trypsin was added, followed by a 2 min incubation. Detached cells were collected and pelleted by the Eppendorf® 5415R benchtop centrifuge (Merck, SA) at 400 x*g* for 4 mins and resuspended in a ml of fresh media.

Cellular respiration activity in MCF-7 and MDA-MB-231 cell lines were assessed by the CellTiter-Glo® Luminescent ATP assay (Promega, USA). Equal volumes (25 µl) of cell suspension and CellTiter-Glo® reagent (Promega, USA) (1:1) were added to a 96-well plate and covered with foil and left on an orbital shaker (Gemmy industrial corp, Taiwan) for 30 mins. The luminescence proportional to ATP production was measured by the VICTOR® Nivo™ (PerkinElmer, USA) microplate reader.

2.5 Exploring the preferred mode of cell death induced by UJ3

2.5.1 Annexin V and 7-AAD to differentiate cell death populations in malignant cell lines

Cells were seeded (as in section 2.4.2) and left either untreated or treated with 1% DMSO, UJ3 (20 µM), CDDP (200 µM) and hydrogen peroxide (Associated chemical enterprise, SA) (positive necrosis control). After cell collection (as in section 2.4.2), the Muse® Annexin V & Dead Cell Assay Kit (Luminex, USA) was utilized as per the manufacturer's procedure. From the collected cell suspension, 300 µl were rinsed in 100 µl of PBS (heated to 37°C) (Sigma-Aldrich, USA). The cell pellet was exposed to 25 µl of a 1X assay buffer (provided in the kit) and 25 µl of Annexin V reagent and then vortexed. An incubation period was then followed at RT for 20 mins in the dark. Thereafter, 50 µl of 1X assay buffer was pipetted into each sample

and vortexed. Samples were recorded at 5000 events and analyzed on the Muse® Cell Analyzer (Merck Millipore, USA) with Muse 1.5 analysis software (Merck Millipore, USA).

2.5.2 The Muse® Mitopotential assay

Cells were seeded (as in section 2.5.1) and left either untreated or treated with 1% DMSO, UJ3 (20 µM) and CDDP (200 µM). After cell collection (as in section 2.4.2), the Muse® Mitopotential Assay Kit (Luminex, USA) was utilized as per the manufacturer's procedure. From the collected cell suspension, 300 µl of cells were rinsed in 100 µl of PBS (heated to 37°C). The cell pellet was then exposed to 50 µl of a 1X assay buffer (provided in the kit). A working solution consisting of MitoPotential dye and 1X assay buffer was made and 47.5 µl was pipetted per tube and vortexed. An incubation period was the followed for 20 mins at 37°C. Thereafter, 2.5 µl of 7-AAD reagent was pipetted, vortexed and incubated at RT for 5 mins in the dark. Samples were recorded at 5000 events and studied on the Muse® Cell Analyzer and its corresponding software.

2.5.3 The Muse® Oxidative Stress assay

Seeded cells (as in section 2.5.1) were left either untreated or treated with 1% DMSO, UJ3 (20 µM) and CDDP (200 µM). After cell collection (as in section 2.4.2), the Muse® Oxidative Stress assay kit (Luminex, USA) was utilized as per the manufacturer's procedure. From the collected cell suspension, 300 µl were rinsed in 100 µl of PBS (heated to 37°C). The pellet was then exposed to 100 µl of 1X assay buffer (provided in the kit). A working solution consisting of Muse® Oxidative Stress Reagent intermediate solution and 1X assay buffer was made and 190 µl were pipetted and vortexed. An incubation period was then followed for 30 mins at 37°C. Samples were recorded at 5000 events and studied by the Muse® Cell Analyzer and it corresponding software.

2.6 Intracellular labeling of organelles to observe UJ3-induced morphological changes

Cells were seeded (as in section 2.4.2) directly onto coverslips and left untreated or treated with 1% DMSO, UJ3 (10 µM), UJ3 IC_{50}, UJ3 (20 µM), CDDP IC_{50} and CDDP (200 µM). A 100 nM MitoTracker Orange probe (Life Technologies, USA) made up in DMEM media was heated and 2 ml were pipetted per dish followed by incubation for 30 mins at 37°C. After media removal, cells were rinsed twice in 2 ml pre-heated PBS. Cells underwent fixation by the addition of 2 ml of 4% formaldehyde (Sigma-Aldrich, Netherlands) (made up in pre-heated PBS) followed by an incubation of 20 mins at 37°C. Cells were then rinsed in 1 ml PBS. Cells were permeabilized in 2 ml of 0.1% Triton X-100 (Merck, England) at 4°C for 25 mins. Removal of Triton X-100 (Merck, England) was followed by incubation in 1 ml blocking buffer comprising of 1% bovine serum albumin (BSA) (ChemCruz, Dallas, Texas) and 0.05% Tween-20 (Sigma-

Aldrich, USA) in PBS at a pH of 7.4 for 30 mins at RT. After removing the blocking buffer, 600 µl of 0.5 µg/ml Alexa Fluor® 488 anti-cytochrome *c* antibody (ab154476) (Abcam, UK) in PBS was pipetted followed by an hr incubation at RT. The cells were rinsed in 1 ml of PBS. Thereafter, 1 ml of 1 µg/ml Hoechst 33258 dye (Invitrogen, USA) in PBS was pipetted per dish followed by a 20 min incubation at RT. Cells were rinsed three times in 2 ml of pre-heated PBS. The coverslip was removed and mounted to a slide by adding a drop of 9% glycerol (Rochelle chemicals, SA). The sides of the coverslip were closed with nail polish and kept in the dark at 4°C. The Axioplan 2 fluorescent microscope (Carl Zeiss, Germany) was used to visualize the changes in nuclear (excitation: 343; emission: 483), mitochondrial (excitation; 554; emission: 576) or cytochrome *c* (excitation: 499; emission: 519) morphology at 630X magnification and with the aid of Axiovision 4.7 software.

2.7 Western Blots and apoptotic protein detection

2.7.1 Extraction of proteins

Seeded malignant cells (as in section 2.4.2) were either left untreated or treated with 1% DMSO, UJ3 (20 µM), UJ3 (IC_{50}) or CDDP (200 µM). After the cell collection (as in section 2.4.2), the pelleted cells were exposed to 100 µl of RIPA buffer (ThermoScientific, USA) while kept on ice. The samples were vortexed and had undergone an incubation at 4 °C for 15 mins. Samples were left at -20 °C until further usage.

2.7.2 Amido black protein quantification

A standard stock of 10 mg/ml of BSA (ChemCruz, Dallas Texas) was serially diluted in a concentration range (5 mg/ml, 2.5 mg/ml, 1.25 mg/ml and 0.625 mg/ml). The stock and extracted protein samples were loaded on a 0.45 µm nitrocellulose membrane (Osmonics, UK) in triplicate at a volume of 1.5 µl. The membrane was then covered in 50% methanol (Merck, SA) for 5 mins. The membrane was immersed for 5 mins in an Amido black solution consisting of 30% methanol, 10% acetic acid (Sigma-Aldrich, USA) and 0.1% Amido black (Sigma-Aldrich, USA). The membrane was then destained thrice with 50% methanol. After the membrane was dried, the loaded samples were cut out and placed in a 24-well plate (Nest Biotechnology, China). Thereafter, 800 µl of 0.1 M NaOH (Saarchem, SA) was pipetted per well and left for 24 hrs on a shaker. Nitrocellulose membrane was then removed from the solution and the plate was read at 600 nm on the VICTOR® Nivo™ microplate reader. The BSA concentrations and absorbance were used to construct the standard curve to evaluate protein concentration and quantification.

2.7.3 Protein preparation and resolution on SDS-PAGE

The BIO-RAD mini electrophoresis casting cassette and apparatus were set up. The 12% separating gel was made up of 30% Acrylamide/ 0.8% bisacrylamide (Sigma-Aldrich, USA), 4 x Tris-Cl (Melford bio laboratories, UK) / Sodium dodecyl sulfate (SDS) (Merck, Germany) at pH 8.8, 10% Ammonium persulfate (APS) (Sigma-Aldrich, USA) and N,N,N′,N′-Tetramethylethylenediamine (TEMED) (MP biomedicals, France). The separating gel was allowed to set for 50 mins, followed by the casting of the stacking gel. The stacking gel comprised of 30% Acrylamide/ 0.8% bisacrylamide, 4 x Tris-Cl / SDS at pH 6.8, 10% APS and TEMED. Thereafter, 100 µl of extraction buffer consisting of 1X Laemmli buffer, including protease inhibitors (BIO-RAD, USA) and β-Mercaptoethanol (Sigma-Aldrich, USA) was added to all samples. Samples were left on a heating block for 5 mins at 95°C. The samples were then allowed to cool on ice, vortexed, and loaded onto the gel. A concentration of 15 µg/µl was used to load proteins and the Precision Plus Protein™ Standards dual color marker (BIO-RAD, USA) was added (250-10 kDa). The gel was assembled in an electrophoresis chamber with 1X electrophoresis buffer containing TRIS, glycine (Saarchem, RSA) and SDS. After the power pack was connected, 15 mA per gel was required to resolve the protein solution.

2.7.4 Western Blot: protein transfer

A 0.45 µm polyvinylidene difluoride (PVDF) membrane (Pall Corporation, Mexico) was exposed to 100% methanol for 5 mins and left on an orbital shaker to facilitate membrane activation. The membrane was rinsed thrice with dH_2O for 5 mins. The separating gel was immersed in 1X Towbin buffer for 15 mins. The Towbin buffer comprised of 25 mM Tris, 192 mM glycine, and 20% methanol. The grid consisting of sponges, filter paper, PVDF and gel was packed appropriately to favour protein transfer. The transfer tank was occupied with 1X Towbin buffer and conditions to promote transfer occurred at 4°C, 70 V for 1 hr 20 mins.

2.7.5 Western Blot: Antibody treatment and detection

The PVDF membrane containing the transferred proteins and marker was washed twice with 1X TBS for 10 mins. The 1X TBS consisted of 5 mM Tris and 15 mM NaCl (Promark chemicals, RSA) at pH 7.5. Refer to Table 2.1 for the primary (1° Ab) and secondary antibody (2° Ab) conditions. The membrane was blocked by immersion in 5% non-fat powdered milk (Spar, SA) consisting of 1X TBS. After removal of milk solution, 1° Ab was added followed by an overnight incubation on an orbital shaker at 4°C. TBST solution was used to rinse the membrane thrice for 10 mins. TBST comprised of 0.1% Tween-20 (Sigma-Aldrich, USA) in 1X TBS. After removal of the TBST solution, the membrane was immersed in the 2° for an hr. TBST was then used to rinse the membrane thrice for 15 mins each, which was repeated four times. The protein bands were detected by means of a Clarity Western Enhancer Reagent (BIO-RAD, USA) as per the manufacturer's procedure with an equal volume of substrate and enzyme

(1:1). The membrane was placed on the orbital shaker for 5 mins while immersed in 5 ml of detection solution. Protein bands were detected on the ChemiDoc ™ with Image lab 6.1 software (BIO-RAD, USA).

Table 2.1: The primary and secondary antibodies, dilution factors and blocking milk solution (non-fat milk powder in 1X TBS) required for the optimized detection of β-actin, caspase-3, caspase-7, caspase-8 and PARP activity levels in the **MCF-7** and **MDA-MB-231** cell lines.

Protein Evaluated	MCF-7		MDA-MB-231	
	1° Ab, dilution factor and blocking solution	**2° Ab, dilution factor and blocking solution**	**1° Ab, dilution factor and blocking solution**	**2° Ab, dilution factor and blocking solution**
β-actin	• 1° Ab: mouse-anti monoclonal anti-β-actin (Sigma-Aldrich, USA) (A1978) • 1:1000 • 2.5% milk solution	• 2° Ab: goat-anti-mouse IgG – HRP (Sigma-Aldrich, USA) • 1:5000 • 2.5% milk solution	• 1° Ab: mouse-anti monoclonal anti-β-actin • 1:1000 • 2.5% milk solution	• 2° Ab: goat-anti-mouse IgG – HRP • 1:2500 • 2.5% milk solution
Caspase-3	• Not applicable	• Not applicable	• 1° Ab: rabbit anti-human caspase-3 (Cell-signalling, USA) (#9762) • 1:5000 • 2.5% milk solution	• 2° Ab: anti-rabbit IgG – HRP (Sigma-Aldrich, USA) • 1:2000 • 4% milk solution
Caspase-7	• 1° Ab: rabbit anti-human caspase-7 (Cell-signalling, USA) (#9492) • 1:1000 • 2.5% milk solution	• 2° Ab: anti-rabbit IgG – HRP • 1:2000 • 4% milk solution	• 1° Ab: rabbit anti-human caspase-7 (Cell-signalling, USA) (#9492) • 1:5000 • 2.5% milk solution	• 2° Ab: anti-rabbit IgG – HRP • 1:5000 • 5% milk solution
Caspase-8	• 1° Ab: rabbit anti-human caspase-8 (Immunotech, France) (FLICE) • 1:2000 • 2.5% milk solution	• 2° Ab: anti-rabbit IgG – HRP • 1:2000 • 4% milk solution	• 1° Ab: rabbit anti-human caspase-8 • 1:2000 • 2.5% milk solution	• 2° Ab: anti-rabbit IgG – HRP • 1:2000 • 4% milk solution
PARP	• 1° Ab: rabbit monoclonal anti-PARP (E102) (Abcam, USA) • 1:5000 • 2.5% milk solution	• 2° Ab: anti-rabbit IgG – HRP • 1:5000 • 4% milk solution	• 1° Ab: rabbit monoclonal anti-PARP • 1:2000 • 5% milk solution	• 2° Ab: anti-rabbit IgG – HRP • 1:2500 • 4% milk solution

2.8 Caspase-independent cell death via AIF translocation

Cells were seeded (as in section 2.4.2) directly onto coverslips and were either left untreated or treated with 1% DMSO, UJ3 (10 μM), UJ3 IC_{50}, UJ3 (20 μM) and CDDP (200 μM). A 100 nM MitoTracker Orange probe was made up in pre-heated DMEM and 2 ml were pipetted per dish and incubated for half an hr at 37°C. After media removal, cells were rinsed twice with 2 ml pre-heated PBS. Cell fixation occurred by the addition of 2 ml of 4% formaldehyde (made up in pre-heated PBS) followed by an incubation period of 15 mins at RT. The cells were then rinsed with a ml of PBS. Permeabilization of cells occurred by the addition of a ml of 2% Triton X-100 at RT for 15 mins. After removing the Triton X-100, cells were exposed to a ml of blocking buffer for an hr at RT. The blocking buffer consisted of 3% BSA and 1% Triton X-100 in PBS at a pH of 7.4. After removing the blocking buffer, 800 μl of 1 μg/ml Alexa Fluor® tagged anti-AIF antibody (ab1998) (Abcam, UK) in PBS was pipetted and left at 4°C overnight. Thereafter, PBS was used three times for 5 mins each to rinse cells. The secondary antibody (1:1000 in PBS), Alexa 488 donkey anti-rabbit IgG (ab150073) (Abcam, UK), was incubated with the cells for an hr at RT. Cells were rinsed twice in PBS, followed by a ml of 1 μg/ml Hoechst 33258 dye that was allowed to incubate with the cells for 20 mins at RT. Cells were rinsed thrice with PBS. The coverslip was then mounted to a slide with a drop of 9% glycerol. The sides of the coverslip were closed with nail polish and left in the dark at 4°C until imaging. The Axioplan 2 fluorescent microscope was used to visualize the changes in nuclear (excitation: 343; emission: 483), mitochondrial (excitation; 554; emission: 576) or AIF translocation (excitation: 499; emission: 519) morphology at 630X magnification with the aid of Axiovision 4.7 software.

2.9 Statistical interpretation

Microsoft™ Excel was used to determine the standard error (SEM) per biological repeat of every assay. Data was represented in the form of a bar graph, histogram, or quadrant chart. A student t-test was utilized for comparison of treated cell data to the 1% vehicle control (type 2 and two-tailed test). A *p*-value less than 0.05, 0.01 or 0.001 (*, ** or ***) signified a significant difference when compared against the vehicle control.

Chapter 3: Results

3.1 Cytotoxicity assessment of UJ3

3.1.1 Screening for UJ3 potency and half-maximal inhibitory concentration (IC_{50})

A drug's optimal dosage of cytotoxic activation and selective IC_{50} concentration is essential to understanding its potency profile. The efficacy and selectivity of UJ3 were evaluated against the malignant MCF-7 and MDA-MB-231 cell lines over 24 hrs and 48 hrs. To establish whether UJ3 exhibits enhanced selectivity for the malignant cell lines as opposed to the non-malignant, the HEK-293 and MRHF-1 cell lines were included. In contrast to the HEK-293, the MRHF-1 fibroblasts represent an improved model to assess the cytotoxicity of UJ3 on healthy human cells due to the lack of cell line transformation.

The fluorometric-based alamar blue® proliferation viability assay was chosen for this study based on its high sensitivity and non-toxic viability measurements for time-course experiments (Rampersad, 2012). The assay served as a cell health monitor as only metabolically viable cells could reduce the blue, non-fluorescent, resazurin dye to a fluorescent pink resorufin product via mitochondrial reductase or diaphorase activity. The measured fluorescence was proportional to the quantification of cellular viability (Kamiloglu *et al*., 2020). Therefore, cellular viability was expressed as a function of mitochondrial activity in cells (Figure 3.1, Figure 3.2, Figure 3.3 A and B).

In both the MCF-7 and MDA-MB-231 cell lines (inclusive of 24 hr and 48 hr studies), the high viability percentages represented by the untreated control (> 100%) and 1% DMSO vehicle control (100%) represent efficient mitochondrial activity for a controlled *in vitro* cell culture system model. Studies of the MCF-7 and MDA-MB-231 cell lines post-24 hr UJ3 treatment indicated that UJ3 significantly ($p < 0.001$) reduced mitochondrial activity in a dose-dependent manner with respect to the vehicle control (Figure 3.1). UJ3 displayed high cytotoxic selectivity for both malignant cell lines over the non-malignant HEK-293 across the entire concentration range. Furthermore, UJ3 was highly selective for both malignant cell lines when compared to the MRHF-1 fibroblasts except at the highest treatment concentration of 20 µM (Figure 3.1). UJ3 appears more cytotoxic to the MCF-7 cell line, with mitochondrial activity decreasing at 10 µM (66%) and 20 µM (27%) compared to the MDA-MB-231 cell line at 10 µM (74%) and 20 µM (33%) (Figure 3.1).

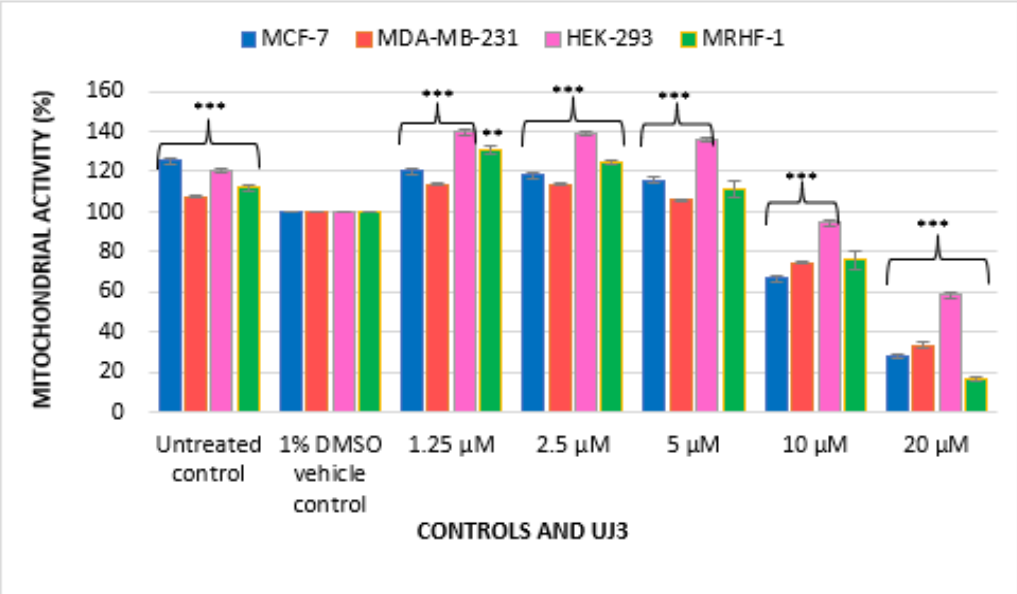

Figure 3.1: Mitochondrial activity as a function of cell viability (%) in **MCF-7**, **MDA-MB-231**, **HEK-293** and **MRHF-1** cell lines **post-24 hrs**. Cells were either left untreated or treated with 1% DMSO (vehicle control) or UJ3 (concentration range 1,25 µM – 20 µM) as determined by alamar blue® proliferation assay. The error bars are a representative of ± SEM (n = 9), the asterisks represent significant differences with respect to the vehicle control (100%) ($p < 0.001$ = ***; $p < 0,01$ = **).

Many malignant cell lines are notorious for cytotoxic recovery post-24 hr treatment (Patwardhan *et al*., 2021). As a result, the study included a 48 hr post-treatment with UJ3 to evaluate whether cytotoxicity was sustained. The 48 hr study highlighted that the MCF-7 cell line remained susceptible to UJ3 and the mitochondrial activity decreased even further across the entire concentration range with respect to the 24-hr study. However, the MDA-MB-231 cell line recovered and viability increased by 15% (10 µM) in the 48 hr study compared to the 24 hr study. Similar to the 24 hr study, UJ3 illustrated higher toxicity and selectivity to the MCF-7 than the non-malignant cell lines (Figure 3.2).

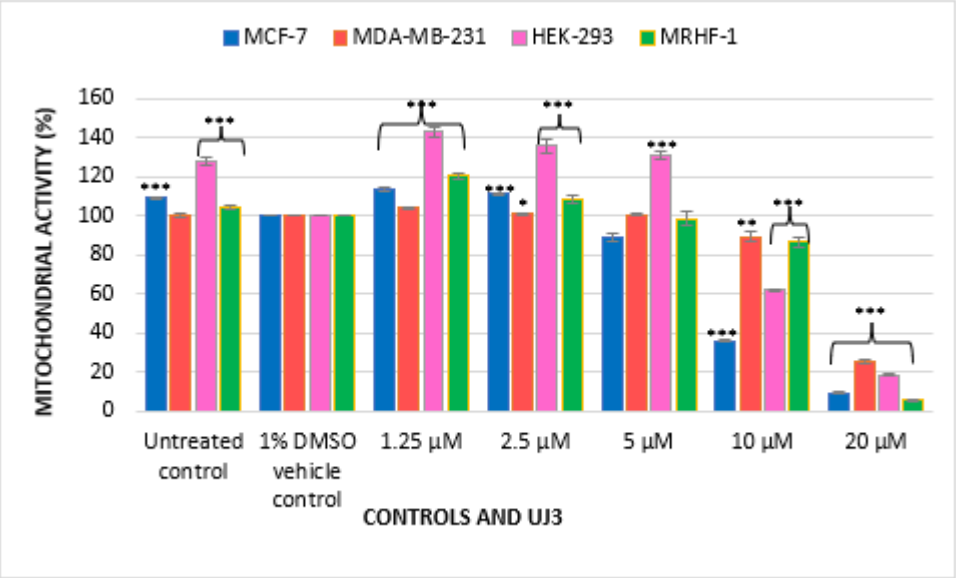

Figure 3.2: Mitochondrial activity as a function of cell viability (%) in **MCF-7**, **MDA-MB-231**, **HEK-293** and **MRHF-1** cell lines **post-48 hrs**. Cells were either left untreated or treated with 1% DMSO (vehicle control) or UJ3 (concentration range 1,25 µM – 20 µM) as determined by alamar blue® proliferation assay. The error bars are a representative of ± SEM (n = 9), the asterisks represent significant differences with respect to the vehicle control (100%) ($p < 0.001$ = ***; $p < 0,01$ = **).

The cytotoxicity of UJ3 was compared to a current chemotherapeutic drug used to treat various malignancies, CDDP (Sakagami *et al*., 2004). In our study, UJ3 activity will be compared to CDDP, which also serves as a positive apoptotic control discussed later. The cytotoxicity study of UJ3 and CDDP was undertaken over 24 hrs and 48 hrs. In the CDDP study, a dose-dependent decrease in mitochondrial activity was observed with respect to the vehicle control in all cell lines (Figure 3.3 A and B). During the 24 hr CDDP study (Figure 3.3 A), mitochondrial levels only decreased (< 50%) at a high CDDP concentration (200 µM) in the MCF-7 cell line. The MDA-MB-231 cell line illustrated CDDP resistance with mitochondrial activity levels (> 50%) at the same concentration. CDDP presented preferential toxicity to the malignant cell lines as opposed to the HEK-293. However, CDDP showed high toxicity to the MRHF-1 cell line, with mitochondrial activity levels reduced to 3,28% (200 µM). During the 48-hr CDDP study (Figure 3.3 B), mitochondrial activity levels declined even further in the MCF-7 cell line compared to that of the 24 hr study and the mitochondrial activity decreased (< 50%) at 50 µM treatment. In the 48 hr CDDP study, the MDA-MB-231 acquired greater resistance to CDDP and displayed weak selectivity for this cell line.

A

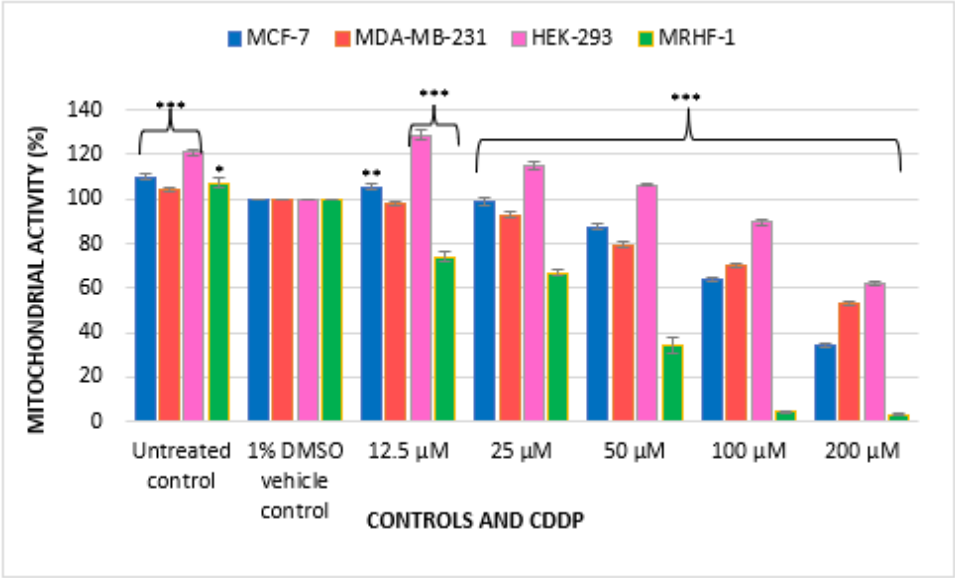

B

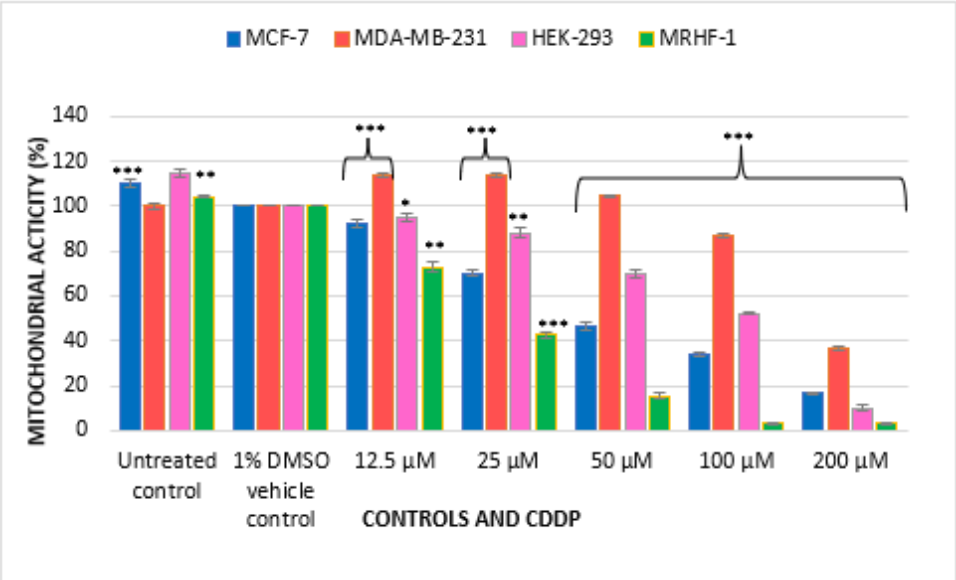

Figure 3.3: Mitochondrial activity as a function of cell viability in **MCF-7**, **MDA-MB-231**, **HEK-293** and **MRHF-1** cell lines **post-24 hrs** (A) **and 48 hrs** (B) with CDDP. Cells were either left untreated or treated with 1% DMSO or CDDP treatment (concentration range 12,5 µM – 200 µM) as determined by alamar blue® proliferation assay. The error bars are a representative of ± SEM (n = 9), the asterisks represent significant differences with respect to the vehicle control (100%) ($p < 0.001$ = ***; $p < 0,01$ = **; $p < 0,05$ = *)

The potency of UJ3 was established by determining the half-maximal inhibitory concentration required to inhibit cellular growth (IC_{50}). The MCF-7 cell line required an IC_{50} of 14.1 μM of UJ3 to inhibit 50% of cellular viability during the 24 hr study. The resultant MCF-7 IC_{50} (14.1 μM) was less than the IC_{50} of both non-malignant cell lines (HEK-293: 22.6 μM and MRHF-1: 15.6 μM), reinforcing the selective nature of UJ3 for the MCF-7 cell line. Furthermore, in the 48-hr study, this cell line failed to recover as the resultant IC_{50} was almost half that in the 24-hr study (7.6 μM) (Table 3.1).

A comparison of UJ3 to CDDP in both 24 hr and 48 hr studies revealed that UJ3 was more cytotoxic to the MCF-7 cell line as characterized by the low IC_{50} compared to CDDP. UJ3 appeared more selective to the MCF-7 cell line than CDDP when compared to the non-malignant cell lines. UJ3 was cytotoxic and selective to the MDA-MB-231 cell line in the 24 hr study with an IC_{50} of 13.6 μM. However, during the 48 hr study, this cell line recovered as the IC_{50} value increased (21.6 μM). As expected, the MDA-MB-231 cell line displayed resistance to CDDP during both 24 hr and 48 hr studies (Table 3.1).

Table 3.1: The half-maximal inhibitory concentration (IC_{50}) (μM) of UJ3 and CDDP required to inhibit 50% of cellular populations in the **MCF-7**, **MDA-MB-231**, **HEK-293** and **MRHF-1** cell lines **post-24 hr** and **48 hr** treatments.

Cell line	**IC_{50} concentration (μM) 24 hr**		**IC_{50} concentration (μM) 48 hr**	
	UJ3	CDDP	UJ3	CDDP
MCF-7	14,08	134,51	7,60	41,70
MDA-MB-231	13,59	219,15	21,61	178,50
HEK-293	22,59	234,06	11,29	108,83
MRHF-1	15,59	41,23	37,78	26,91

3.1.2 Impact of UJ3 on cellular respiration

The CellTiter-Glo® Luminescent viability assay evaluated the influence of UJ3 on cellular respiration and thus mitochondrial health status based on detecting ATP level changes upon treatment. This assay was employed for its high sensitivity, lengthy half-life (approximately 5 hrs) and protection from endogenous ATPases. The CellTiter-Glo reagent contains the luciferase enzyme, luciferin substrate, Mg^{2+}, buffer, ATPase inhibitors and a reagent for cellular lysis. Following cellular lysis with the reagent, ATP expulsion from the cell will serve as a co-factor for the luciferase enzyme. Luciferase will convert luciferin to oxy-luciferin and generate quantifiable luminescence directly proportional to intracellular ATP presence (Hannah *et al*., 2001).

In both MCF-7 and MDA-MB-231 cell lines, the untreated and vehicle controls represent elevated ATP levels indicative of a controlled *in vitro* cell culture system (Figure 3.4 and Figure 3.5). The ATP levels post-UJ3 or CDDP treatment were compared to the vehicle control reference. Previous cancer research with silver phosphine complexes indicated that 100 µM of CDDP produced a similar cytotoxicity profile to 10 µM of silver complexes (Engelbrecht *et al*., 2018). Therefore, this study used 200 µM of CDDP and 20 µM of the complex due to the resistant nature of the cell lines under investigation.

In the MCF-7 cellular respiration bar graph (Figure 3.4), UJ3 significantly ($p < 0.001$) reduced ATP levels (0.8%) compared to the vehicle control. Similarly, CDDP had significantly ($p < 0.001$) reduced ATP levels (7.7%) compared to the vehicle control. UJ3 influenced cellular respiration more drastically than CDDP, as UJ3 generated a 6.9% greater reduction of ATP at a concentration 10X lower than CDDP (Figure 3.4). This correlates with the mitochondrial activity measured by the alamar blue® proliferation assay. UJ3 (20 µM) resulted in a greater reduction of mitochondrial activity (27.95%) compared to CDDP (200 µM) treatment (34.62%) (Figure 3.1 and Figure 3.3 A)

Similarly, in the MDA-MB-231 bar graph (Figure 3.5), UJ3 and CDDP had significantly reduced ATP levels ($p < 0.001$) with respect to the vehicle control. ATP levels were reduced to (9.2%) post-UJ3 and (30.8%) post-CDDP. Therefore, UJ3 resulted in a 21.6% greater ATP reduction and impact on cellular respiration than CDDP (Figure 3.5). This correlates with the mitochondrial activity measured by the alamar blue® proliferation assay. UJ3 (20 µM) resulted in a greater reduction of mitochondrial activity (33.72%) compared to CDDP (200 µM) treatment (52.98%) in the MDA-MB-231 cells (Figure 3.1 and Figure 3.3 A). Overall, UJ3 influenced cellular respiration and mitochondrial activity more severely in the MCF-7 than in the MDA-MB-231 cell line.

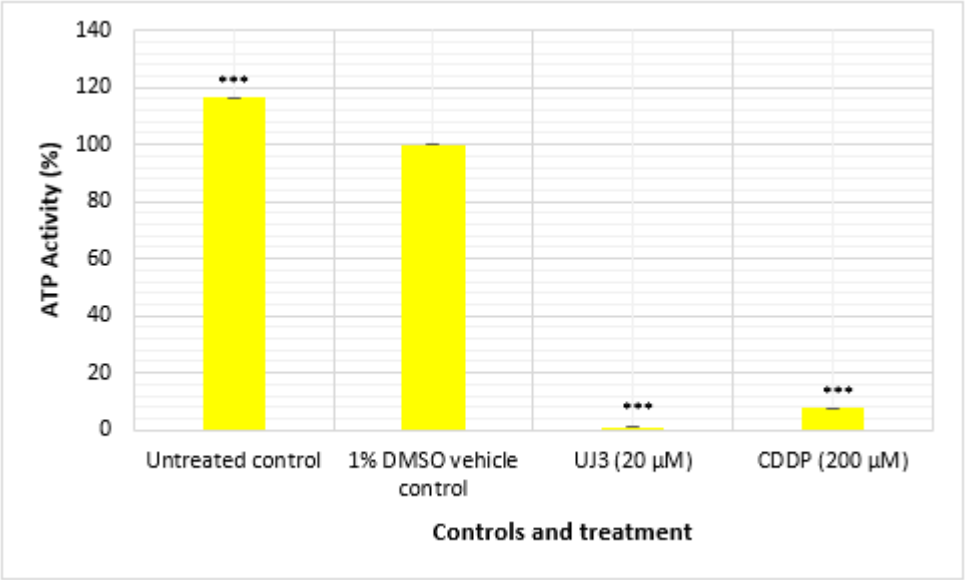

Figure 3.4: Cellular respiration is characterized as a percentage of ATP activity (%) in the **MCF-7** cell line. The cells were either untreated or treated with 1% DMSO vehicle control, UJ3 (20 µM) and CDDP (200 µM). Luminescence was detected **post-24 hrs** by the CellTiter-Glo® Luminescent assay. The error bars are a representative of ± SEM (*n* = 9), the asterisks represent significant differences with respect to the vehicle control (100 %) ($p < 0.001$ = ***).

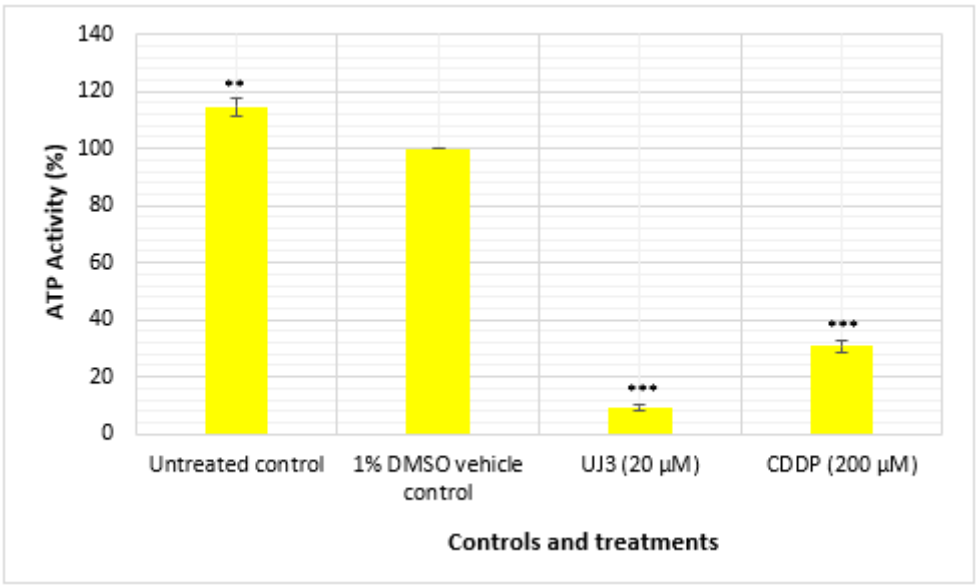

Figure 3.5: Cellular respiration is characterized as a percentage of ATP activity (%) in the **MDA-MB-231** cell line. The cells were either untreated or treated with either 1% DMSO vehicle control, UJ3 (20 µM) and CDDP (200 µM). Luminescence was detected **post-24 hrs** by the CellTiter-Glo® Luminescent assay. The error bars are a representative of ± SEM (*n* = 9), the asterisks represent significant differences with respect to the vehicle control (100 %) ($p < 0.001$ = ***).

3.1.3 Observing morphological changes induced by UJ3 made evident through light microscopy

Micrographs of the untreated and vehicle controls (Figure 3.6 (A - B)) of the MCF-7 and MDA-MB-231 cell lines depict thriving cells of epithelial morphology and high cellular confluency with no sign of cellular stress. MCF-7 cells appeared dome-shaped, whereas the MDA-MB-231 appeared spindle-like (Figure 3.6 (A - B)). Both cell lines treated with (1.25 – 5 μM) UJ3 (Figure 3.6 (C – E)) maintained high population numbers and resembled their respective controls (Figure 3.6 (A)). In the MCF-7, a notable reduction of cell populations and marked cytotoxicity were depicted at 10 μM (Figure 3.6 (F)) and 20 μM (Figure 3.6 (G)) UJ3 treatment. A reduction in cell populations post 200 μM CDDP treatment was also observed, highlighting MCF-7 susceptibility to CDDP (Figure 3.6 (H)). Cell population changes with respect to the controls post-UJ3 and CDDP treatment concurs with the alamar blue® proliferation assay (Figure 3.1). Moreover, apoptotic morphology such as cell shrinkage and membrane blebbing were visible at 10 μM UJ3 (Figure 3.6 (F)) and 200 μM CDDP (Figure 3.6 (H)) in the MCF-7 cell line. Apoptotic bodies and cellular detachment were visible at 20 μM UJ3 treatment (Figure 3.6 (G)). In the MDA-MB-231, a notable reduction of cell populations was only observed at 20 μM UJ3 (Figure 3.6 (G)) and apoptosis morphology such as cellular rounding and shrinkage became more apparent at this concentration. CDDP at 200 μM treatment (Figure 3.6 (H)) displayed granularity of cellular contents and cellular debris.

In the 48 hr study, both controls (Figure 3.7 (A - B)) of the MCF-7 and MDA-MB-231 appeared more confluent with respect to the 24 hr study. In the MCF-7, higher cell population reduction post-48 hr UJ3 (2.5 – 20 μM) treatment (Figure 3.7 (D – G)) was observed with respect to the 24 hr study. These findings support the sustained cytotoxicity of UJ3 over 48 hrs (Figure 3.2 and IC_{50} reduction post-48 hr treatment). Morphological changes induced by UJ3 in the MCF-7 included cellular rounding and shrinkage and a portion of cells with membrane impairment at 20 μM (Figure 3.7 (G)) concurring with the decreased viability determined by the alamar blue® proliferation assay (Figure 3.1). The MCF-7 remained susceptible to 200 μM CDDP over 48 hrs (Figure 3.7 (H)). In the MDA-MB-231, cell recovery was evident by the rise in cell population numbers despite UJ3 (1.25 – 10 μM) treatment (Figure 3.7 (C - F)) (Figure 3.2 and IC_{50} rise post-48 hr treatment). However, only at 20 μM UJ3 treatment (Figure 3.7 (G)) was a reduction of cell populations observed, coinciding with the alamar blue® proliferation assay (Figure 3.2).

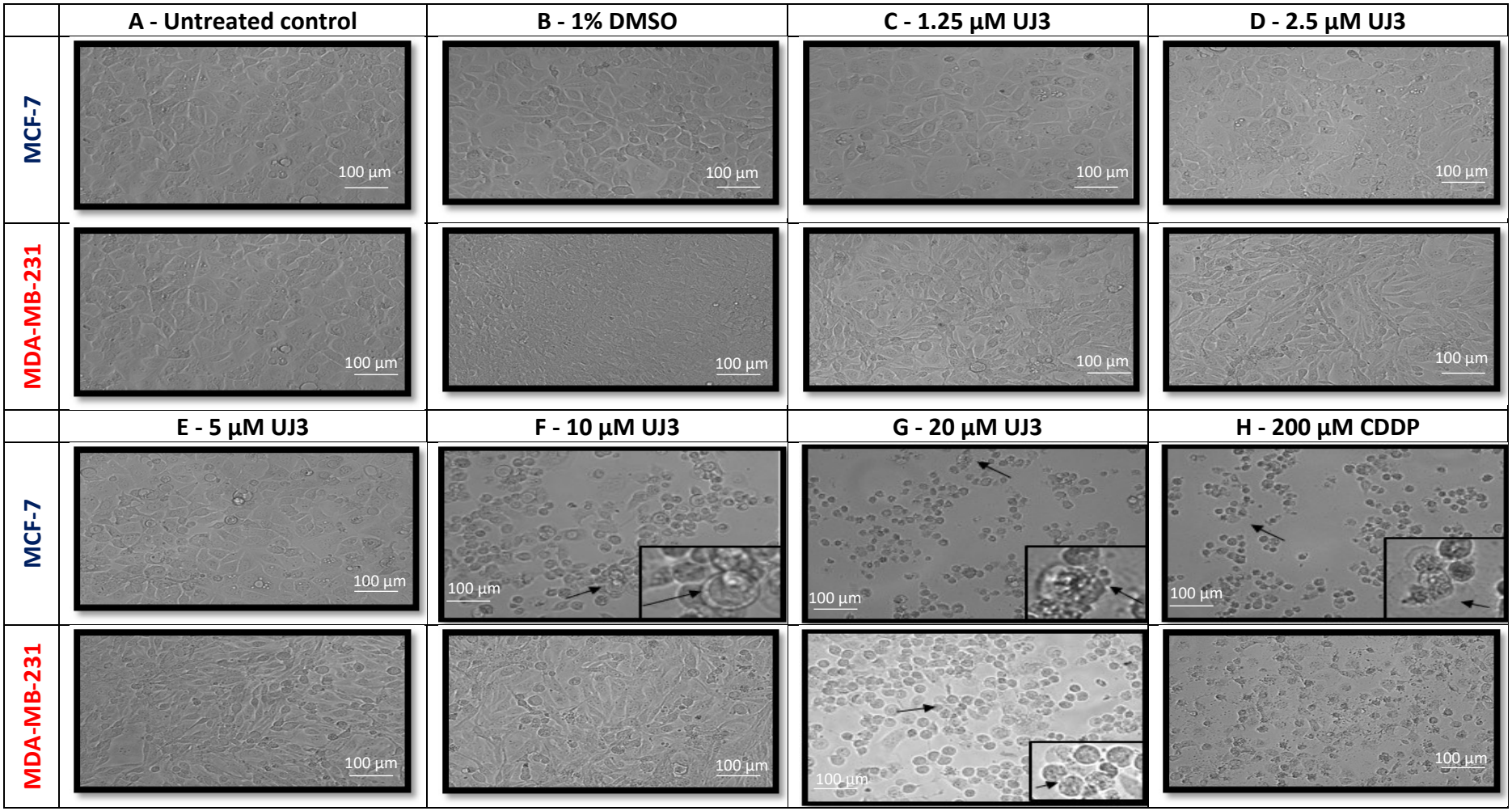

Figure 3.6: Cellular morphology light micrographs (200x magnification) of **MCF-7** and **MDA-MB-231** **post-24 hrs.** Cells were left untreated (A) or treated with either 1% DMSO (B), UJ3 (1,25 µM (C), 2.5 µM (D), 5 µM (E), 10 µM (F), 20 µM(G)) and CDDP 200 µM (H)). Black arrows are indicative of apoptotic morphology (**MCF-7**: (F) and (H) - apoptotic membrane blebbing; (G) - apoptotic bodies and **MDA-MB-231**: (G) - cell shrinkage) enlarged at the bottom right of the image. Both cell lines untreated and vehicle controls (A - B) represent thriving cell populations with epithelial morphology. UJ3 notably reduced the MCF-7 cell line population more severely than the MDA-MB-231 cell line (F - G). Similarly, CDDP (H) appears more cytotoxic to the MCF-7 cell line.

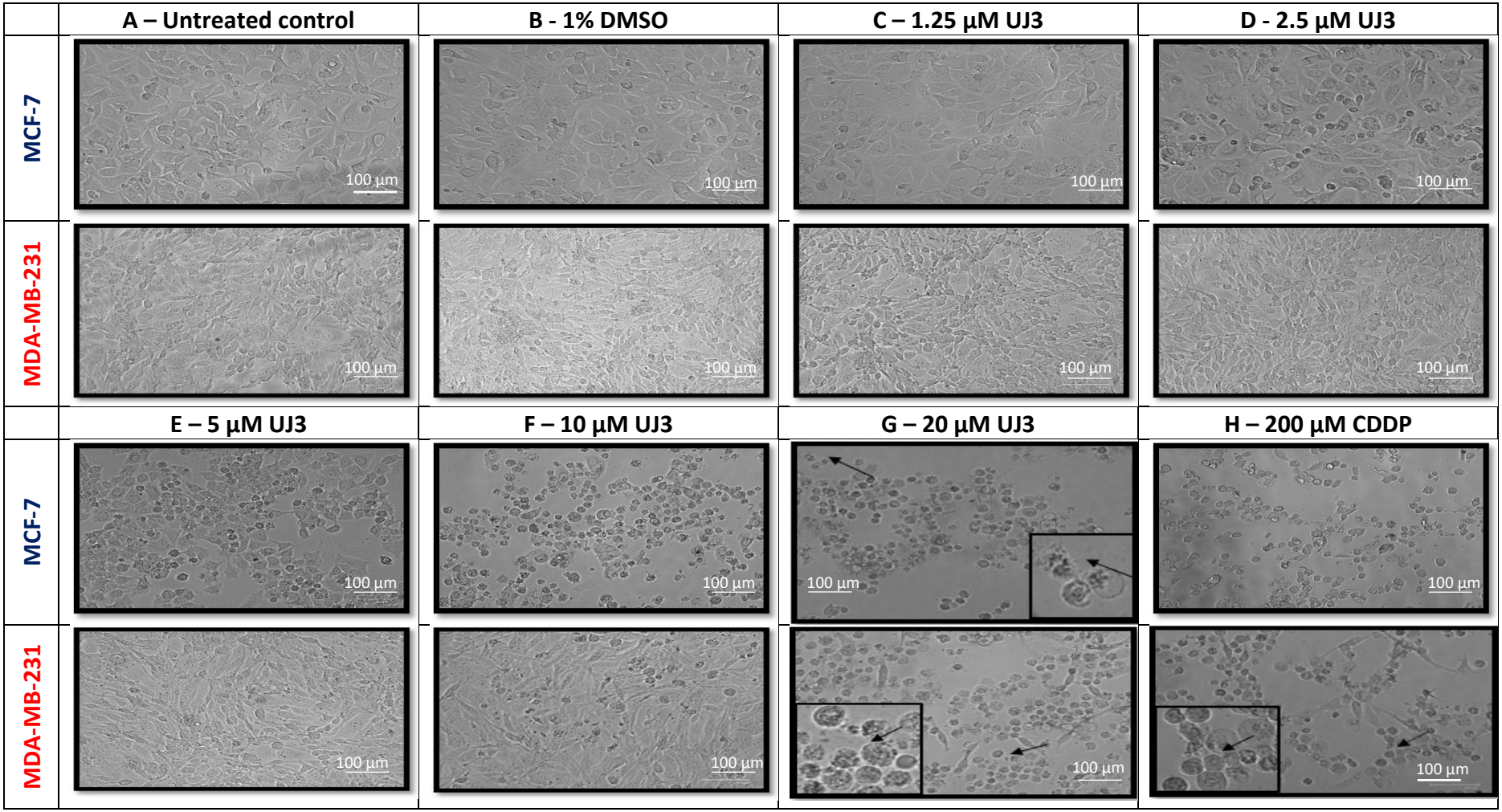

Figure 3.7: Cellular morphology light micrographs (200x magnification) of **MCF-7** and **MDA-MB-231** **post-48 hrs**. Cells were left untreated (A) or treated with either 1% DMSO (B), UJ3 (1,25 µM (C), 2.5 µM (D), 5 µM (E), 10 µM (F), 20 µM(G)) and CDDP 200 µM (H)). Black arrows are indicative of apoptotic morphology (**MCF-7**: (G) – membrane impairment and **MDA-MB-231**: (G) and (H) – cell shrinkage) enlarged at the bottom right or left of the image. The controls (A - B) of both cell lines maintained confluency, as observed in the 24 hr study. UJ3 sustained cytotoxicity in the MCF-7 cell line over 48 hrs (D – G) and MCF-7 cells remained sensitive to CDDP (H). The MDA-MB-231 cell line recovered (C – F) and was only susceptible at 20 µM UJ3 treatment (G).

Micrographs of the untreated and vehicle controls (Figure 3.8 (A - B)) of the HEK-293 and MRHF-1 non-malignant cell lines depicted healthy confluent cells. The HEK-293 controls appeared epithelial-like and the MRHF-1 with an oval, flat nucleus (Figure 3.8 (A – B)). In both cell lines, UJ3 (1.25 – 10 μM) (Figure 3.8 (C – F)) did not negatively influence cell growth or health status as the treated cells resembled the thriving controls. In both cell lines, major cell population reduction, cellular rounding and stress only occurred at 20 μM UJ3 (Figure 3.8 (G)) and CDDP 200 μM (Figure 3.8 (H)) during the 24 hr study.

In the 48 hr study, both controls (Figure 3.9 (A - B)) of the HEK-293 and MRHF-1 appeared more confluent with respect to the 24 hr study. In both cell lines, the viability increased further with no sign of cellular stress post-UJ3 (1.25 – 5 μM) treatment (Figure 3.9 (C – E)). In the HEK-293, reduced populations were observed at UJ3 (10 – 20 μM) (Figure 3.9 (F – G)) and CDDP 200 μM (Figure 3.9 (H)) (in accordance with Figure 3.2). In the MRHF-1, no cellular stress was depicted at UJ3 (1.25 – 10 μM) treatment (Figure 3.9 (C – F)). In contrast, to the HEK-293, the MRHF-1 did not depict any cellular stress at 10 μM UJ3 (Figure 3.9 (F)). However, cellular stress was depicted at 20 μM UJ3 (Figure 3.9 (G)) (Figure 3.2) and 200 μM CDDP treatment (Figure 3.9 (H)).

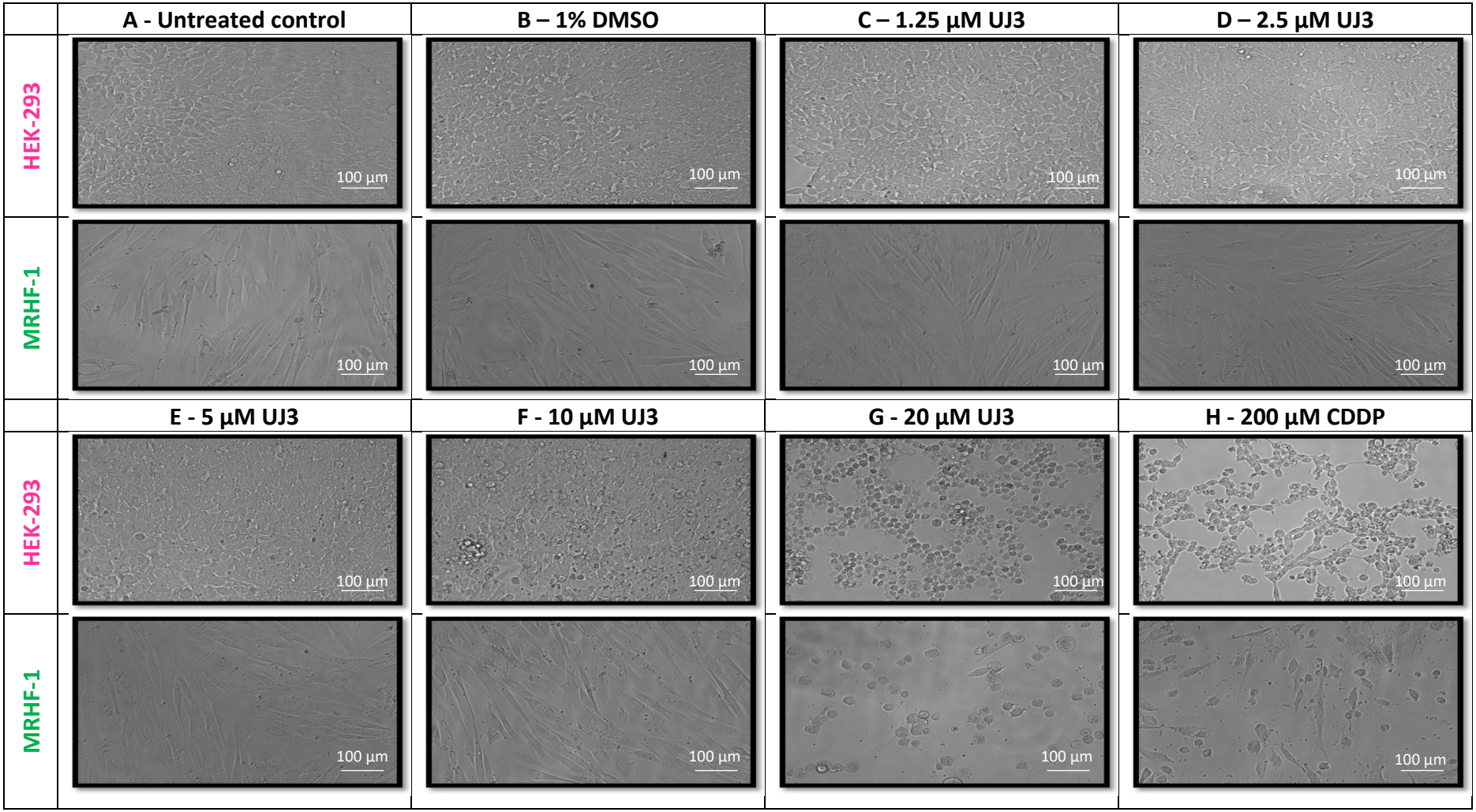

Figure 3.8: Cellular morphology light micrographs (200x magnification) of **HEK-293** and **MRHF-1** **post-24 hrs.** Cells were left untreated (A) or treated with either 1%DMSO (B), UJ3 (1,25 µM (C), 2.5 µM (D), 5 µM (E), 10 µM (F), 20 µM(G)) and CDDP 200 µM (H)). Both cell lines untreated and vehicle controls (A - B) represent healthy, thriving cell populations. No major reduction of cell populations was observed in both cell lines (C – F) except at the highest UJ3 (G) and CDDP (H) concentration.

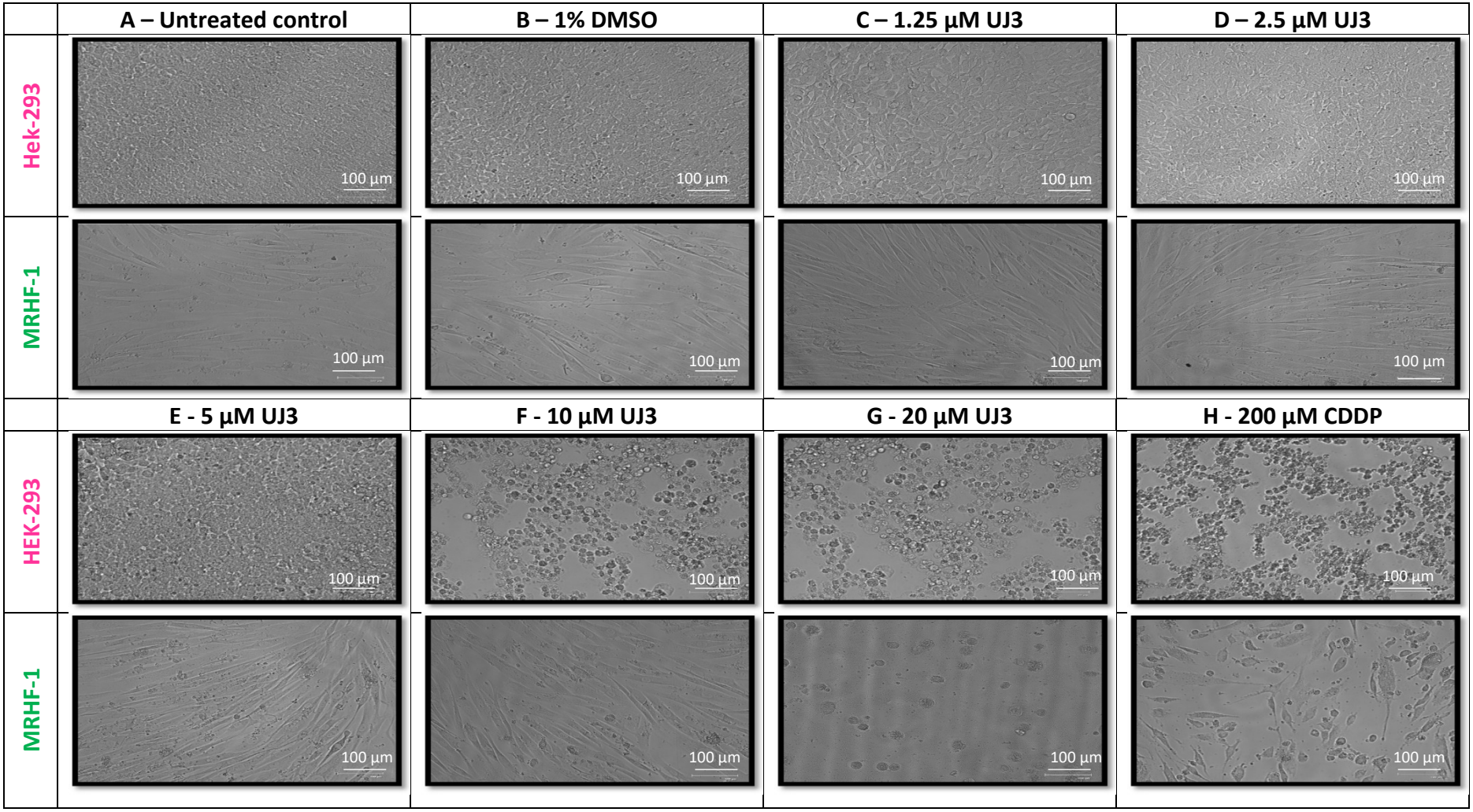

Figure 3.9: Cellular morphology light micrographs (200x magnification) of **HEK-293** and **MRHF-1** **post-48 hrs**. Cells were left untreated (A) or treated with either 1% DMSO (B), UJ3 (1,25 µM (C), 2.5 µM (D), 5 µM (E), 10 µM (F), 20 µM(G)) and CDDP 200 µM (H)). Both cell lines' controls (A - B) represent healthy, thriving cell populations. UJ3 appeared more cytotoxic to the HEK-293 than the MRHF-1. In the HEK-293, UJ3 treatment resembled the controls morphology (C – E) except at (F – G), where cellular stress became apparent. In the MRHF-1, high cellular confluency was observed (C – F), with the morphology resembling the controls except at the highest UJ3 concentration (G). In both cell lines, CDDP reduced cell populations (H).

3.2 Exploring the preferred mode of cell death induced by UJ3

3.2.1 Annexin V and 7-AAD to differentiate cell death populations

Annexin V possess high-affinity attachment to phosphatidylserines (PS). When a cell undergoes early apoptosis, a shift in PS occurs from the cytoplasmic side of the cell membrane to the outer membrane surface. The translocation of PS in apoptotic cells acts as a molecular tag recognized by macrophages for their subsequent capture and degradation. During late apoptosis or necrosis, cellular membrane integrity is impaired, permitting DNA binding dyes into the cell. This assay exploits the binding affinity of Annexin V to PS and conjugates Annexin V to fluorochromes enabling the detection of apoptotic cells. Annexin V is often accompanied by a 7-aminoactinomycin D (7-AAD) DNA dye. The dye is a necrotic or dead cell marker that enters cell membranes with impaired structural integrity. It permits 7-AAD to bind to intracellular DNA, detecting late apoptotic or necrotic cells based on their impaired plasma membrane. The Annexin V and 7-AAD assay quantitatively analyze cell populations based on their type of cell death. The cell populations may be live (Annexin V (-) and 7-AAD (-)), early apoptotic (Annexin V (+) and 7-AAD (-)), late apoptotic (Annexin V (+) and 7-AAD (+)), or dead/necrotic cell populations (Annexin V (-) and 7-AAD (+)) (Dong *et al*., 2009; Zimmermann and Meyer, 2011).

In both MCF-7 (Figure 3.10) and MDA-MB-231 (Figure 3.11) dot plots, the untreated (A) and vehicle control DMSO (B) had most cell populations located in the live cell quadrant (> 80%). This represents healthy unstained cells with intact membranes and non-exposed surface PS. UJ3 treatment (C) resulted in a population shift to the late apoptotic quadrant for both the MCF-7 (52%) (Figure 3.10) and MDA-MB-231 cell lines (74%) (Figure 3.11). This revealed that the preferred mode of cell death elicited by UJ3 is apoptosis. In the MCF-7, the positive apoptotic control CDDP (D) resulted in a population shift into the late apoptotic quadrant (42 %) as expected (Figure 3.10). In the MDA-MB-231, CDDP (D) had a high cell population percentage within the live cell quadrant (60%); this is expected as MDA-MB-231 displays resistance to CDDP (Figure 3.11). In the MCF-7 cell line, the positive necrosis control H_2O_2 (E) resulted in a population shift into the dead or necrotic cell quadrant (90%) as expected (Figure 3.10). In the MDA-MB-231 cell line, the positive necrosis control H_2O_2 (E) resulted in an unexpected population shift into the late apoptotic quadrant (82%) instead of the necrotic quadrant (Figure 3.11).

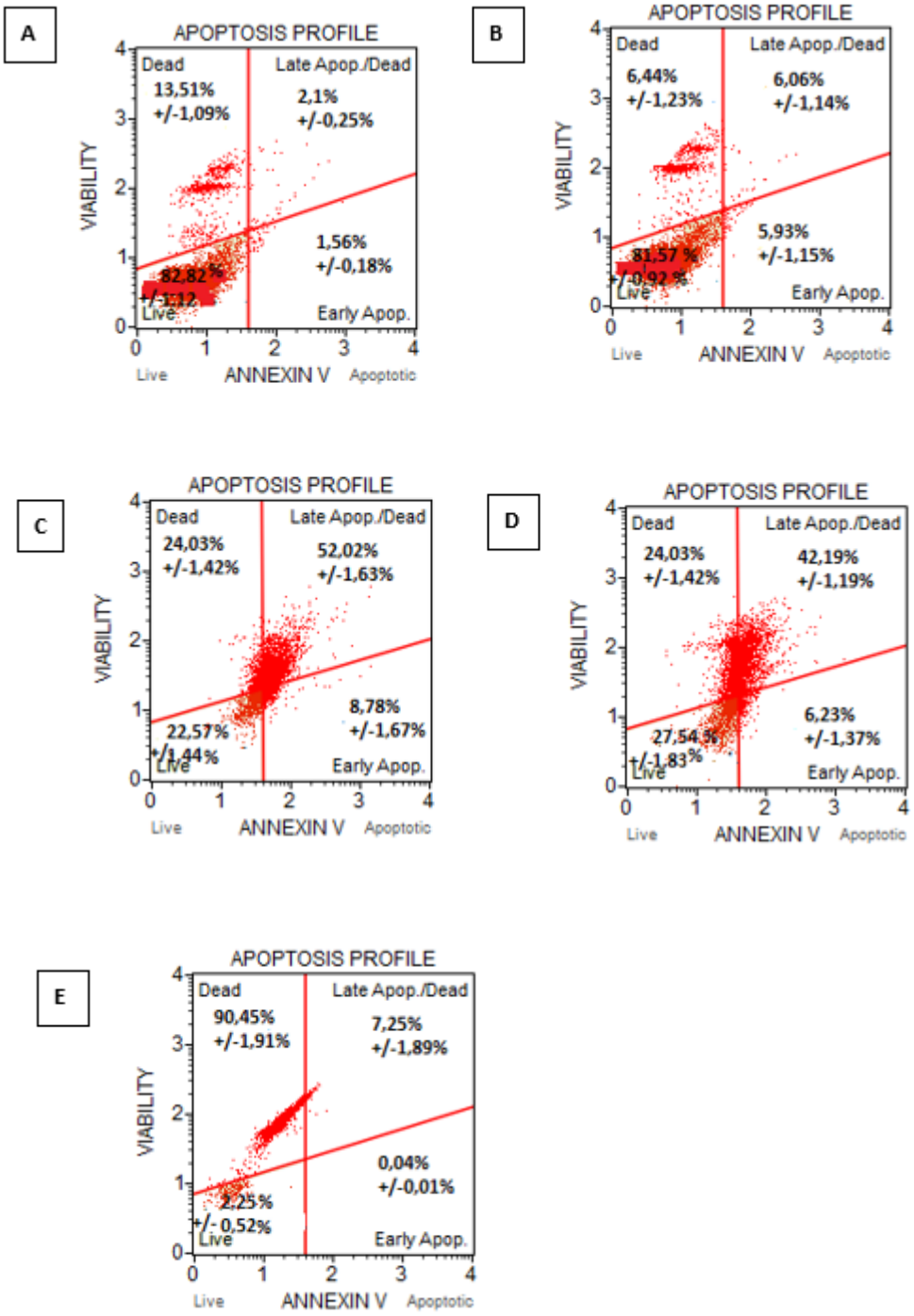

Figure 3.10: Dot plots differentiating the modes of cell death in **MCF-7** cells by Annexin V and 7-AAD reagent determined on the Muse cell analyzer **post-24 hrs** ((A) untreated control, (B) 1% DMSO vehicle control, (C) UJ3 treatment (20 μM), (D) CDDP (200 μM) positive apoptosis control and (E) Hydrogen peroxide (50%) positive necrosis control). Dot plots display a particular biological representative, while the average values shown in the plot include an average of three biological repeats (SEM: n=3).

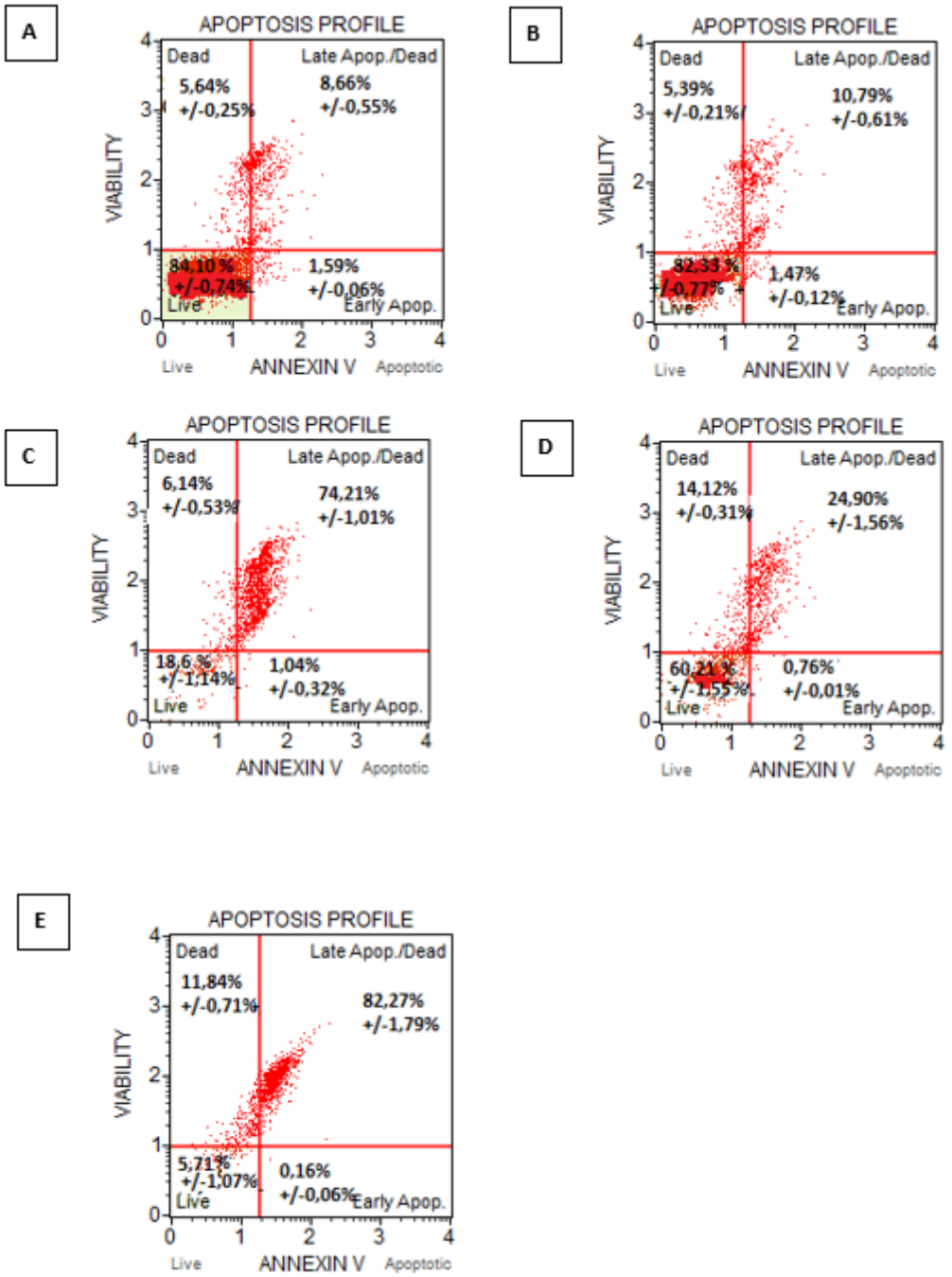

Figure 3.11: Dot plots differentiating the modes of cell death in **MDA-MB-231** cells by Annexin V and 7-AAD reagent determined on the Muse cell analyzer **post-24 hrs** ((A) untreated control, (B) 1% DMSO vehicle control, (C) UJ3 treatment (20 μM), (D) CDDP (200 μM) positive apoptosis control and (E) Hydrogen peroxide (50%) positive necrosis control). Dot plots display a particular biological representative, while the average values shown in the plot include an average of three biological repeats (SEM: n=3).

Table 3.2: Table summarizing the cell death populations in **MCF-7** and **MDA-MB-231** detected using the Annexin V and 7-AAD assay on the Muse cell analyzer. The cells were either untreated or treated with 1% DMSO vehicle control, UJ3 (20 µM) and CDDP (200 µM) **post-24 hrs**. Values represent the mean of triplicate experiments.

MCF-7 viability (%)				
	Live	**Early Apoptotic**	**Late Apoptotic**	**Dead**
Untreated Control	82,82 (+/- 1,12)	1,56 (+/- 0,18)	2,1 (+/- 0,25)	13,51 (+/- 1,09)
1% DMSO	81,57 (+/- 0,92)	5,93 (+/- 1,15)	6,06 (+/- 1,14)	6,44 (+/- 1,23)
UJ3 (20 µM)	22,57 (+/- 1,44)	8,78 (+/- 1,67)	52,02 (+/- 1,63)	24,03 (+/- 1,42)
CDDP (200 µM)	27,54 (+/- 1,83)	6,23 (+/- 1,37)	42,19 (+/- 1,19)	24,03 (+/- 1,42)
Hydrogen Peroxide (50%)	2,25 (+/- 0,52)	0,04 (+/- 0,01)	7,25 (+/- 1,89)	90,45 (+/- 1,91)
MDA-MB-231 Viability (%)				
	Live	**Early Apoptotic**	**Late Apoptotic**	**Dead**
Untreated Control	84,10 (+/- 0,74)	1,59 (+/- 0,06)	8,66 (+/- 0,55)	5,64 (+/- 0,25)
1% DMSO	82,33 (+/- 0,77)	1,47 (+/- 0,12)	10,79 (+/- 0,61)	5,39 (+/- 0,21)
UJ3 (20 µM)	18,6 (+/- 1,14)	1,04 (+/- 0,32)	74,21 (+/- 1,01)	6,14 (+/- 0,53)
CDDP (200 µM)	60,21 (+/- 1,55)	0,76 (+/- 0,01)	24,90 (+/- 1,56)	14,12 (+/- 0,31)
Hydrogen Peroxide (50%)	5,71 (+/- 1,07)	0,16 (+/- 0,06)	82,27 (+/- 1,79)	11,84 (+/- 0,71)

3.2.2 Mitochondrial membrane potential (ΔΨm) as a parameter of cell death

The mitochondria, renowned as the cellular ''powerhouse'' are essential to not only cellular bioenergetics and biosynthesis but to governing cellular fate and health status as well. The mitochondrion houses central cell death mediators and variations in the ΔΨm have been associated with many modes of cell death, such as apoptosis, necrosis and even caspase-independent cell death. Energy production by the mitochondrion is accumulated into an electrochemical gradient resulting in the formation of a ΔΨm that supplies the cell with its required ATP. In the early stages of apoptosis, the ΔΨm is reduced due to the expulsion of cytochrome *c* through the mitochondrial pore known as MOMP (Henry-Mowatt *et al*., 2004; Krysk *et al*., 2001; Tait and Green, 2013). Subsequent depolarization of the mitochondrial membrane is linked to cellular stress and specific modes of cellular death. The Muse MitoPotential assay utilizes a MitoPotential reagent that generates high fluorescence in the presence of a strong driving membrane potential. In contrast, a depolarized membrane potential will result in reduced fluorescence detection. The 7-AAD marker is again used to determine membrane integrity and will not be associated with live and early cells undergoing apoptosis (Schmid *et al*., 1992). This section involves studying the mitochondrial membrane potential after UJ3 subjection to provide insight into the mode of cell death elicited.

The MitoPotential assay separates cells into specific cell populations. The lower left quadrant represents live cells with depolarized membranes (MitoPotential (-) due to decreased membrane potential and 7-AAD (-) due to intact membrane in live cells). The lower right quadrant represents live cells with intact plasma membranes (MitoPotential (+) intact membrane can drive a potential gradient and 7-AAD (-)). Upper left quadrant dead cells with a depolarized mitochondrial membrane (MitoPotential (-) due to decreased membrane potential and 7-AAD (+) due to loss of structural integrity in the plasma membrane of dead cells). The upper right quadrant represents dead cells with an intact mitochondrial membrane (MitoPotential (+) intact mitochondrial membrane can drive a membrane potential and 7-AAD (+) dead cells lose structural integrity of plasma membrane).

The MCF-7 dot plots (Figure 3.12) of the untreated (A) and DMSO control (B) had most of the cell population in the live cell quadrant (untreated control: 79.10%, DMSO: 78.84%), indicating that the cells are healthy, capable of driving a high mitochondrial membrane potential and maintaining an intact plasma membrane. UJ3 (C) shifted the population to the depolarized dead quadrant (84%), indicating that UJ3 reduced the mitochondrial membrane potential and impaired the plasma membrane (Figure 3.12). This may be implicated as late apoptotic death as observed in Annexin V and 7-AAD assay (Figure 3.10). These findings are in conjunction with the decreased mitochondrial activity and ATP levels determined by the viability assays (Figure 3.1 and Figure 3.4). Furthermore, the UJ3 (20 μM) morphology micrograph depicts

apoptotic morphology (Figure 3.6 (G)). Similarly, CDDP treatment (D) resulted in a population shift to the depolarized dead quadrant (81%) (Figure 3.12). These findings correlate to the population shift into the late apoptotic quadrant as observed in the Annexin V and 7-AAD assay (Figure 3.10). These findings are also in conjunction with the reduced mitochondrial activity levels (Figure 3.3A), reduced ATP levels (Figure 3.4) and apoptotic blebbing morphology (Figure 3.6 (H)).

The MDA-MB-231 (Figure 3.13) untreated (A) and DMSO control (B) had most of the cell population in the live cell quadrant (untreated control: 84.54%, DMSO: 85.63%), indicating healthy cells, capable of driving a high mitochondrial membrane potential and maintaining an intact plasma membrane. UJ3 (C) shifted the cell population to the depolarized dead quadrant (46%), indicating mitochondrial membrane potential reduction and plasma membrane impairment (Figure 3.13). This may be implicated as late apoptotic cellular death as observed in Annexin V and 7-AAD assay (Figure 3.11). These findings correlate to the reduced mitochondrial activity (33.72%) (Figure 3.1), reduced ATP levels (Figure 3.5) and morphological cellular rounding (Figure 3.7). CDDP (D) had a high cell population percentage within the live cell quadrant (59%) as the MDA-MB-231 cells are resistant to CDDP (Figure 3.13). These findings correlate to the high cell population percentage in the live cell quadrant (60%) determined by the Annexin V and 7-AAD assay (Figure 3.11) and mitochondrial activity levels (52.98%) (Figure 3.3 A).

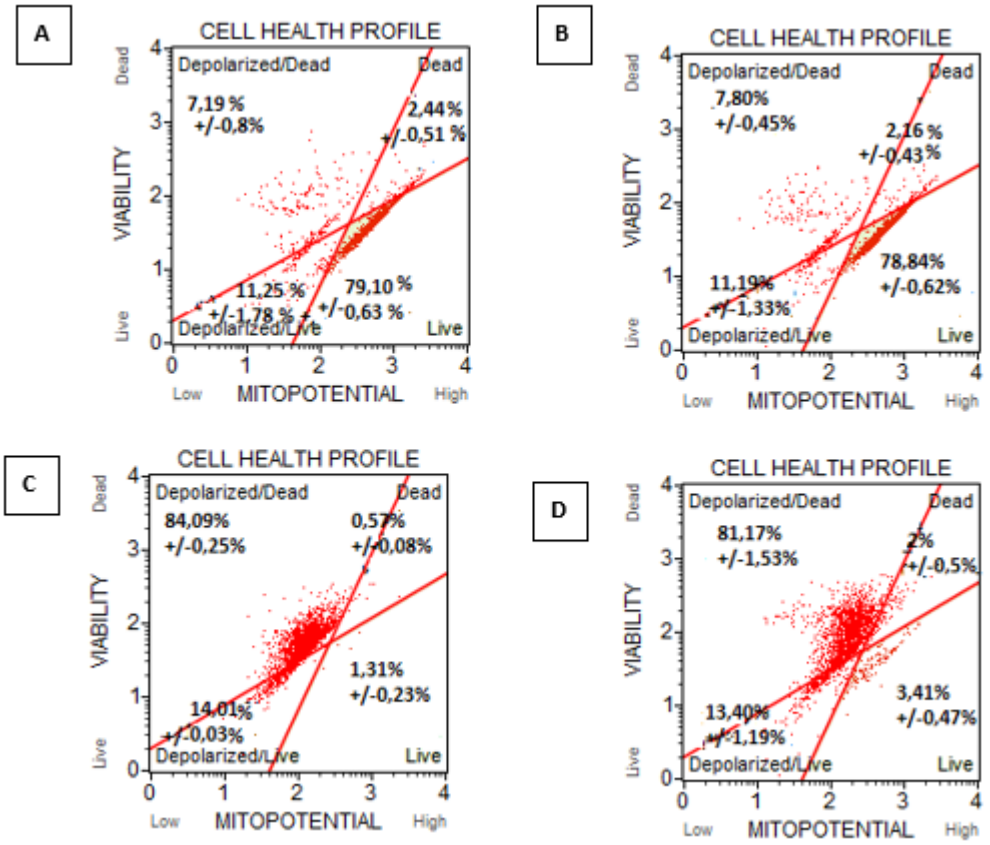

Figure 3.12: Dot plots representing changes in mitochondrial membrane potential ($\Delta\Psi m$) and membrane integrity associated with cell death in **MCF-7** cells determined by MitoPotential and 7-AAD reagent detected on the Muse cell analyzer **post-24 hrs** ((A) untreated control, (B) 1%DMSO vehicle control, (C) UJ3 treatment (20 µM) and (D) CDDP (200 µM) positive apoptosis control). Dot plots display a particular biological representative, while the average values shown in the plot include an average of three biological repeats (SEM: n=3).

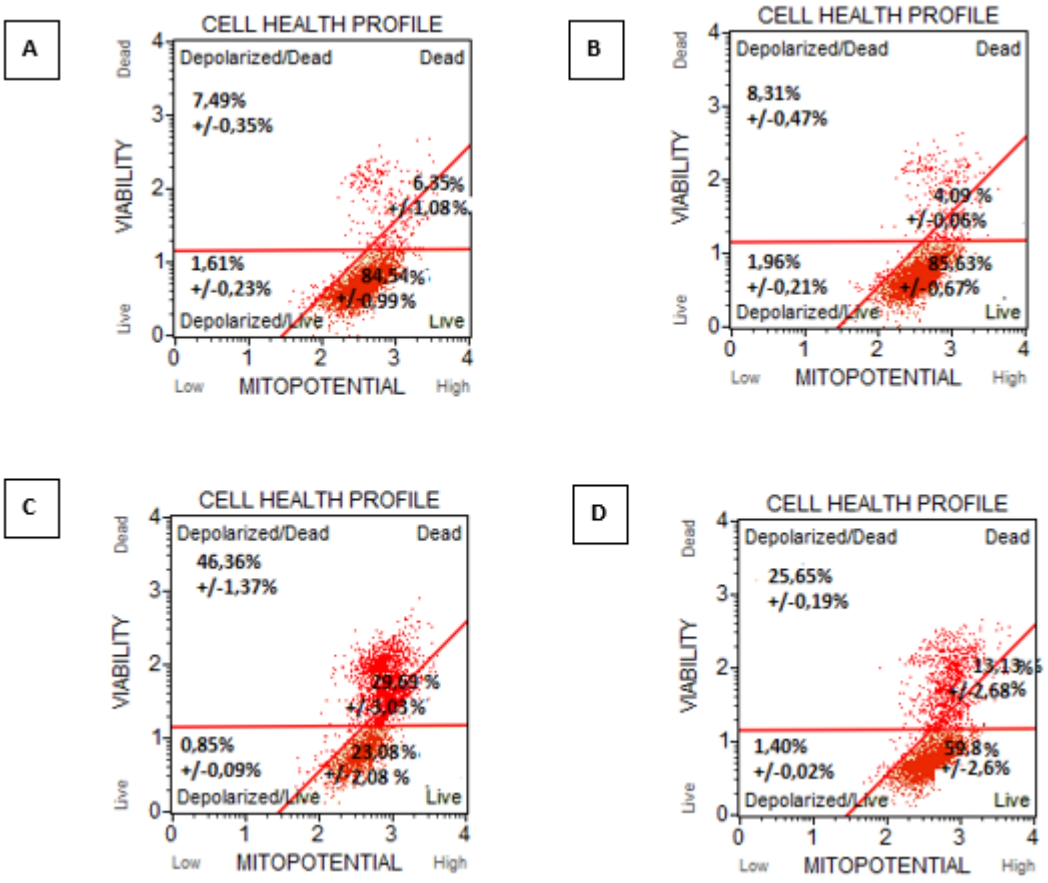

Figure 3.13: Dot plots representing changes in mitochondrial membrane potential ($\Delta\Psi m$) and membrane integrity associated with cell death in MDA-MB-231 cells determined by MitoPotential and 7-AAD reagent detected on the Muse cell analyzer **post-24 hrs** ((A) untreated control, (B) 1%DMSO vehicle control, (C) UJ3 treatment (20 μM) and (D) CDDP (200 μM) positive apoptosis control). Dot plots display a particular biological representative, while the average values shown in the plot include an average of three biological repeats (SEM: n=3).

Table 3.3: Table summarizing changes in mitochondrial membrane potential (ΔΨm) and membrane integrity in **MCF-7** and **MDA-MB-231** using the MitoPotential and 7-AAD reagent detected on the Muse cell analyzer. The cells were either untreated or treated with 1% DMSO vehicle control, UJ3 (20 µM) and CDDP (200 µM) **post-24 hrs**. Values represent the mean of triplicate experiments.

MCF-7 (%)				
	Live	**Depolarized/Live**	**Depolarized/Dead**	**Dead**
Untreated Control	79,10 (+/- 0,63)	11,25 (+/- 1,78)	7,19 (+/- 0,18)	2,44 (+/- 0,51)
1% DMSO	78,84 (+/- 0,62)	11,19 (+/- 1,33)	7,80 (+/- 0,45)	2,16 (+/- 0,43)
UJ3 (20 µM)	1,31 (+/- 0,23)	14,01 (+/- 0,03)	84,09 (+/- 0,25)	0,57 (+/- 0,08)
CDDP (200 µM)	3,41 (+/- 0,47)	13,40 (+/- 1,19)	81,17 (+/- 1,53)	2 (+/- 0,5)
MDA-MB-231 (%)				
Untreated Control	84,54 (+/- 0,99)	1,61 (+/- 0,23)	7,49 (+/- 0,35)	6,35 (+/- 1,08)
1% DMSO	85,63 (+/- 0,67)	1,96 (+/- 0,21)	8,31 (+/- 0,47)	4,09 (+/- 0,06)
UJ3 (20 µM)	23,08 (+/- 2,08)	0,85 (+/- 0,09)	46,36 (+/- 1,37)	26,69 (+/- 3,03)
CDDP (200 µM)	59,8 (+/- 2,6)	1,40 (+/- 0,02)	25,65 (+/- 0,19)	13,13 (+/- 2,68)

3.2.3 Oxidative stress as a parameter of cell death

Reactive oxygen species (ROS) such as hydrogen peroxide or hydroxyl radicles are end products of aerobic respiration made by the mitochondria and nicotinamide adenine dinucleotide phosphate (NADPH) oxidases. Healthy cells have an antioxidant defense mechanism in place to get rid of the toxicity associated with ROS. When high levels of ROS production prevail and cellular antioxidant defense mechanisms fail, oxidative stress results. Consequently, initiating DNA, protein, and lipid injury and inducing overall cellular stress or death. Malignant cells retain high levels of ROS due to strenuous metabolic activity and proliferating ability. However, malignant cells employ enzymes such as manganese superoxide dismutase (SOD), glutathione peroxidase and catalase to eradicate ROS (Chen *et al*., 2007; Kannan and Jain, 2000; Shehat and Tigno-Aranjuez, 2019). As a result, malignant cells may have enhanced sensitivity to increased oxidative stress as a high level of endogenous ROS already exists intracellularly. The high level of oxidative stress may promote caspase-dependent apoptosis or inhibition of caspase and disruption to catalase may promote autophagy. Lysosomal necrotic cell death may also be associated with high ROS production (Chen *et al*., 2007).

The Muse® Oxidative Stress assay detects superoxide radicles to study the percentage of cells undergoing oxidative stress. Dihydroethidium contained in the reagent undergoes an oxidation reaction in the presence of superoxide anions and forms an ethidium bromide fluorophore that binds to DNA and emits red fluorescence (Jackson, 2013)—subsequently separating cell populations into low-level ROS-producing (M1) or high-level ROS positive cells (M2).

ROS profiles of the MCF-7 (Figure 3.14) untreated control, vehicle control and UJ3 produced low levels of superoxide radicles (M1 > 90 %). CDDP had greater levels of superoxide radicles (35.46%) than UJ3 (5.57%). However, most of the cell population (64.47 %) was in the M1 region post-CDDP treatment (Figure 3.14). In the MDA-MB-231 ROS profile (Figure 3.15), the untreated and vehicle controls produced low levels of superoxide radicles (M1 > 90%). UJ3 resulted in a higher M1 population (59.10%) than the M2 positive ROS cell population (40.66%). UJ3 produced higher ROS levels in the MDA-MB-231 cell line (M2: 40.66%) than in the MCF-7 cell line (M2: 5.57%). Furthermore, UJ3 generated higher ROS in the MDA-MB-231 cell line than CDDP (M2: 19.37%). In contrast, the MCF-7 cell line presented with higher ROS levels post-CDDP treatment (35.46%) compared to UJ3 (5.57%) (Figure 3.15).

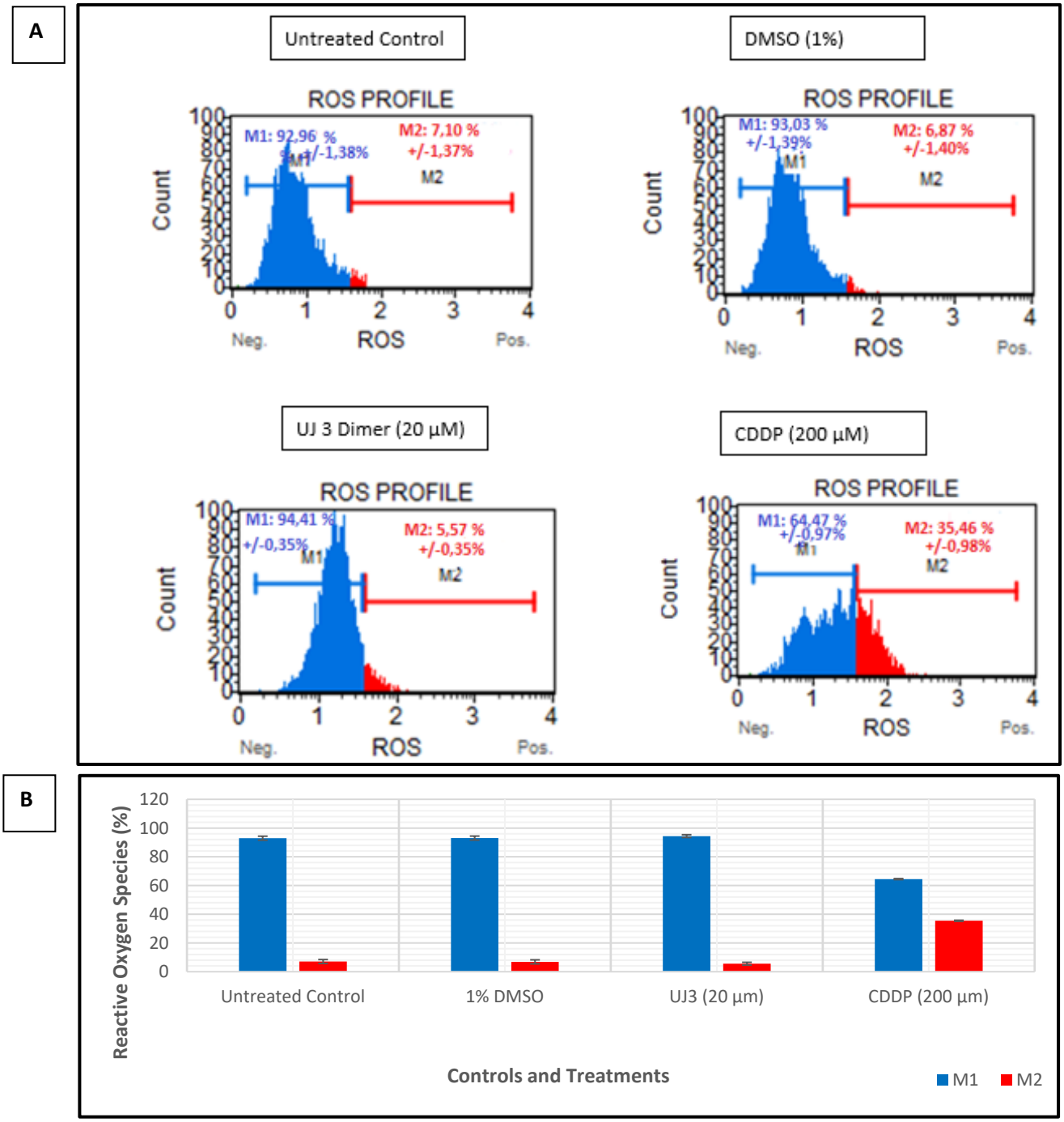

Figure 3.14: Histograms (A) and bar chart (B) representing reactive oxygen species levels in **MCF-7** untreated control, 1% DMSO vehicle control, UJ3 (20 µM) and CDDP (200 µM) **post-24 hrs**. Histograms display a particular biological representative, while the average values shown in the plot include an average of three biological repeats (SEM: n=3).

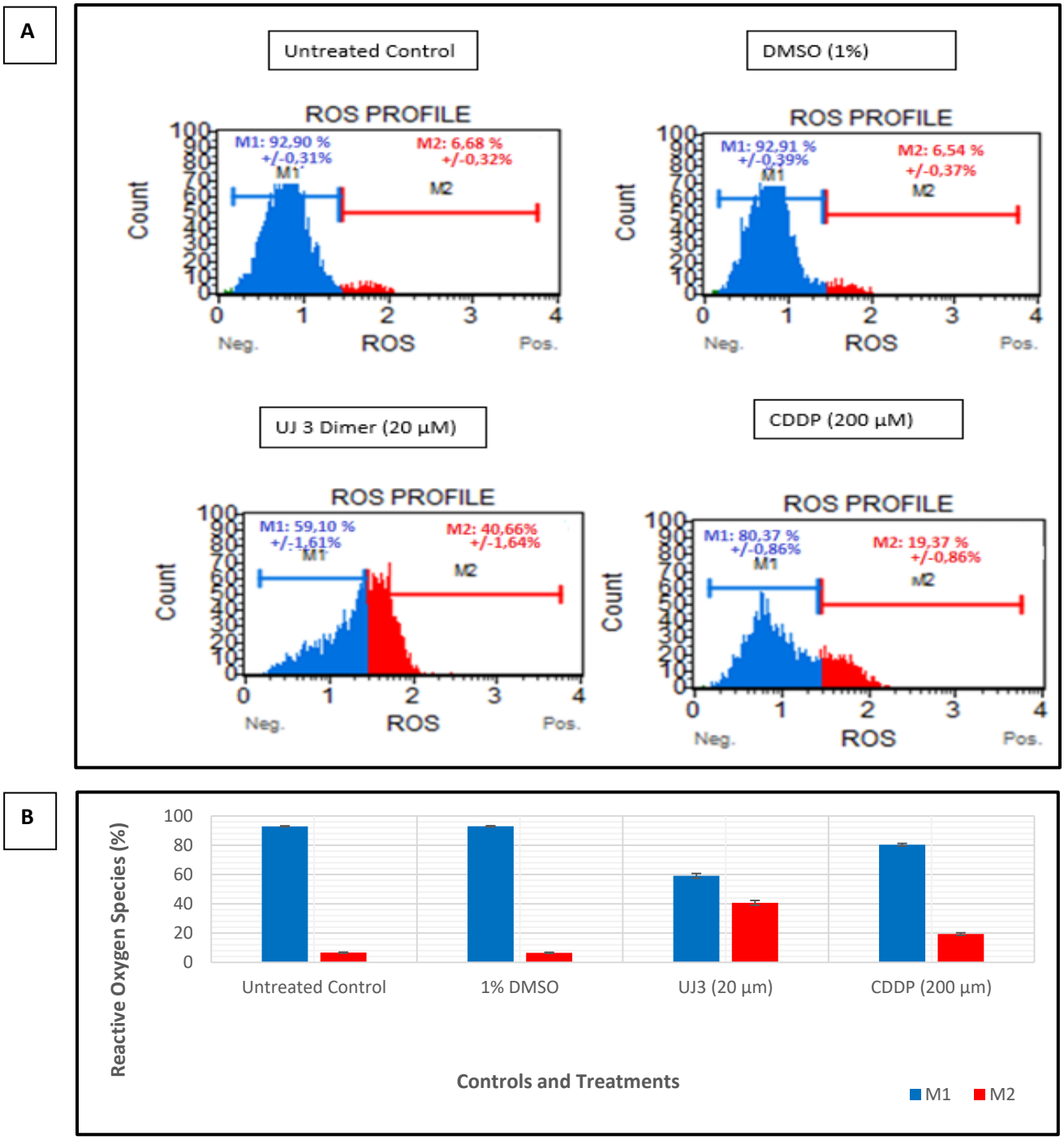

Figure 3.15: Histograms (A) and bar chart (B) representing reactive oxygen species levels in **MDA-MB-231** untreated control, 1% DMSO vehicle control, UJ3 (20 µM) and CDDP (200 µM) **post-24 hrs**. Histograms display a particular biological representative, while the average values shown in the plot include an average of three biological repeats (SEM: n=3).

3.3 Intracellular labeling of organelles to observe UJ3 induced morphological changes

The cell's intracellular organelles or proteins were fluorescently labeled. The nuclei were labeled with Hoechst 33258, the mitochondria with MitoTracker orange and cytochrome *c* with Alexa 488 dye. Full images of the labeled MCF-7 (Figure 3.16) and MDA-MB-231 (Figure 3.18) were included. The cells marked with arrows in the full images are depicted as enlarged images for the MCF-7 (Figure 3.17) and MDA-MB-231 (Figure 3.19) and will be discussed in more detail. In addition to the UJ3 and CDDP treatments previously used, 10 μM of UJ3 and the IC_{50} of CDDP for both cell lines were included to detect apoptotic morphology at concentrations not included in previous assays.

3.3.1 Tracking the nucleus

Hoechst 33258 is a bisbenzimide dye used to fluorescently label the cell nucleus and stain DNA by attaching to the minor groove of DNA that is rich in Adenine – Thymine. Hoechst 33258 was chosen for this study as opposed to other DNA staining dyes due to its negligible cytotoxicity, enhanced cellular permeability and high signal-to-noise ratio when excited by UV illumination (Bucevičius *et al*., 2018). Since apoptotic cell death encompasses many alterations to DNA, studying associated morphological changes post-UJ3 treatment will provide insight as to how UJ3 executes apoptosis as suggested by prior results (Figure 3.6 (G), Figure 3.10 (C), Figure 3.11(C), Figure 3.12 (C) and Figure 3.13 (C)). DNA damage may be the result of apoptotic death or the signal that initiates apoptotic death in cells depending on the mechanistic action of UJ3. Moreover, changes in DNA morphology may further establish the mode of cell death.

The untreated and vehicle controls (Figure 3.17(A - B)) of the MCF-7 depicted unimpaired nuclei with a consistent chromatin distribution based on the equal distribution of the Hoechst 33258 dye. UJ3 treatments (10 μM, 14.1 μM and 20 μM) (Figure 3.17 (C – E)) depicted no extreme chromatin condensation (karyorrhexis) or fragmentation. However, UJ3 (20 μM) treatment (Figure 3.17 (E)) depicted a change in the spherical shape of the nuclei. The positive apoptotic control CDDP (134.5 μM) (Figure 3.17 (F)) resulted in brighter Hoechst 33258 fluorescence with chromatin condensation along the nuclear periphery and shrinkage of nuclei (pyknosis). CDDP (200 μM) (Figure 3.17 (G)) promoted DNA fragmentation.

The MDA-MB-231 controls (Figure 3.19 (A - B)) depicted a similar distribution profile of the Hoechst 33285 dye as in the MCF-7. UJ3 (10 μM) treatment (Figure 3.19 (C)) portrayed minor chromatin condensation. UJ3 IC_{50} (13.6 μM) treatment (Figure 3.19 (D)) displayed bright Hoechst 33258 fluorescence with major DNA fragmentation observed near the nuclei periphery as well as nuclei shrinkage. Chromatin condensation was not observed in UJ3 (20

μM) and CDDP (219.2 μM) treatments (Figure 3.19 (E – F)); however, a shift in fluorescence and change in nuclei shape was depicted. CDDP (200 μM) treatment (Figure 3.19 (G)) depicted peripheral chromatin condensation in the nuclei. Overall, UJ3 impacted the MDA-MB-231 nuclei morphology more drastically than the MCF-7 cell line.

3.3.2 Tracking the mitochondria and its associated protein – cytochrome c

MitoTracker Orange fluorescent dye tracks mitochondria health status by monitoring $\Delta\Psi m$, changes in mitochondria mass, mitochondria localization and morphology. The cationic fluorophore moves through the mitochondrial membrane according to the Nernst equation. Therefore, its accumulation in the mitochondrial matrix is inversely proportional to the $\Delta\Psi m$ such that high polarization results in more dye accumulation detected. The dye contains a chloromethyl group that covalently attaches to proteins in the mitochondria (Kholmukhamedov *et al*., 2013; Perry *et al*., 2011). MitoTracker Orange was chosen for its strong selectivity for active mitochondria and retainment during cell fixation or permeabilization (Han *et al*., 2013). The electron transport protein cytochrome c is an essential protein of study due to its relation to oxidative phosphorylation, ATP generation and crucial involvement in the intrinsic apoptosis pathway *(*Ow *et al*., 2008). The Alexa 488 dye contains a succinimidyl ester that facilitates conjugation to an antibody or cytochrome *c* protein allowing for its fluorescent detection. Alexa 488 dye was chosen due to its advantageous pH insensitivity over a broad range and superior photostability compared to other dyes (Panchuk-Voloshina *et al*., 1999).

The untreated and vehicle controls (Figure 3.17(A - B)) of the MCF-7 depicted highly polarized, intact mitochondria made evident through the intense accumulation of MitoTracker Orange dye. UJ3 treatments (10 μM, 14.1 μM and 20 μM) (Figure 3.17 (C – E)) depicted a reduction in dye accumulation with respect to the controls, indicative of a decrease in $\Delta\Psi m$ and polarisation. Additional mitochondrial depolarisation was observed as the CDDP concentration increased from (134.5 μM) (Figure 3.17 (F)) to CDDP (200 μM) (Figure 3.17 (G)). Alexa 488 dye revealed that cytochrome *c* remained intact and localized during UJ3 treatments (10 μM and 14.1 μM) (Figure 3.17 (C) and (E)) as depicted in the controls (Figure 3.17(A - B)). However, UJ3 IC_{50} treatment (14.1 μM) (Figure 3.17 (D)) depicted cytochrome *c* expulsion and a higher intensity of Alexa 488 dye with respect to the controls.

The MDA-MB-231 controls (Figure 3.19 (A - B)) depict highly polarized mitochondria similar to the distribution profile of the MCF-7 controls. UJ3 (10 μM, 13.6 μM and 20 μM) and CDDP treatments (219.2 μM and 200 μM) (Figure 3.19 (C - G)) depicted a decrease in polarisation. Moreover, the polarization profiles of UJ3 (20 μM) and CDDP (200 μM) correspond to a reduction in both $\Delta\Psi m$ and ATP (Figure 3.5 and Figure 3.13 (C) and (D)). Cytochrome *c*

appears localized and intact in all UJ3 (10 μM, 13.6 μM and 20 μM) and CDDP (219.2 μM and 200 μM) treatments (Figure 3.19 (C – G)) with respect to the controls (Figure 3.19 (A – B)).

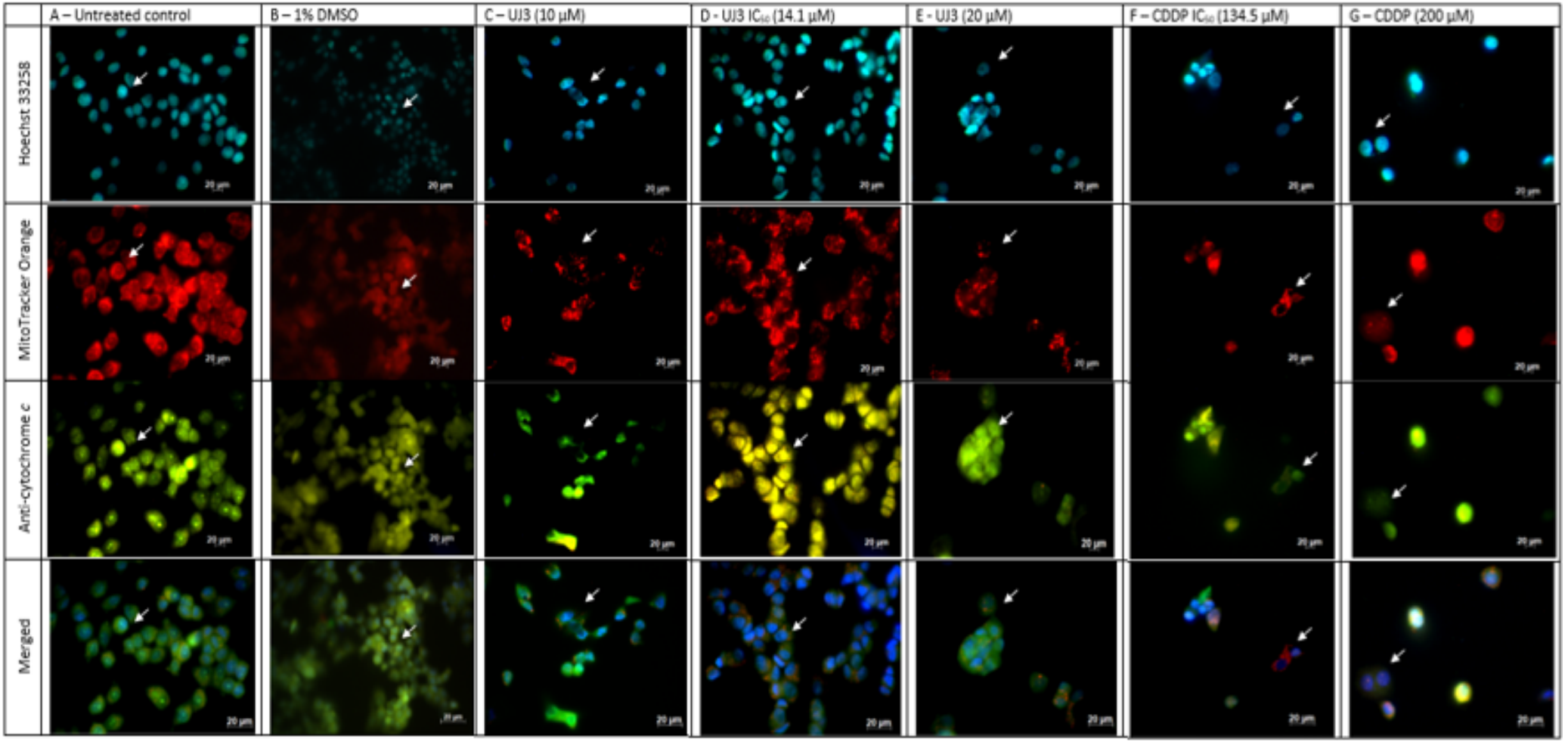

Figure 3.16*:* Intracellular fluorescent micrographs (1000X magnification) of **MCF-7** cells. Cells were left untreated (A) or treated with either 1% DMSO (B), UJ3 10 µM (C), UJ3 IC_{50} 14.1 µM (D), UJ3 20 µM (E), CDDP IC_{50} 134.5 µM (F) and CDDP 200 µM (G) **post-24 hrs**. The nuclei were labeled with Hoechst 33258, mitochondria with MitoTracker Orange and cytochrome *c* with Alexa 488 dye. Cells marked with an arrow are enlarged in Figure 3.17.

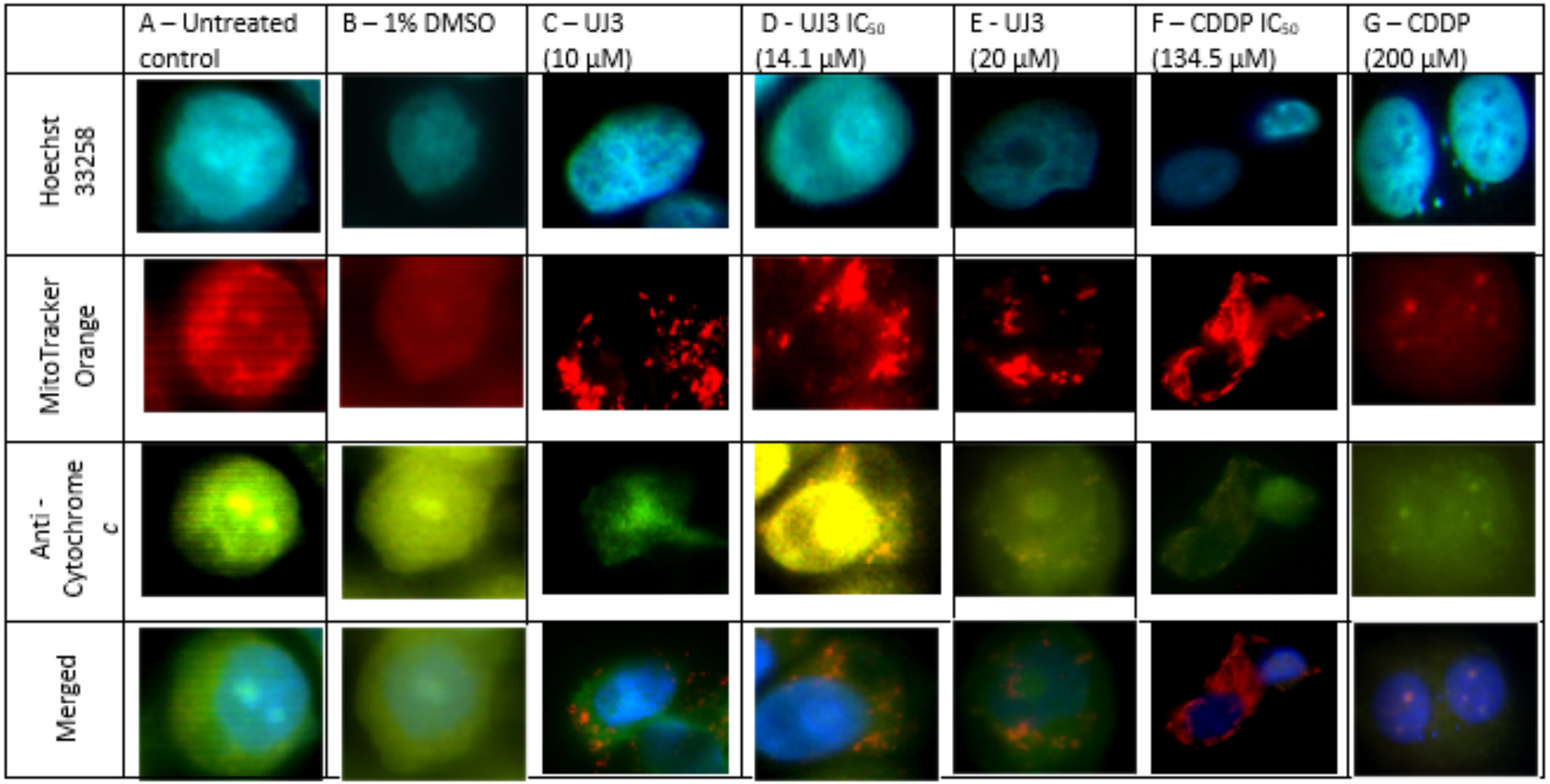

Figure 3.17*:* Intracellular fluorescent micrographs of **MCF-7** enlarged from Figure 3.16. Cells were left untreated (A) or treated with either 1% DMSO (B), UJ3 10 µM (C), UJ3 IC_{50} 14.1 µM (D), UJ3 20 µM (E), CDDP IC_{50} 134.5 µM (F) or CDDP 200 µM (G) **post-24 hrs**. The nucleus was labeled with Hoechst 33258, mitochondrion with MitoTracker Orange and cytochrome *c* with Alexa 488 dye. Chromatin condensation and fragmentation were most observable in the positive apoptosis control CDDP (F – G). UJ3 treatments influenced the $\Delta\Psi m$ (C -E) with cytochrome *c* expulsion at UJ3 IC_{50} treatment (D).

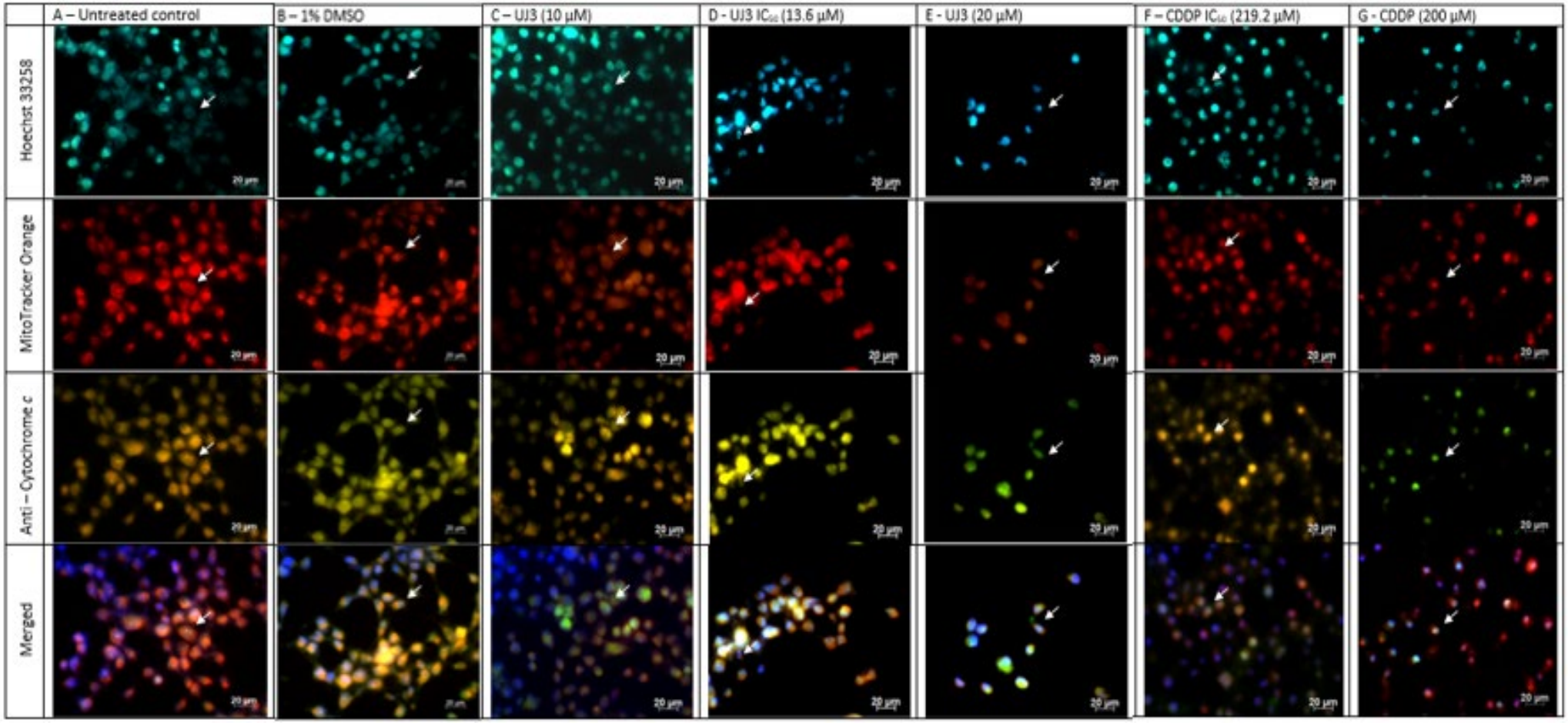

Figure 3.18*:* Intracellular fluorescent micrographs (1000X magnification) of **MDA-MB-231** cells. Cells were left untreated (A) or treated with either 1% DMSO (B), UJ3 10 μM (C), UJ3 IC_{50} 13.6 μM (D), UJ3 20 μM (E), CDDP IC_{50} 219.2 μM (F) and CDDP 200 μM (G) **post-24 hrs**. The nuclei were labeled with Hoechst 33258, mitochondria with MitoTracker Orange and cytochrome *c* with Alexa 488 dye. Cells marked with an arrow are enlarged in Figure 3.19.

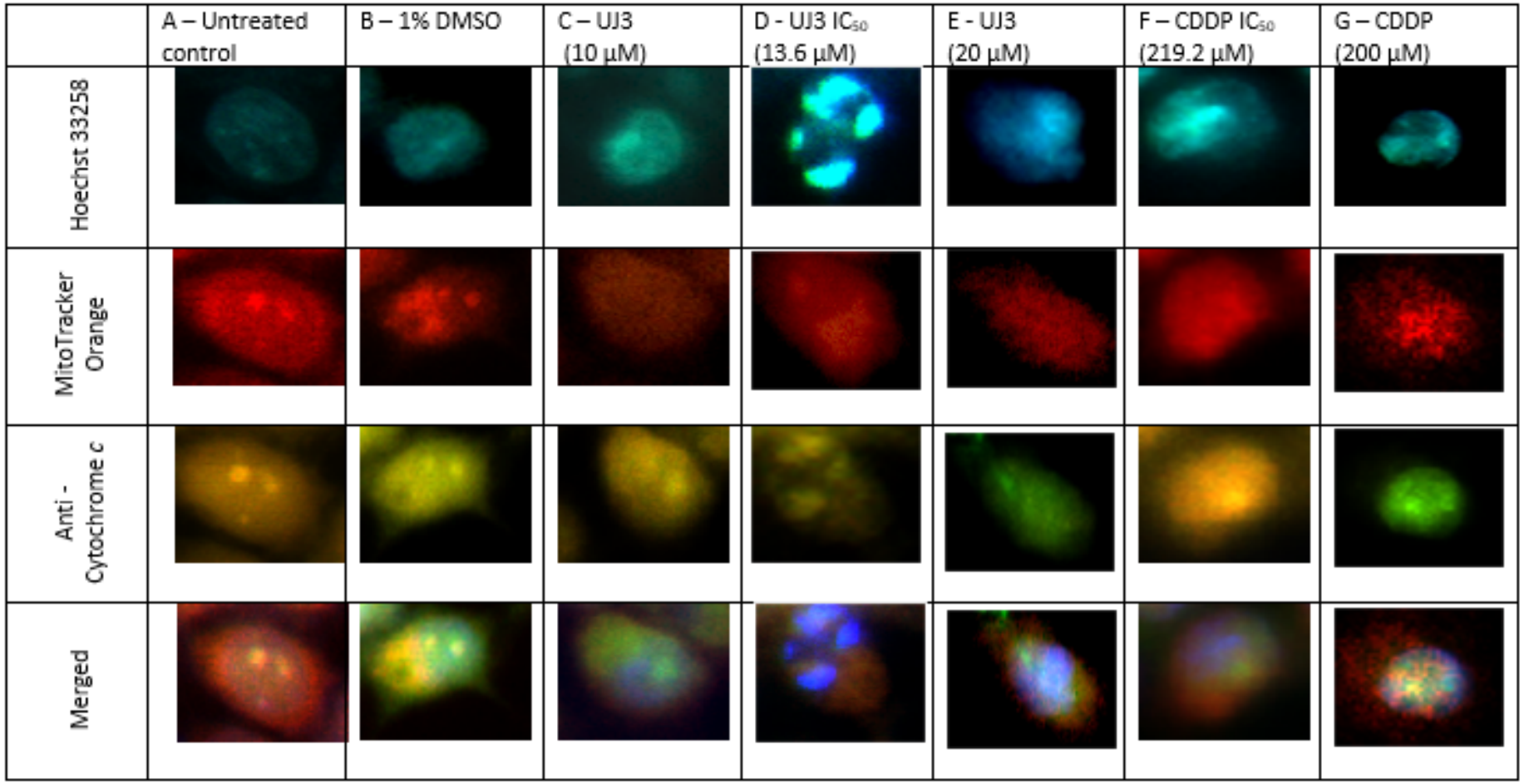

Figure 3.19: Intracellular fluorescent micrographs of **MDA-MB-231** enlarged from Figure 3.18. Cells were left untreated (A) or treated with either 1% DMSO (B), UJ3 10 µM (C), UJ3 IC_{50} 13.6 µM (D), UJ3 20 µM (E), CDDP IC_{50} 219.2 µM (F) and CDDP 200 µM (G) **post-24 hrs**. The nucleus was labeled with Hoechst 33258, mitochondrion with MitoTracker Orange and cytochrome *c* with Alexa 488 dye. Major DNA fragmentation was observed at UJ3 IC_{50} treatment (D) and UJ3 influenced the $\Delta\Psi m$ (C – E). This was visible as a diffusion of the MitoTracker Orange dye. No cytochrome *c* leakage was visible for UJ3 treatments.

3.4 Western Blots and apoptotic protein detection

Intracellular labeling of the MCF-7 cytochrome *c* and mitochondria support cell death induction via the intrinsic apoptosis pathway (Figure 3.17). Whereas mitochondrial bioenergetics and cell death assays suggest apoptosis death in the MDA-MB-231 (Figure 3.11, Figure 3.13 and Figure 3.19), whether the intrinsic pathway facilitates this remains to be investigated. A western blot was conducted to evaluate the activity of crucial pro-apoptotic proteins such as caspase-3, caspase-7, caspase-8 and PARP associated with apoptosis to confirm and further explore these findings. Caspase-3 detection was omitted for the MCF-7 cell line as these cells do not express caspase-3 (Jänicke, 2008). Cells were either left untreated or treated with 1% DMSO, UJ3 IC_{50}, UJ3 (20 µM) and CDDP (200 µM) post-24 hrs. Pro-forms and cleaved forms of the apoptotic proteins were normalized against the beta-actin (42 kDa) loading control.

The MCF-7 caspase-7 profile (Figure 3.20A) indicates the presence of the full-length pro-caspase-7 (35 kDa) in all controls and treatments. A dark band (20 kDa) was visible post-UJ3 IC_{50} (14.1 µM) treatment (D); this represents the cleaved active form of caspase-7. However, no cleaved caspase-7 was detected in CDDP treatment (E) (Figure 3.20A). In the PARP profile (Figure 3.20A), the full-length PARP (116 kDa) was present in the controls, visible as a dark, intense band. However, a faint band was detected in the UJ3 (20 µM) treatment (C), corresponding to the full-length PARP. The full-length PARP in the UJ3 IC_{50} (D) and CDDP (E) lanes are not visible. However, this corresponds to cleaved PARP (24 kDa) presence for both treatments with the absence of the larger cleaved PARP fragment (89 kDa) (Figure 3.20A). Moreover, PARP cleavage for UJ3 IC_{50} (14.1 µM) treatment corresponds to caspase-7 cleavage detection at the same concentration. Although active caspase-7 was not detected during CDDP treatment, its apoptotic effect was detected by PARP cleavage (Figure 3.20A). To further confirm UJ3's association with the intrinsic apoptosis pathway, the extrinsic pathway initiator caspase-8 was detected (Figure 3.20B). Pro-caspase-8 (55 / 53 kDa) was visible in the controls and treatments with no presence of cleaved active caspase-8 (43 / 41 kDa).

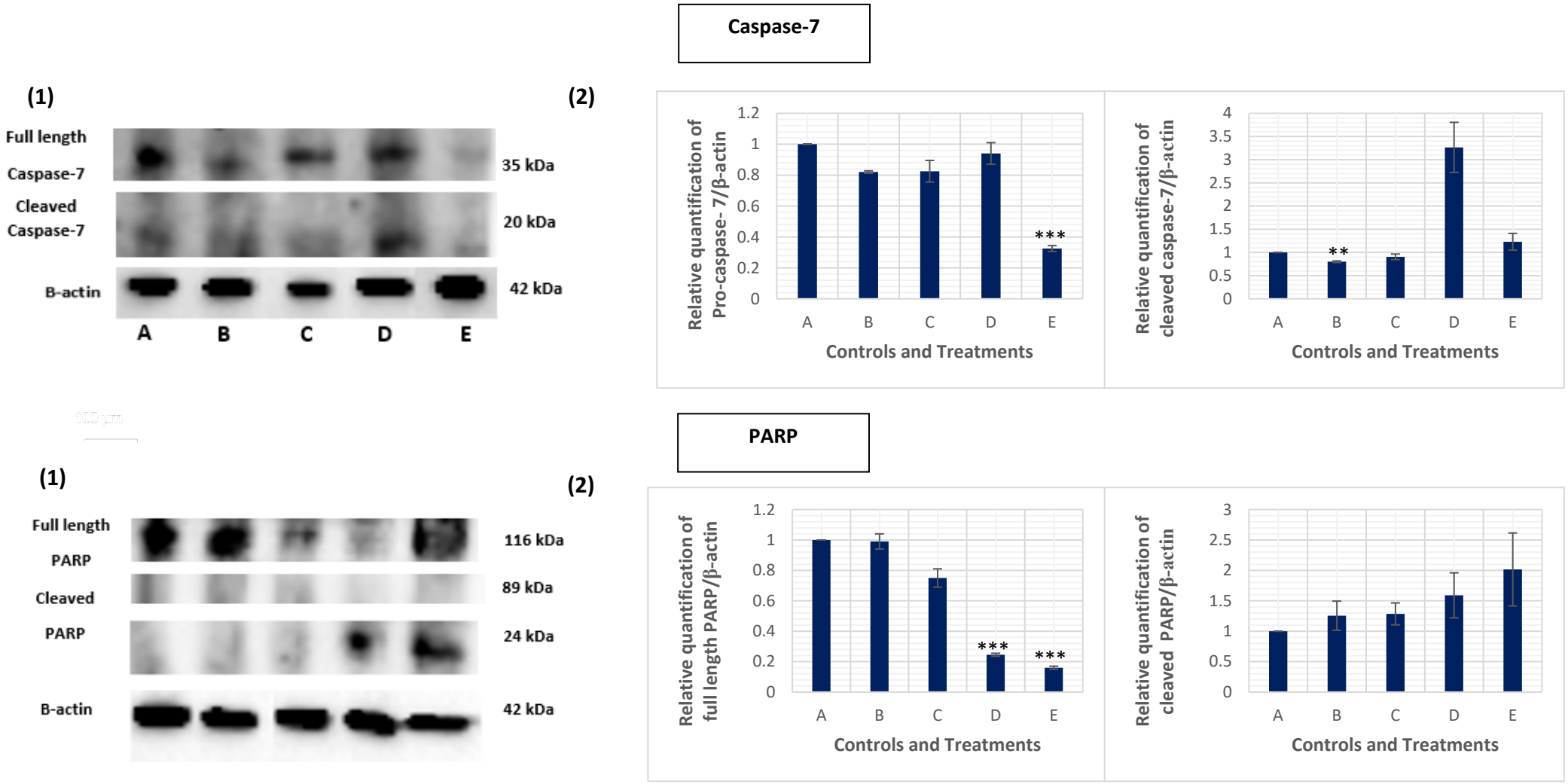

Figure 3.20A*:* Western blot profiles of pro-apoptotic proteins Caspase-7 and PARP (1) and their respective relative quantification (2) in the **MCF-7** cell line. Cells were either left untreated (A) or treated with 1% DMSO (B), UJ3 20 µM (C), UJ3 IC_{50} 14.1 µM (D) and CDDP 200 µM (E) **post-24 hrs**. Pro-forms and cleaved forms of the *apoptotic* proteins were normalized against the beta-actin loading control. The error bars are representative of ± SEM (n = 2), the asterisks represent significant differences with respect to the untreated control (100%) (p < 0.001 = ***; p < 0,01 = **).

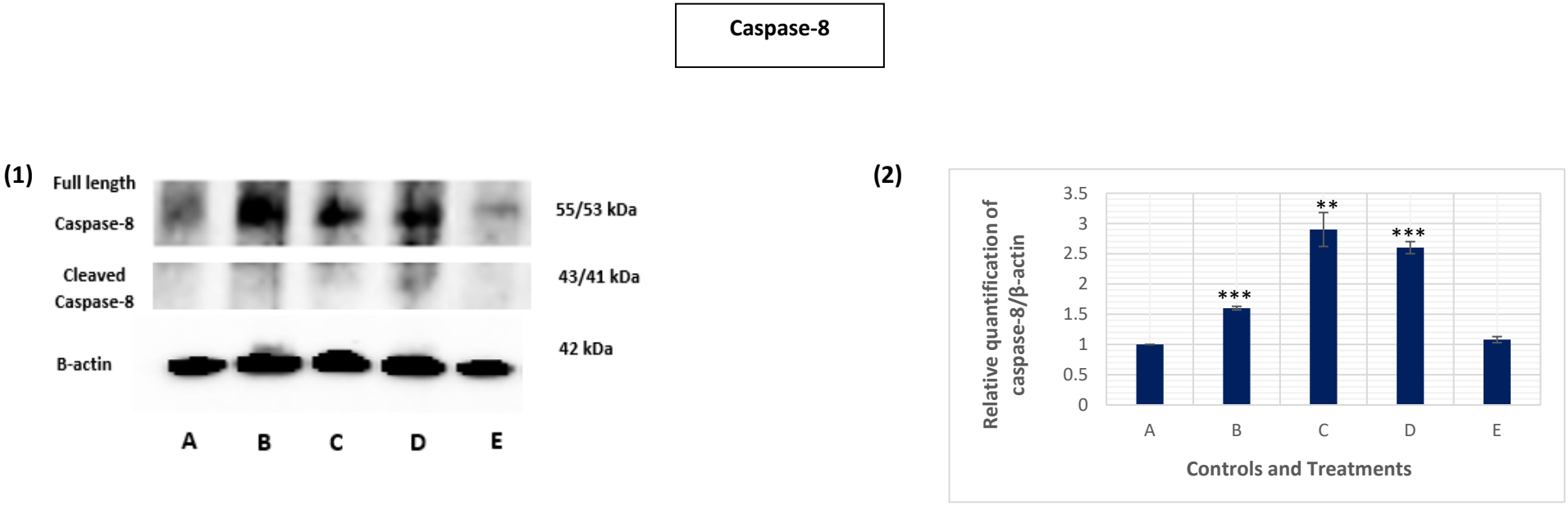

Figure 3.20B*:* Western blot profile of pro-apoptotic protein Caspase-8 (1) and its respective relative quantification (2) in the **MCF-7** cell line. Cells were either left untreated (A) or treated with 1% DMSO (B), UJ3 20 μM (C), UJ3 IC_{50} 14.1 μM (D) and CDDP 200 μM (E) **post-24 hrs**. Pro-forms and cleaved forms of the apoptotic proteins were normalized against the beta-actin loading control. The error bars are representative of ± SEM (*n* = 2), the asterisks represent significant differences with respect to the untreated control (100%) ($p < 0.001$ = ***; $p < 0{,}01$ = **).

The MDA-MB-231 caspase-3 profile (Figure 3.21A) detects the presence of the full-length pro-caspase-3 (35 kDa) with no active form for all controls and treatments. Similarly, the entire length of PARP (116 kDa) (Figure 3.21A) and pro-caspase-7 (35 kDa) (Figure 3.21B) was detected for all controls and treatments with no corresponding active form presence. Pro-caspase-8 was detected in all controls and treatments (55 / 53 kDa). However, the active form was absent (Figure 3.21B).

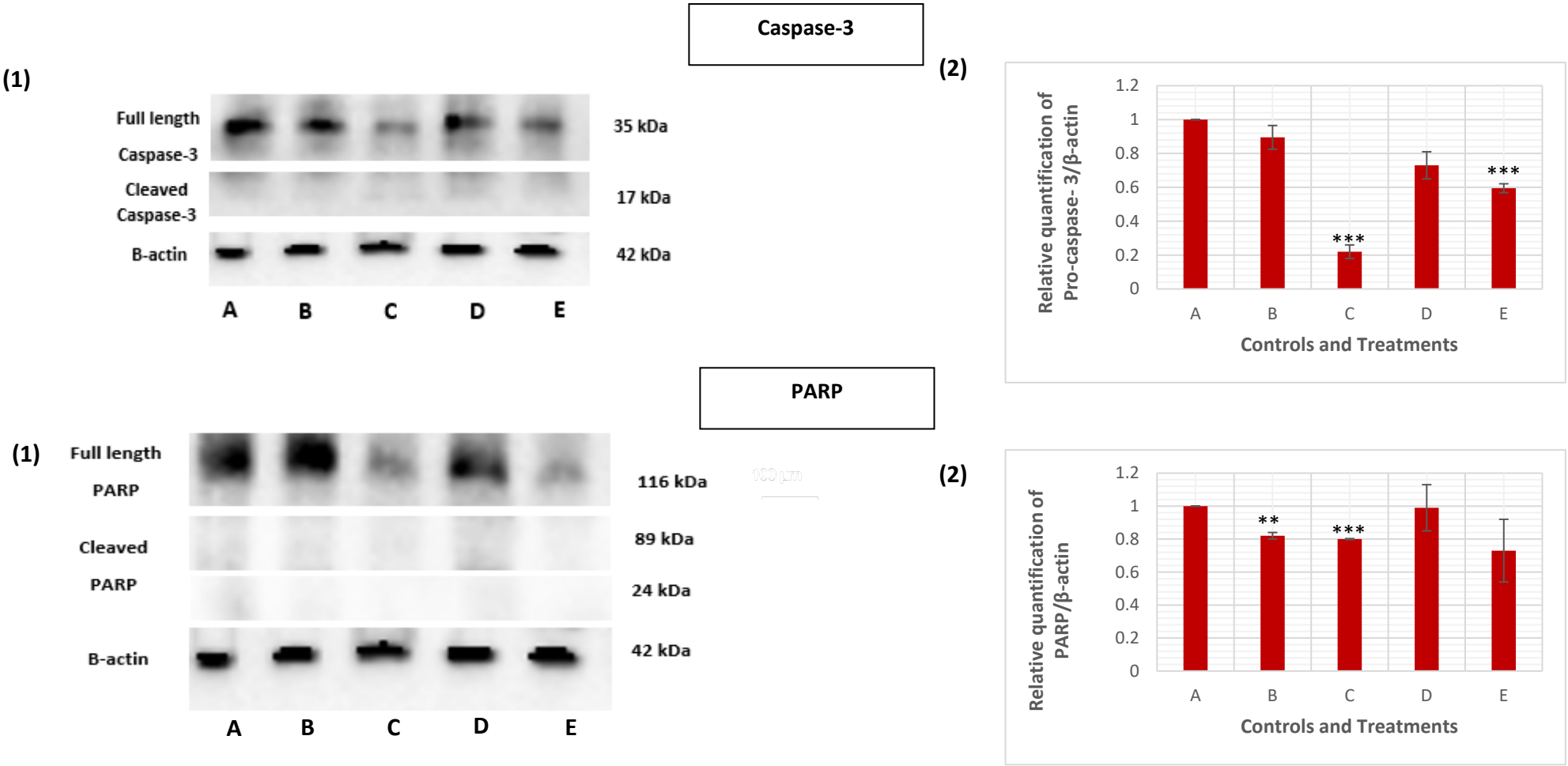

Figure 3.21A*:* Western blot profiles of pro-apoptotic proteins Caspase-3 and PARP (1) and their respective relative quantification (2) in **MDA-MB-231**. Cells were either left untreated (A) or treated with 1% DMSO (B), UJ3 IC_{50} 13.6 µM (C), UJ3 20 µM (D) and CDDP 200 µM (E) **post-24 hrs**. Pro-forms and cleaved forms of the apoptotic proteins were normalized against the beta-actin loading control. The error bars are representative of ± SEM (n = 2), the asterisks represent significant differences with respect to the untreated control (100%) (p < 0.001 = ***; p < 0,01 = **).

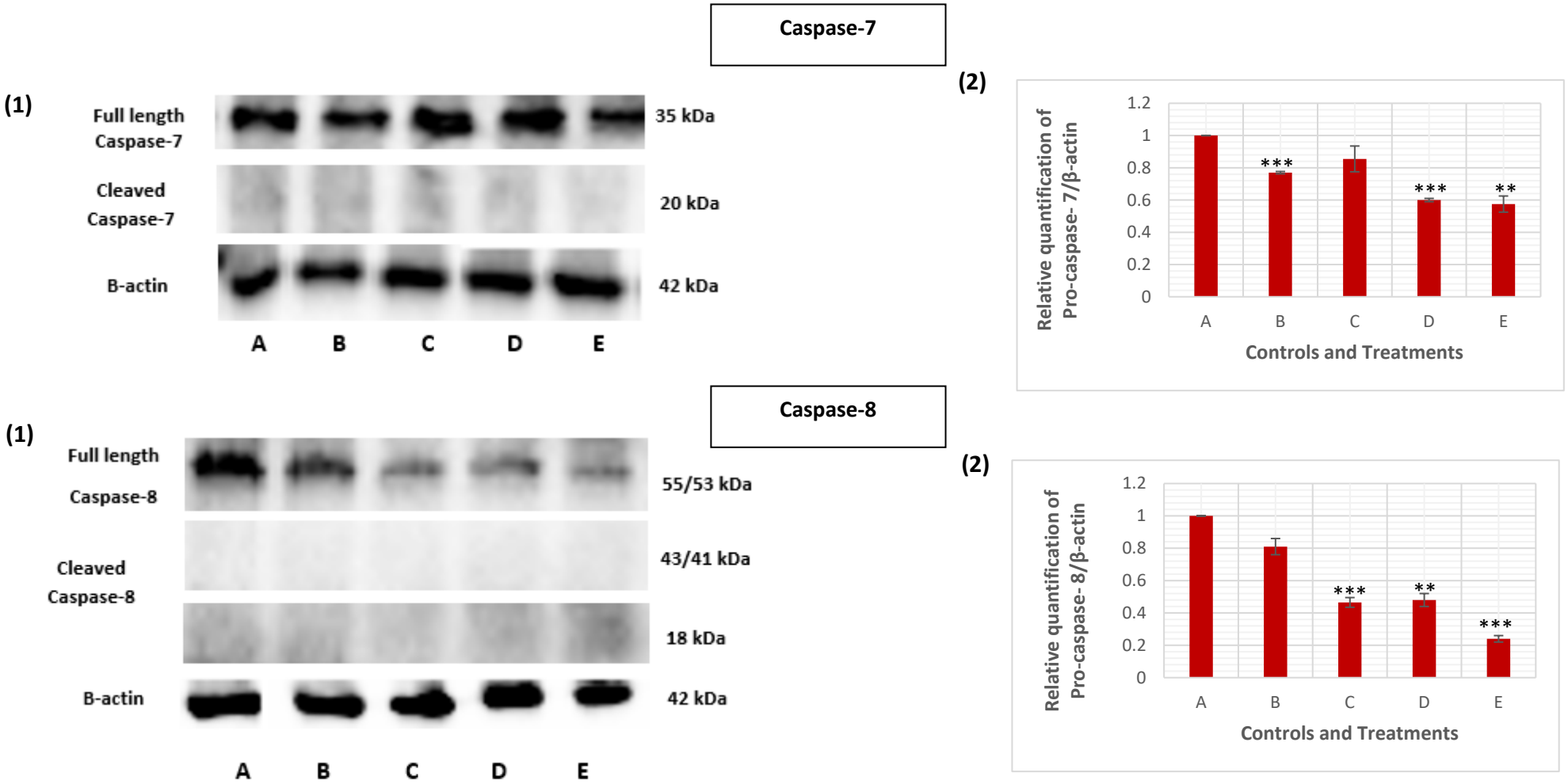

Figure 3.21B*:* Western blot profiles of pro-apoptotic proteins Caspase-7 and Caspase-8 (1) and their respective relative quantification (2) in **MDA-MB-231**. Cells were either left untreated (A) or treated with 1% DMSO (B), UJ3 IC_{50} 13.6 µM (C), UJ3 20 µM (D) and CDDP 200 µM (E) **post-24 hrs**. Pro-forms and cleaved forms of the apoptotic proteins were normalized against the beta-actin loading control. The error bars are representative of ± SEM (n = 2), the asterisks represent significant differences with respect to the untreated control (100%) ($p < 0.001$ = ***; $p < 0,01$ = **).

3.5 Caspase Independent cell death and AIF

Western blot results of the MDA-MB-231 cell line prompted the study of AIF and its role in CICD due to the absence of caspase cleavage (Figure 3.21). The AIF flavoprotein is a ROS scavenger and an apoptosis assistant independent of caspases. AIF is a resident of the mitochondrial intermembrane space and when acted upon by an apoptotic stimulus, AIF translocates into the cytosol and interacts with nuclei. Subsequently, promoting chromatin condensation along the periphery and extensive DNA fragmentation (Barbosa *et al*., 2016; Loane *et al*., 2015). The MDA-MB-231 depicted extensive DNA fragmentation (Figure 3.19 (D)) and chromatin condensation (Figure 3.19 (C)). Furthermore, when AIF is overexpressed, a swift loss in $\Delta\Psi m$ is noted and more PS is exposed (Feng and Koh, 2013). A loss in $\Delta\Psi m$ was observed in both MCF-7 and MDA-MB-231 post-UJ3 treatment (Figure 3.12 (C), Figure 3.13 (D), Figure 3.17 (C - E)) and Figure 3.19 (C - E)). UJ3 stimulated PS exposure in both cell lines (Figure 3.10 (C)) and Figure 3.11 (C)).

The localization and migration of AIF were tracked in the MCF-7 and MDA-MB-231 by Alexa-488 dye. The cell nuclei were labeled with Hoechst 33258, the mitochondria with MitoTracker orange and AIF protein with Alexa-488 tagged anti-AIF antibody. Full images of the MCF-7 (Figure 3.22) and MDA-MB-231 (Figure 3.24) were included. The cells marked with arrows in the full images are depicted as enlarged images for the MCF-7 (Figure 3.23) and MDA-MB-231 (Figure 3.25) and will be discussed in more detail. In addition to the UJ3 and CDDP treatment concentrations used in the western blot technique, a 10 µM UJ3 treatment was included to detect whether any AIF leakage would occur at a lower concentration.

The MCF-7 controls (Figure 3.23 (A – B)) indicate the localization of AIF within the mitochondrial intermembrane space. Similarly, AIF appeared as green, fluorescent speckles within the mitochondrial intermembrane space post-UJ3 treatment (10 µM and 14.1 µM) (Figure 3.23 (C – D)). UJ3 (20 µM) treatment (Figure 3.23 (E)) indicated that the majority of AIF was localized to the mitochondrial intermembrane space; however, minor fluorescence within the nuclei space was observed when compared to the Hoechst 33258 nuclei staining (which depicted chromatin condensation as well). AIF appeared localized to the mitochondrial intermembrane space post-CDDP treatment (200 µM) (Figure 3.23 (F)).

The MDA-MB-231 controls (Figure 3.25 (A – B)) indicate the localization of AIF to the mitochondrion. Similarly, AIF was localized when treated with UJ3 (10 µM) (Figure 3.25 (C)). However, UJ3 treatment (13.6 µM and 20 µM) (Figure 3.25 (D - E)) resulted in bright green fluorescence detection corresponding to the area of the nuclei space (marked by white arrows). As the UJ3 concentration rised from (13.6 µM) to (20 µM) so did AIF fluorescence become more prominent (Figure 3.25 (D - E)). As a result, UJ3 treatment promoted apoptotic

AIF translocation to the nuclei. Moreover, AIF translocation was made evident by the co-localization of the dyes in the merged images (Figure 3.25 (D – E)). This confirms that the MDA-MB-231 follows a caspase-independent apoptotic cell death mechanism. AIF appeared localized to the mitochondrial intermembrane space post (200 μM) CDDP treatment (Figure 3.25 (F)).

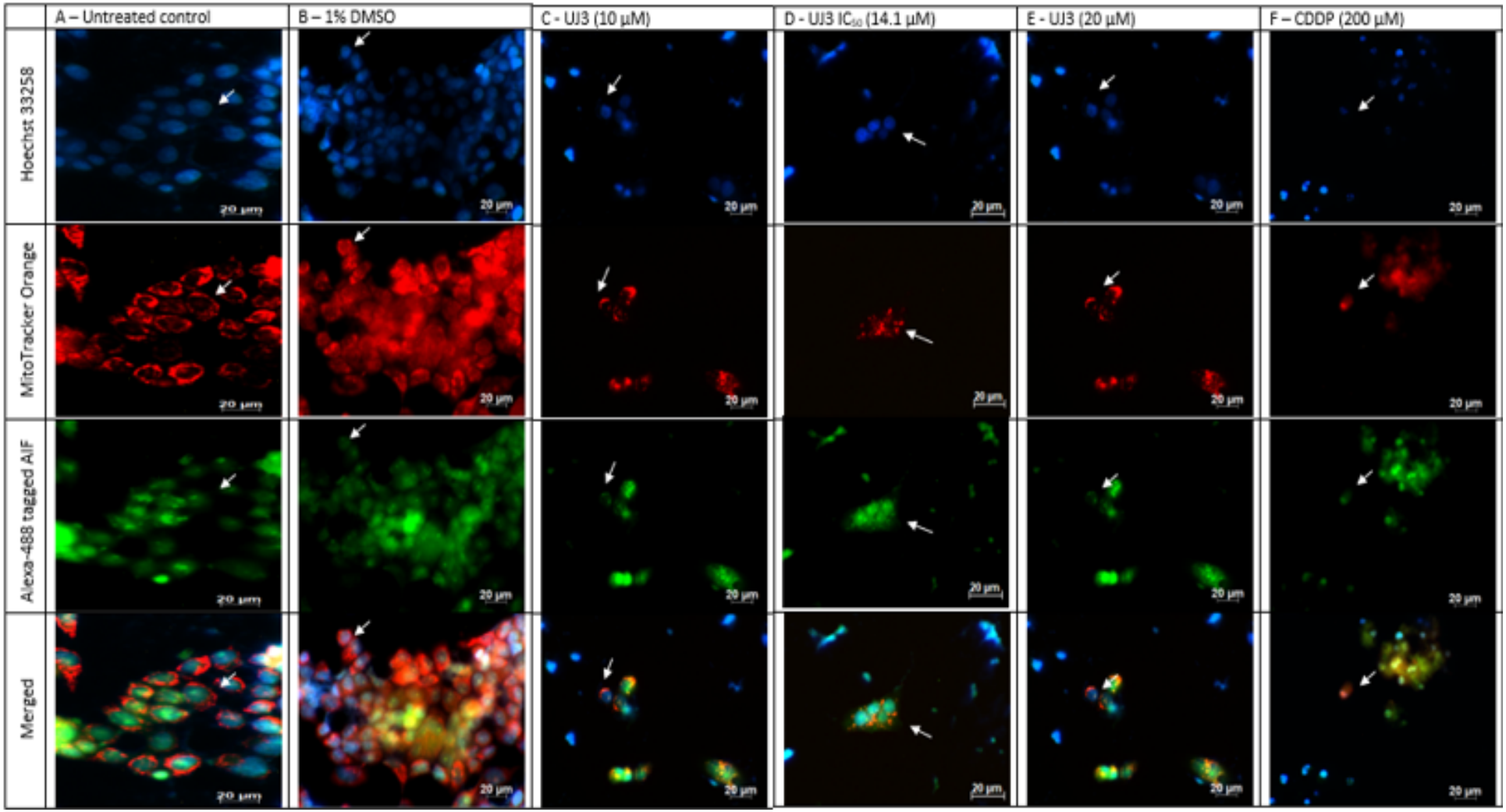

Figure 3.22: Intracellular fluorescent micrographs (1000X magnification) of **MCF-7** cells. Cells were left untreated (A) or treated with either 1% DMSO (B), UJ3 10 µM (C), UJ3 IC_{50} 14.1 µM (D), UJ3 20 µM (E) and CDDP 200 µM (F) **post-24 hrs**. The nuclei were labeled with Hoechst 33258, mitochondria with MitoTracker Orange and AIF with Alexa-488 tagged anti-AIF antibody. Cells marked with an arrow are enlarged in Figure 3.23.

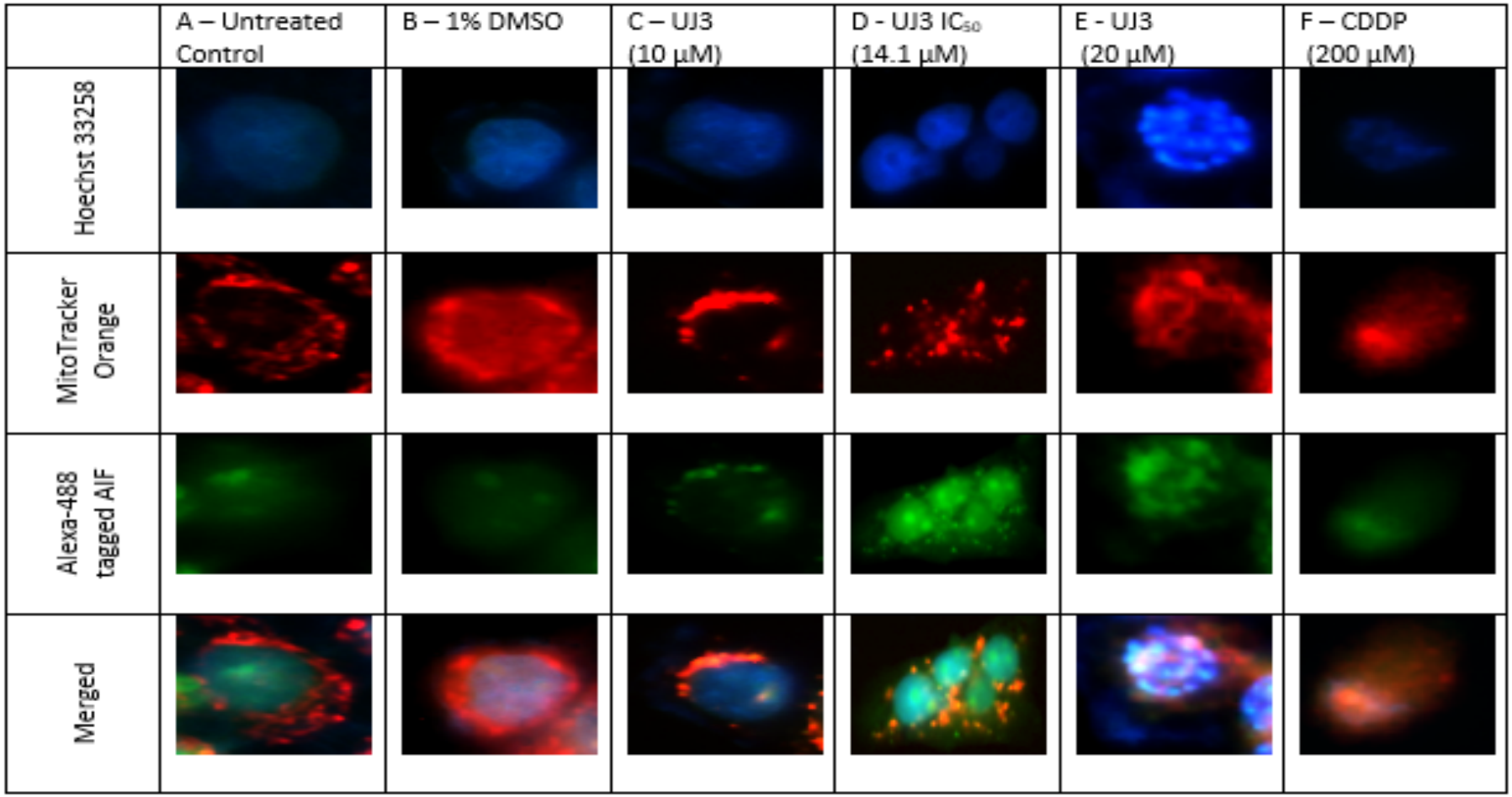

Figure 3.23*:* Intracellular fluorescent micrographs of **MCF-7** enlarged from Figure 3.22. Cells were left untreated (A) or treated with either 1% DMSO (B), UJ3 10 µM (C), UJ3 IC_{50} 14.1 µM (D), UJ3 20 µM (E) and CDDP 200 µM (F) **post-24 hrs**. The nucleus was labeled with Hoechst 33258, mitochondrion with MitoTracker Orange and AIF with Alexa-488 tagged anti-AIF antibody. Minor translocation of AIF to the nuclei was observed post-UJ3 treatment (E).

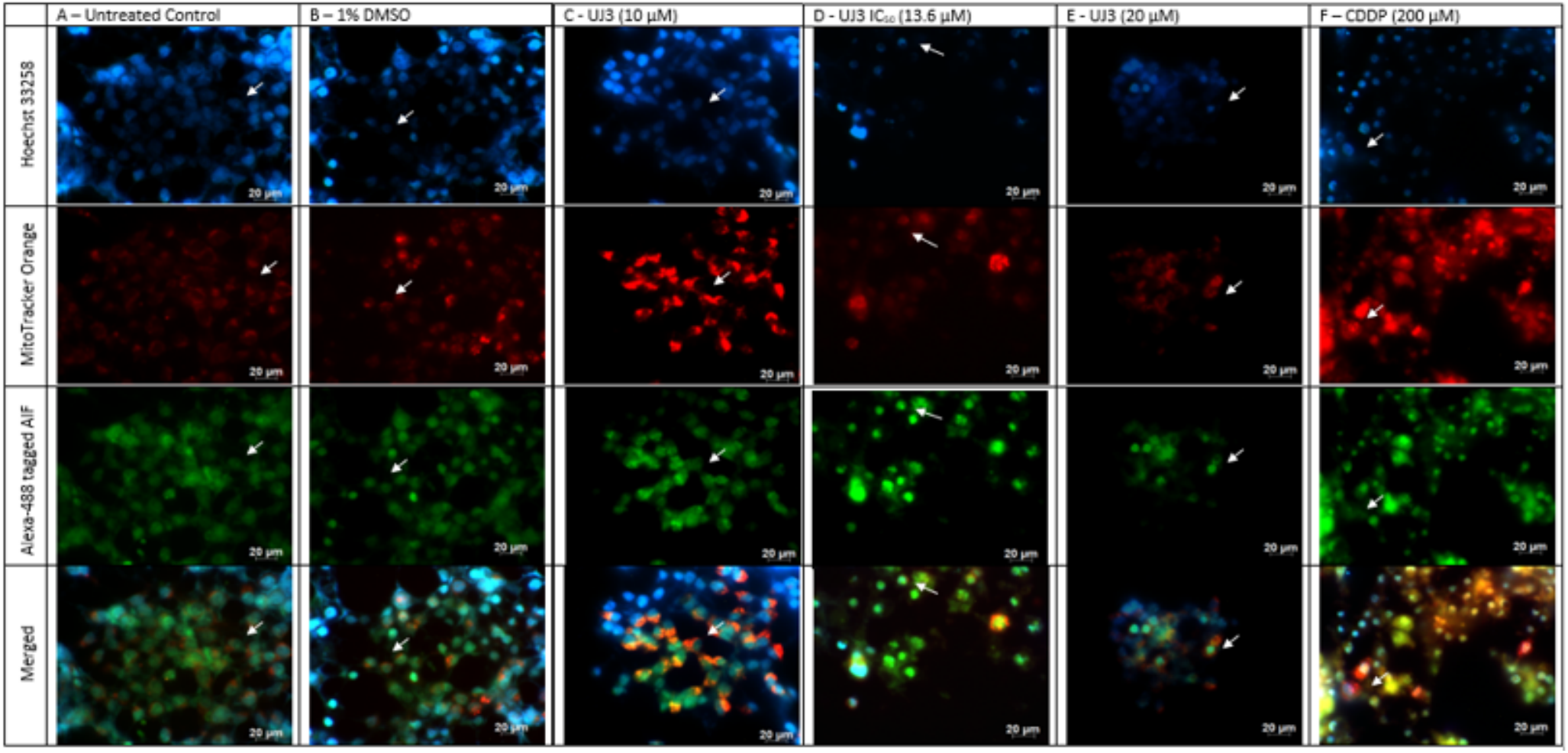

Figure 3.24: Intracellular fluorescent micrographs (1000X magnification) of **MDA-MB-231** cells. Cells were left untreated (A) or treated with either 1% DMSO (B), UJ3 10 µM (C), UJ3 IC_{50} 13.6 µM (D), UJ3 20 µM (E) and CDDP 200 µM (F) **post-24 hrs**. The nuclei were labeled with Hoechst 33258, mitochondria with MitoTracker Orange and AIF with Alexa-488 tagged anti-AIF antibody. Cells marked with an arrow are enlarged in Figure 3.25.

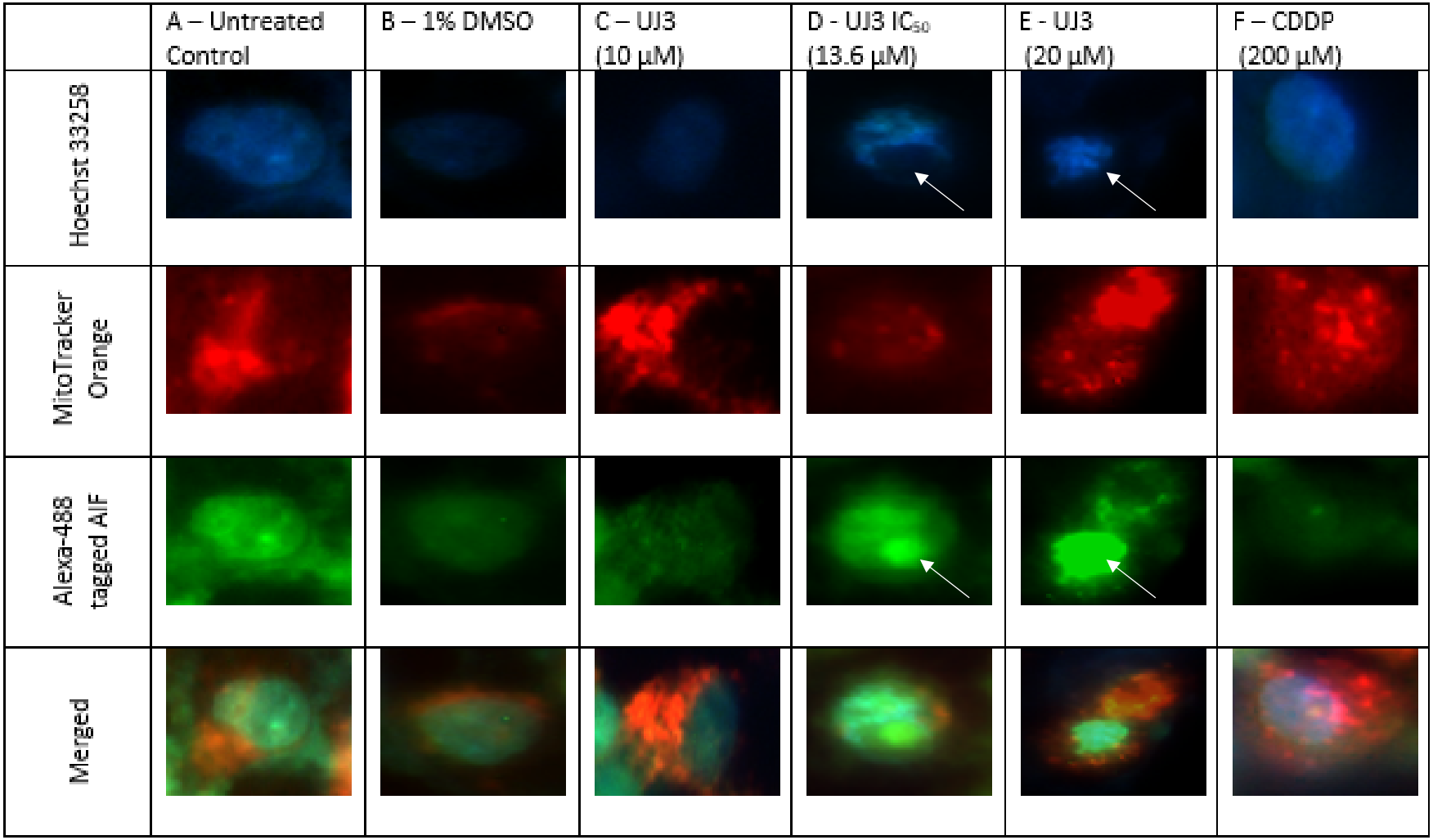

Figure 3.25: Intracellular fluorescent micrographs of **MDA-MB-231** enlarged from Figure 3.24. Cells were left untreated (A) or treated with either 1% DMSO (B), UJ3 10 µM (C), UJ3 IC_{50} 13.6 µM (D), UJ3 20 µM (E) and CDDP 200 µM (F) **post-24 hrs**. The nucleus was labeled with Hoechst 33258, mitochondrion with MitoTracker Orange and AIF with Alexa-488 tagged anti-AIF antibody. Major translocation of AIF to the nuclei was observed post-UJ3 treatment (E)

Chapter 4: Discussion

Introduction

The potency of CDDP and its derived analogues set off the study of diverse gold complexes in pursuit of metals with high potency and reduced toxicity. Gold complexes ligated to phosphines demonstrated significant cytotoxicity. Phosphines are often exploited as ligands in organic synthesis and anti-cancer metallodrugs due to their involvement in biological reactions such as interactions with ROS, disulfides, or phosphonium salts. Furthermore, phosphines possess a strong affinity for transition metals and when conjugated to metals, their complexes are kinetically stable in many oxidation states (Berners-Price and Sadler, 1988). Studies with bischelated Au (I) phosphines which contain a diphenylphosphine (dppe), revealed that the active component of the complex was induced by the cationic ion and was applicable in treating various tumors in mice models. However, the application of many Au (I) complexes were limited by severe toxicity in dogs due to non-selective lipophilic mitochondrial dysfunction in all cells (Berners-Price and Sadler, 1988; Harker *et al*., 1991; Kriel and Coates, 2012). The high toxicity of gold and platinum-based complexes and the accompaniment of cell death resistance led researchers to explore the cytotoxicity of safer metals such as silver (Raju *et al*., 2022).

Numerous studies reported the anti-proliferative effects of silver complexes. Silver metals were adjoined to various ligands such as carboxylates, N-heterocyclic carbenes (NHC), NSAIDS, Schiff bases and phosphines all of which demonstrated anti-cancer properties. Silver ligand complexes with a higher amount of silver ions had enhanced activity and appeared less toxic (Raju *et al*., 2022). More specifically, binuclear Ag (I) complexes possessed significant anti-cancer activity. Binuclear Ag (I)-triphenylphosphine complexes were cytotoxic against MDA-MB-231 cells, Ag (I)-5,5-diethyl barbiturate-bis(dppe) alkane complexes produced higher cytotoxicity to MCF-7 than carboplatin complexes with minimal toxicity to non-malignant cell lines. Silver complexes with phosphines or thiazolidine ligands demonstrated *in vitro* cytotoxicity against MDA-MB-231 and MCF-7 cell lines. The use of silver complexes in treating breast, colorectal, lung and ovarian tumors has been well documented and recorded to show greater cytotoxicity than CDDP (Canudo-Barreras *et al*., 2021; Harurluoglu *et al*., 2021; Raju *et al*., 2022).

A novel class of complexes without the conventional ‘coinage’ metal type were synthesized and exhibited high anti-cancer potential. The Ag (I) thiocyanate complexes fall into this category (Meijboom *et al*., 2009). Ag (I) thiocyanate complexes with varying ratios of metal to ligand revealed anti-cancer activity against MCF-7 cells with minimal cytotoxicity to non-malignant cell lines. Ag (I) thiocyanate complexes were cytotoxic to the MCF-7 cell line and

the isolated ligand appeared non-toxic (Ferreira *et al*., 2015). UJ3 demonstrated high cytotoxicity to SNO oesophageal cells with greater efficacy than CDDP and minimal toxicity (Engelbrecht *et al*., 2018).

In the current study, UJ3 (Figure 4.1) cytotoxicity was assessed on MCF-7 and MDA-MB-231 breast cancer cell lines. Both cell lines are invasive ductal carcinomas but are vastly different regarding phenotypical and genotypical characteristics. MCF-7 cell lines are hormone receptor (ER α+) (luminal A subtype) positive. In contrast, MDA-MB-231 cell lines are of the triple-negative subtype, related to poor prognosis and limited treatments. Moreover, high penetrance *BRCA* mutations make this cell line highly resistant to many treatment options. Concerning ATP generation, MCF-7 cells prefer oxidative phosphorylation and increase glycolytic activity as conditions of hypoxia increase. MDA-MB-231 cells, conversely, are reliant mainly on glycolysis and select the Warburg effect (Theodossiou *et al*., 2019). Lastly, MCF-7 cells are epithelial type and are sensitive to CDDP, whereas MDA-MB-231 are CDDP-resistant and appear mesenchymal in phenotype (Koh *et al*., 2021; Theodossiou *et al*., 2019). Therefore, the effect of UJ3 on these two vastly different malignant breast cancer types is of interest.

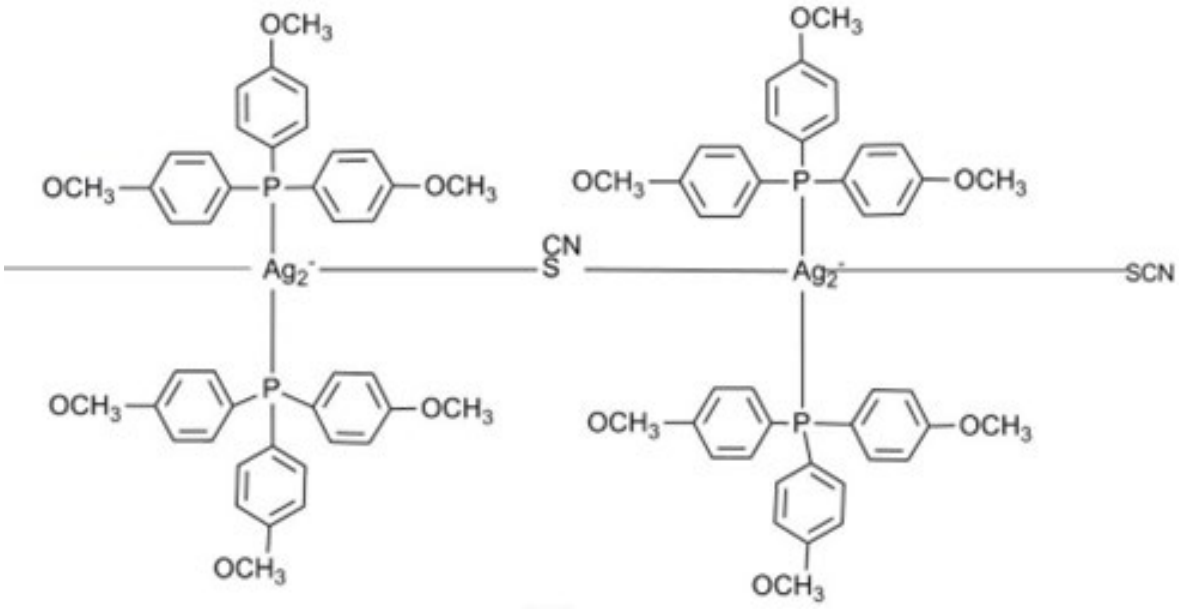

Figure 4.1: Molecular structure of dimeric Silver (I) thiocyanate 4-methoxyphenyl phosphine (UJ3) [Ag SCN{p(4-$MeOC_6H_4$)$_3$}$_2$]$_2$. The thiocyanate anion is co-ordinately bound to binuclear silver atoms; each silver atom is adjoined to two phosphine ligands (Adapted from Engelbrecht *et al*., 2018).

4.1 Cytotoxicity assessment of UJ3

4.1.1 Screening for potency

In keeping with the aforementioned anti-cancer potential of Ag (I) phosphine complexes, UJ3 demonstrated cytotoxicity in both MCF-7 and MDA-MB-231 malignant cell lines during the 24 hr alamar blue® dose-response study (Figure 3.1). In the 24 hr study, UJ3 required an IC_{50} of 14.1 µM to inhibit 50 % of the MCF-7 cell population and an IC_{50} of 13.6 µM for the MDA-MB-231 cell line (Table 3.1). The resultant IC_{50} in the present study falls within the range of reported *in vitro* IC_{50} concentrations of anti-cancer silver complexes. For instance, silver thiosulfate complexes had an IC_{50} of 21.3 µM against MCF-7 (Ota *et al*., 2021) and amino-NHC Ag complexes had an IC_{50} of 28.68 µM against the MCF-7 cell line (Wang *et al*., 2011). Furthermore, UJ3 against SNO cells had an IC_{50} of 3.5 µM (Engelbrecht *et al*., 2018) and Ag (I) phosphine complexes with varying ligand ratios against MCF-7 cells had an IC_{50} range of 3 - 3.59 µM (Ferreira *et al*., 2015). Silver complexes with tri(*p*-tolyl) phosphine ligands had an IC_{50} range of 1.8 - 28 µM in murine leukemia cells (Zartilas *et al*., 2009). Novel Ag (I) triphenylphosphine complexes had IC_{50} values ranging from 5.6 - 18 µM post-48 hr incubations in A549, MCF-7 and MDA-MB-231 cell lines (Silva *et al*., 2020).

4.1.2 Selectivity evaluation

According to Chatelut *et al*. (2003), A limiting factor in the drug discovery process of cytotoxic anti-cancer agents is their toxicity to non-malignant cell lines, which may predict possible side effects later in the drug discovery process. A drug with high toxicity to non-malignant cell lines hinders its pharmacodynamic profile and is eliminated early in the drug discovery process (Chatelut *et al*., 2003). A drug's *in vitro* toxicity and selectivity pave the future for *in vivo* and potential clinical trials (Zhang *et al*., 2020). Thus, UJ3 toxicity to non-malignant HEK-293 and MRHF-1 cell lines was evaluated by the alamar blue® proliferation assay (Figure 3.1). The immortalized HEK-293 cell line is a standard non-malignant cell line adopted in cancer research. HEK-293 cells grow well due to transformation with adenovirus 5 DNA (Lin *et al*., 2014). The MRHF-1 fibroblasts are a primary cell line and represent an improved model to assess drug screening on healthy human cells. MRHF-1 has not been transformed and represents high relevance to the origin of isolation (Lee *et al*., 2000). UJ3 appeared selective to both malignant cell lines over the HEK-293 across the entire concentration range (Figure 3.1). Furthermore, UJ3 was highly selective for both malignant cell lines compared to the MRHF-1 fibroblasts except at the highest treatment concentration of 20 µM (Figure 3.1). The UJ3 IC_{50} concentrations for both malignant cell lines are lower than the non-malignant cell lines (Table 3.1); this indicates that UJ3 has greater selectivity for malignant cell lines and desirably lower toxicity to non-malignant cell lines. The higher selectivity profiles of Ag (I)

phosphine complexes for malignant over non-malignant cell lines were reported in many studies (Engelbrecht *et al*., 2018; Ferreira *et al*., 2015; Yilmaz *et al*., 2017).

Many anti-cancer agents aim to target the mitochondria. The $[Au(dppe)_2]Cl$ complexes displayed cytotoxic activity but their application was limited due to the non-selective uptake of the drug into the mitochondria, which promoted high toxicity. The non-selective uptake was based on the high lipophilicity of the cationic complex (McKeage *et al*., 2000). Many researchers aimed to design complexes with a selective hydro-lipophilicity balance to target the mitochondria. A study altered the lipophilic characteristics of Ag (I) complexes via the addition of heteroatoms or hydrazine bridges, which influenced the lipophilic character of the complex. Au (I) hydrazine bridged-diphosphine complexes and Ag (I) bischelated complexes with altered lipophilicity demonstrated enhanced mitochondrial selectivity in a panel of malignant cell lines including MCF-7 at low nM or μM IC_{50} concentrations (Kriel and Coates, 2012). It has been suggested that Au (I) and Ag (I) lipophilic cations or ligated phosphine lipophilicity are linked to the entrance and accumulation of these complexes in the mitochondria of malignant cells (Engelbrecht *et al*., 2018; Berners-Price and Sadler, 1988; Medici *et al*., 2016). The cytotoxicity profile of Au (I) diphosphine complexes may be attributed to their strong lipophilicity allowing mitochondrial entrance. In addition, active phosphines with thermodynamic and kinetic stability at the target region inhibited toxicity to non-malignant cells *in vivo* (Berners-Price and Sadler, 1988). UJ3 demonstrated high selectivity and since the ligated phosphines are lipophilic, it may be hypothesized that a favorable balance of lipophilic character in UJ3 may influence its selective uptake in the mitochondria of malignant cells.

The mitochondrial inner membrane has a negative membrane potential; thus, positive lipophilic cations can bind to the matrix and accumulate in the mitochondria against the concentration gradient. Alkyltriphenylphosphonium, rhodamine and cyanine are cations that may be ligated to complexes to accumulate in the matrix of the mitochondria based on the Nernst equation (Mahepal *et al*., 2008; Zielonka *et al*., 2017). In order for the cationic lipophilic complex to accumulate in the mitochondria, it needs to migrate through the plasma and mitochondrial membrane, both of which have a negative membrane potential. Subsequently, allowing the accumulation of the cationic drug in the cytosol and then in the mitochondria. The plasma membrane potential initiates a 3-5-fold accumulation of the cationic drug in the cytosol compared to that in the extracellular medium. Thereafter, the higher mitochondrial membrane potential further amplifies the drug concentration by a factor of 100-1000 (Zielonka *et al*., 2017). According to McKeage *et al*. (2000), malignant cells are associated with higher transmembrane potentials; this may be implicated due to the preference of glycolysis in the cytosol for ATP production rather than oxidative phosphorylation in the mitochondria of certain malignancies. Therefore, this amplified accumulation of cytotoxic anti-cancer agents is

beneficial in targeting malignant cells with their high membrane potentials (McKeage *et al*. 2000). Accordingly, UJ3 may exert its selectivity based on the high membrane potentials of malignant cells compared to the non-malignant and its cytotoxicity may have been influenced by accumulation in the mitochondria.

4.1.3 Drug recovery/resistance evaluation

Recovery or drug resistance is a significant impediment in developing anti-cancer drugs, highly potent drugs such as CDDP are susceptible to cancer recovery (Patwardhan *et al*., 2021; Skowron *et al*., 2021). Approximately 90% of chemotherapeutic agents fail to treat invasive malignancies due to resistance (Mansoori *et al*., 2017). In the present study, UJ3 sustained cytotoxicity in the 48 hr study against the MCF-7 cell line and had an IC_{50} of almost half that in the 24 hr study (7.6 μM) (Figure 3.2 and Table 3.1). Similar to the 24- hr study, UJ3 illustrated higher cytotoxicity and selectivity to the MCF-7 than the non-malignant cell lines in the 48 hr study. This indicates that UJ3 features potential pharmacological properties against the MCF-7 cell line with no recovery post-48 hrs.

However, the MDA-MB-231 cell line recovered in the 48 hr study as the IC_{50} increased (21.6 μM) (Figure 3.2 and Table 3.1). Multi-drug resistance (MDR) is facilitated by the high expression of p-glycoprotein (P-gp), which subsequently serves as an efflux pump for a spectrum of therapeutic drugs. Many chemotherapeutic drugs may activate MAPK or protein kinase c pathways which stimulate the expression of P-gp and this influences the transport of the drug in MDR cell lines (Bagowski, 1999; Chen *et al*., 2011; Hofmann, 2004). Protein kinase D (PKD) regulates many signaling pathways, including the MAPK pathway and thus MDR. PKD2 is an isoform of PKD and is highly expressed in MDR cell lines such as MDA-MB-231. As a result, overexpression of P-gp in MDA-MB-231 has been linked to resistance in a range of chemotherapeutic drugs. A study that used shRNA to knock down PKD2 in MDA-MB-231 reported lower IC_{50} and resistance indexes against the therapeutic agent paclitaxel (Chen *et al*., 2011). The increased IC_{50} in the MDA-MB-231 may be a result of high P-gp expression in this cell line that promoted high efflux of UJ3 enabling cell recovery.

Since drug resistance is multifactorial other recovery mechanisms include inactivation of the drug, decreased drug cumulation, altered expression of genes involved in cell survival, protein trafficking, changes in cell transporters and ABC transporters promoting drug expulsion, signals or circuits that promote apoptosis evasion, alterations to drug targets such that the drug can no longer elicit a response from the target, changes in metabolism or epigenetics and enhancement of DNA repair mechanisms (Mansoori *et al*., 2017; Molinaro *et al*., 2020). Intrinsic factors influencing genetic stability and epigenetics promote tumor heterogeneity, stimulating drug resistance. Mutations involved in drug transporters may prevent drug binding

or reduce the number of available transporters limiting the absorption of the drug. Recovery may be through up-regulation of anti-apoptotic genes (*BCL-2* or *AKT*) and down-regulation of pro-apoptotic genes (*Bax* or *Bak*) (Mansoori *et al*., 2017). High expression or modification of enzymes (glutathione) that metabolize drugs or carrier molecules were also reported to promote cell recovery and reduce drug plasma concentrations (Luqmani, 2005).

4.1.4 Evaluation of UJ3 to the reference drug CDDP

CDDP has been a standard anti-cancer agent for over four decades (Skowron *et al*., 2021). CDDP is currently used to treat many malignancies ranging from head and neck carcinomas, breast cancer, non-Hodgkin's lymphoma, non-small lung cancer, reproductive organ malignancies, osteosarcomas to neuroendocrine malignancies. Systemic treatment regimens often include CDDP with a combination of drugs such as 5-fluorouracil or etoposide for enhanced treatment response. The positive charge of CDDP facilitates interaction with DNA, RNA and proteins (Dasari and Bernard Tchounwou, 2014; Skowron *et al*., 2021). CDDP has an affinity for interacting with the N7 region of the guanosine and adenosine bases. Subsequently, forming mono adducts with inter/ intrastrand crosslinks. The DNA crosslinks inhibit the replication of DNA and transcription of RNA. The unrepaired DNA will lead to single or double-strand breaks and trigger apoptosis. CDDP may also affect the G2/M and S phases of the cell cycle to promote apoptosis (Jafarzadeh *et al*., 2022; Skowron *et al*., 2021). However, the high anti-cancer potency of CDDP induces toxicity to non-malignant cells. The high toxicity raises side effects, including hair loss, damaged nerves, renal damage, ototoxicity, hemolytic anemia, gastrointestinal symptoms and myelosuppression (Astolfi *et al*., 2013; Jafarzadeh *et al*., 2022). Moreover, tumors employ multiple pathways to promote CDDP resistance. Tumors may promote high CDDP efflux and low drug influx, enhance intracellular inactivation or DNA repair mechanisms, promote low adduct development and high anti-apoptotic signals. CDDP resistance may be intrinsic to the cell or acquired over time (Skowron *et al*., 2021).

In the present study, CDDP served as the positive apoptosis control and was compared to the efficacy of UJ3. In both 24 hr and 48 hr studies, the resultant IC_{50} values indicated that UJ3 was more cytotoxic to the MCF-7 cell line than CDDP. Moreover, UJ3 resulted in lower toxicity to the non-malignant cell lines than CDDP (Figure 3.1, Figure 3.2, Figure 3.3 A and B and Table 3.1). UJ3 demonstrated cytotoxicity and selectivity to MDA-MB-231 during the 24 hr study (Figure 3.1 and Table 3.1) but recovered in the 48 hr study (Figure 3.2). MDA-MB-231 was highly resistant to CDDP in both 24 hr and 48 hr studies (Figure 3.3 A and B and Table 3.1). The improved cytotoxicity and selectivity of Ag (I) complexes compared to CDDP *in vitro* have been well documented (Engelbrecht *et al*., 2018; Canudo-Barreras *et al*., 2021; Ferreira *et al*., 2015; Harurluoglu *et al*., 2021; Medvetz *et al*., 2008; Potgieter *et al*., 2016; Stryjska *et al*., 2020).

4.1.5 Evaluation of UJ3 on cellular respiration

The CellTiter-Glo® Luminescent viability assay was employed to monitor UJ3s influence on cellular respiration by detecting changes in ATP levels. In the MCF-7, UJ3 generated a 6.9% greater reduction of ATP at a concentration 10X lower than CDDP (Figure 3.4). This coincides with the mitochondrial activity measured by the alamar blue® assay (Figure 3.1 and Figure 3.3 A). In the MDA-MB-231, UJ3 resulted in a 21.6% greater ATP reduction and impact on cellular respiration than CDDP (Figure 3.5). This correlates with the mitochondrial activity measured by the alamar blue® proliferation assay. Overall, UJ3 influenced cellular respiration, mitochondrial activity and consequently mitochondrial bioenergetics more severely in the MCF-7 than in the MDA-MB-231 cell line.

Metabolically MCF-7 cells are of the Pasteur type implying they prefer oxidative phosphorylation and increase glycolytic activity as conditions of hypoxia increase. In contrast, MDA-MB-231 mainly relies on glycolysis and selects the Warburg effect during normoxia and hypoxia (Theodossiou *et al*., 2019). The electron transport chain (ETC) is crucial to ATP generation and oxidative phosphorylation. ETC comprises complexes I - IV that participate in redox reactions and electron transfers. Nicotinamide adenine dinucleotide (NADH), reduced flavin adenine dinucleotide (FADH2) and succinate donate electrons to oxygen with the aid of transmembrane proteins that serve as carriers of electrons (Ashton *et al*., 2018; Dong *et al*., 2020). The electron transfer and ATP synthase establish the electrochemical gradient in the inner membrane of the mitochondria (Ashton *et al*., 2018). According to Berners-Price *et al*. (1988), phosphines retain the potential to disrupt cellular respiration by acting as an electron acceptor or donor in the ETC (Berners-Price and Sadler, 1988). UJ3 is a tertiary phosphine complex; the above literature suggests that mitochondrial bioenergetics were disrupted via the phosphine ligand and may have influenced oxidative phosphorylation more significantly in the MCF-7 (due to MCF-7 metabolic preference) than the MDA-MB-231 (Warburg effect preference). Nevertheless, both cell lines suffered severe bioenergetic dysfunction.

According to Olelewe *et al*. (2022), AuPhos-19 is a small molecule with a phosphine ligand that exerts cytotoxic effects in TNBC cell lines via disruption of oxidative phosphorylation in murine and human TNBC. The cytotoxicity was facilitated via the lipophilic cationic properties of the complex (Olelewe *et al*., 2022). As previously discussed, the lipophilic nature and possible accumulation of UJ3 in the mitochondria may have enabled UJ3 to execute the bioenergetic dysfunction in MCF-7 and MDA-MB-231 (Figure 3.4 and Figure 3.5), possibly via interference with the electron transport chain.

4.1.6 Light micrographs confirm viability measured biochemically.

The light micrographs depicting MCF-7 and MDA-MB-231 morphology and population numbers visibly concur with the viability percentages measured biochemically via the alamar blue® proliferation assay and CellTiter-Glo® Luminescent assay (Figure 3.6, Figure 3.1, Figure 3.4 and Figure 3.5). More specifically, these micrographs confirm that UJ3 was more cytotoxic to the MCF-7 than the MDA-MB-231 with the latter demonstrating resistance to treatment in the 48 hr study (10 μM UJ3) (Figure 3.6, Figure 3.7). Furthermore, the selective nature of UJ3 was depicted in the HEK-293 and MRHF-1 cell lines (Figure 3.8 and Figure 3.9). UJ3 represented superior cytotoxicity and selectivity in both cell lines compared to CDDP, correlating to the previously described observations of mitochondrial activity and cellular viability. In addition to changes in the cell population number and overall cellular health, light microscopy provided a clue on the possible type of cell death elicited by UJ3 based on morphological changes (discussed further in the next section).

4.2 UJ3 targets the mitochondria to trigger apoptosis in both malignant cell lines

4.2.1 Light and fluorescent microscopy

According to the National Committee on cell death (NCCD), in addition to drug-induced biochemical changes, morphology plays a crucial role in investigating the death modality. For example, caspase activity may not be detected in CICD apoptotic mechanisms. In such a case, morphology will aid as an apoptosis identifier (Galluzzi *et al*., 2007). In the MCF-7 cell line, light microscopy revealed apoptotic morphology induced by UJ3 such as cell shrinkage and membrane blebbing (Figure 3.6 (F)), cellular rounding, cellular shrinkage and apoptotic bodies (Figure 3.6 (G)). These findings are in conjunction with the renowned apoptotic morphology described by Kerr *et al*. (1972). Similarly, the MDA-MB-231 depicted cellular rounding and shrinkage post-UJ3 treatment (Figure 3.6 (G)). Apoptosis is also associated with characteristic nuclear morphology features (Wong, 2011). In the MCF-7 cell line, UJ3 induced nuclear apoptotic features such as DNA fragmentation (Figure 3.23 (E)) and changes in the spherical nuclei shape (Figure 3.17 (E)). In the MDA-MB-231, nuclear karyorrhexis and pyknosis were observed post-UJ3 treatment (Figure 3.19 (D) and (E)). Alterations in nuclear and chromatin structure indicate an apoptosis modality post-UJ3 treatment. DNA damage may be the end effect or the initiated stimulus of apoptosis (Wong, 2011).

Various Ag (I) complexes were reported to target DNA to initiate cell death (Pettinari *et al*., 2011). A study focusing on heteroleptic Ag (I) phosphino complexes reported that the complex promoted moderate DNA destabilization, exhibited DNA binding affinity as determined by

competitive binding studies, promoted DNA fragmentation as determined via the Comet assay, inhibited the activity of thioredoxin reductase (TrxR) to increase ROS levels and increased caspase-3 activity to promote apoptosis in ovarian cancer (Dammak *et al*., 2020). Ferreira *et al* (2015), reported that Ag (I) phosphine complexes induced cell cycle arrest at the G2/M phase, which may have prevented DNA synthesis and repair in MCF-7 cells and contributed to apoptosis. Engelbrecht *et al*. (2017), reported that SNO cells treated with a Ag (I) cyanide moiety resulted in apoptotic nuclear morphology such as chromatin condensation and DNA fragmentation after treatment. Therefore, these studies indicate that Ag (I) phosphine complexes, including UJ3, may target DNA to initiate apoptosis, or the resultant changes in nuclear morphology may be an end effect of the apoptosis pathway. To biochemically confirm whether apoptosis was the mode of cell death, PS exposure, mitochondrial membrane potential and oxidative stress were studied.

4.2.2 PS exposure and membrane integrity

The biochemical translocation of PS from the cytoplasmic to the outer membrane surface, along with weakened membrane integrity, is a biochemical characteristic of late apoptotic cell death (Fadok *et al*., 1998). The Annexin V and 7-AAD assay revealed that UJ3 induced late apoptotic cell death in both MCF-7 and MDA-MB-231 cell lines (Figure 3.10 (C) and Figure 3.11 (C)). These findings agree with studies that reported Ag (I) phosphine complexes as apoptosis activating agents in malignant cell lines (Engelbrecht *et al*., 2018; Human-Engelbrecht *et al*., 2017; Ferreira *et al*., 2015; Potgieter *et al*., 2017). According to Wong (2011), in the degradation or late phase of apoptosis, membrane integrity is weakened, membrane blebbing occurs, apoptotic bodies are formed, cytoplasmic organelles are modified and cell components are packaged into apoptotic bodies. The detection of late apoptosis in the Annexin V and 7-AAD assay coincides with the late apoptotic morphology depicted in the light micrographs for both malignant cell lines (Figure 3.6 (F) and (G)).

4.2.3 Mitochondrial membrane potential (ΔΨm) as a parameter of cell death

The mitochondrion governs metabolic signals, proliferation, redox reactions, bioenergetics, cell health and death fate. Mitochondria house crucial death mediators and are actively involved in apoptotic cell death (Dong *et al*., 2020). The energy the mitochondrion supplies is accumulated into an electrochemical gradient, producing a ΔΨm that provides cellular ATP. Subsequent depolarization of ΔΨm is associated with cellular stress and specific cell death modalities (Henry-Mowatt *et al*., 2004; Krysk et al., 2001; Tait and Green, 2013). According to Lee *et al*. (2019), ΔΨm provides insight into mitochondrial activity because it indicates the strength of the ETC and oxidative phosphorylation to generate ATP. Therefore, disrupted ΔΨm reflects disrupted bioenergetics (Lee *et al*., 2019). In the previous section, UJ3 demonstrated

high selectivity. It may be hypothesized that the balance of lipophilic character in UJ3 influenced its selective uptake in the mitochondria of malignant cells with high transmembrane potentials. In support of this hypothesis, UJ3 influenced the mitochondrial activity and bioenergetics of the mitochondria as detected by the altered ATP levels (Figure 3.4 and Figure 3.5). It is, therefore, expected that UJ3 would also impact the ΔΨm of malignant cells. Furthermore, bioenergetic stress and a decreased ΔΨm is an important event that promotes apoptosis and facilitates the expulsion of apoptogenic factors (Gutiérrez *et al*., 2017).

The biochemical MitoPotential assay revealed that UJ3 depolarized the ΔΨm and impaired the plasma membrane in both MCF-7 and MDA-MB-231 cell lines (Figure 3.12 (C) and Figure 3.13 (C)). The morphological MitoTracker Orange dye labeling confirmed that UJ3 reduced ΔΨm and polarisation in both MCF-7 and MDA-MB-231 mitochondria (Figure 3.17 (C – E)) and (Figure 3.19 (C – E)). These findings correlate to the influence of UJ3 on mitochondrial bioenergetics (Figure 3.1, Figure 3.4 and Figure 3.5). Moreover, impaired plasma membranes and depolarization of the ΔΨm are associated with late apoptosis (Wong, 2011). Therefore, these findings coincide with the late apoptotic morphology light micrographs (Figure 3.6 (F) and (G)) and late apoptosis detection via the Annexin V and 7-AAD assay (Figure 3.10 (C) and Figure 3.11 (C)). The likelihood of the mitochondrial permeability transition pore (PTP) opening increases with a reduction in ΔΨm. In response to various stimuli (hypoxia, genetic stress, elevated oxidative stress, excessive cytosol calcium influx, irregular oncogene expression and toxic compounds), the mitochondria will decrease its ΔΨm to proceed with apoptosis that is either caspase-dependent or independent. The BCL-2 family governs the resultant MOMP regulation (Figure 1.8) and the activation of MOMP most often results in a cell's demise (Adams *et al*., 2019, Jäättelä and Tschopp, 2003; Lopez and Tait, 2015; Saraste and Pulkki, 2000; Wong, 2011).

Ag (I)–NHCs induced apoptosis in HL60 (leukemia cells) and many other malignant cell lines via depolarization of ΔΨm, which prompted the release of apoptogenic factors from the intermembrane space of the mitochondria, promoting CICD induction and AIF release. The depolarization of ΔΨm was not induced via primary necrosis but by mitochondrial targeting to elicit apoptosis by silver complexes (Eloy *et al*., 2012). According to Altay *et al*. (2019), Ag (I) complexes ([Ag(I-dicl)]n and AgH(nif)2]) induced apoptosis in MCF-7 via the depolarization of the ΔΨm followed by cytochrome *c* release and activated caspases to initiate intrinsic apoptosis. Habib *et al*. (2019), reported that Ag (I)-NHC induced apoptosis in MDA-MB-231 via a reduction in ΔΨm. Triphenylphosphine groups (TPP^+) have been exploited as a moiety in many complexes for their favorable mitochondrial selectivity, enabling drug accumulation in the mitochondria to influence ΔΨm. Approximately 246 patents of TPP^+ complexes were

reported and 100 are already approved (Zielonka *et al*., 2017). Ag (I) phosphine complexes, including UJ3, have been reported to promote mitochondrial-mediated apoptosis via ΔΨm reduction (Human-Engelbrecht *et al*., 2017; Ferreira *et al*., 2015). In line with these reports, UJ3 reduced the ΔΨm to facilitate apoptosis in MCF-7 and MDA-MB-231.

4.2.4 Oxidative stress as a parameter of cell death

The mitochondrion harbors high ROS levels linked to high tumor proliferation rates and tumorigenic pathways. Malignant cells avoid oxidative stress through the rigorous activity of antioxidant enzymes for example SOD and glutathione peroxidase to eradicate ROS. Metal complexes may suppress antioxidant enzyme activity or influence ROS by targeting the mitochondria. The resultant imbalance in redox activity subsequently promotes lipid peroxidation or MOMP, which indirectly alters cellular DNA and protein structure to activate cell death. The MOMP facilitates the release of pro-apoptotic proteins to trigger apoptosis's biochemical and morphological changes (Chen *et al*., 2007; Kannan and Jain, 2000; Pedrosa *et al*., 2018). Many ruthenium complexes were reported to increase intracellular ROS activity, disrupt oxidative phosphorylation, disrupt ΔΨm and elicit cell death (Li *et al*., 2021). NHC complexes display similar donor characteristics as phosphines and similar transition metal binding affinities. Au and Ag carbene complexes have been reported to induce ROS-mediated mitochondrial targeting to elicit intrinsic apoptosis cell death in MCF-7, MDA-MB-231 and HeLa cells (Iacopetta *et al*., 2017). In the present study, UJ3 resulted in higher ROS activity in the MDA-MB-231 (40.66%) than the MCF-7 (5.57%) (Figure 3.14 and Figure 3.15).

TrxR is a regulator of redox activity and a mitochondrial resident. TrxR converts oxidized thioredoxin (Trx) to its reduced form to eradicate high ROS levels and defend against oxidative stress. Variants of TrxR are up-regulated in many malignancies and contribute to apoptosis prevention, tumor invasion and proliferation (Bhatia *et al*., 2016; Raninga *et al*., 2015; Rubartelli *et al*., 1992). Decreased TrxR levels are associated with high ROS levels and reduced ΔΨm to promote apoptosis (Ly *et al*., 2003). Moreover, up-regulation of TrxR in MDA-MB-231 cells contributed to its invasion and proliferation during *in vitro* studies. Auranofin-treated MDA-MB-231 cells suppressed TrxR activity and increased ROS levels to reduce MDA-MB-231 cell invasion (Bhatia *et al*., 2016). Many studies reported the ability of Au (I) and Ag (I) complexes to suppress the activity of TrxR redox enzymes that contain the selenocysteine residue (Dammak *et al*., 2020; Gandin and Fernandes, 2010; Gandin and Fernandes, 2015). A study conducted by Quintana *et al*. (2022), reported that the cytotoxicity of a dinuclear Au-based complex $[Au_2(bisNHC)_2]^2$ against A2780 ovarian cancer was induced via high ROS activity and inhibition of TrxR. A2780 cells have high basal levels of ROS and were, therefore, sensitive to increased ROS induction via the complex. As a result, these cells

could not withstand the additional ROS and oxidative stress, resulting in their death (Quintana *et al*., 2022).

A study by Sarmiento-Salinas *et al*. (2019), measured intracellular ROS levels in MDA-MB-231 and MCF-7 cells using dihydroethidium. The MDA-MB-231 cells are highly invasive and already possess high basal ROS levels due to high metabolic activity and cellular respiration end products compared to the MCF-7 cell line. As a result, MDA-MB-231 cells are more susceptible to increased ROS levels and, thus, oxidative stress (Sarmiento-Salinas *et al*., 2019). Therefore, this may be a reason for the higher ROS levels detected in the MDA-MB-231 than in the MCF-7 cell line in the present study. Alternatively, UJ3 may also influence antioxidant enzyme activity such as TrxR to increase the MDA-MB-231 cells vulnerability to oxidative stress. However, for confirmation purposes, future studies may measure the expression levels of TrxR post-UJ3 treatment by performing an immunoblot.

Overall, UJ3 induced apoptotic cell death in both MCF-7 and MDA-MB-231 by mitochondrial targeting due to depolarized mitochondrial membrane detection, PS exposure, apoptosis morphology and oxidative stress (ROS activity was prominent in the MDA-MB-231, not the MCF-7). Moreover, the mitochondrial bioenergetics studies in section 4.1 correlate to mitochondrial-mediated apoptosis in section 4.2.

4.3 UJ3 conducts the classical intrinsic apoptosis pathway in MCF-7

In response to numerous apoptotic stimuli, the mitochondrion reduces its ΔΨm to promote MOMP (Wong, 2011). The ΔΨm correlates with the expulsion of pro-apoptotic proteins such as cytochrome *c* (labeled with Alexa 488 dye). UJ3 IC_{50} promoted the release of cytochrome *c* from the mitochondrial intermembrane space into the cytoplasm of MCF-7 cells (Figure 3.17 (D)), suggesting that UJ3 initiates the intrinsic apoptosis pathway. Cytochrome *c* cytosolic expulsion enables interaction with APAF-1 and ATP to form the heptameric apoptosome. The apoptosome interacts with pro-caspase-9. The initiator caspase-9 activates the effector caspase-3 and caspase-7. Therefore, cytochrome *c* activity is central to activating the intrinsic caspase cascade (Wong, 2011).

Caspase-3 cleaves ICAD to activate CAD to embark on nuclear apoptosis and promote its characteristic morphology. As a result, nuclear morphology such as chromatin condensation and DNA fragmentation is aided by caspase-3 activity. Activated downstream caspases cleave proteins involved in the cell cycle, DNA repair, cytoskeleton preservation, kinases and signaling cascades (Wong, 2011). However, the MCF-7 cell line has the caspase-3 gene removed due to a genomic mutation that introduces an early stop codon in the mRNA (Martin *et al*., 1995). A study reported that staurosporine (STS) treatment in MCF-7 cells (null of caspase-3) could cleave many other substrates essential to apoptotic morphology, such as PARP, pRb and protein kinase catalytic subunits (Porter and Jänicke, 1999). Other studies indicate that caspase-3 is necessary for DNA fragmentation and apoptotic features. When caspase-3 activity was restored in caspase-3 null MCF-7, so was the apoptotic morphology (Porter and Jänicke, 1999; Jänicke, 2008). Another study indicated that caspase-3 is essential to cleaving α-fodrin, which is required for membrane blebbing (Martin *et al*., 1995).

In contrast, the present study indicates that UJ3 induced membrane blebbing and nuclear apoptotic morphology in MCF-7 caspase-3 null cells. Gee *et al.* (2002), reported that pyrrolo-1,5-benzoxazepine induced apoptosis in caspase-3 null MCF-7 cells and induced DNA fragmentation and apoptotic morphology via caspase-7 activity instead of caspase-3 or caspase-6. Caspase-7 cleaves the same DEVD substrate as caspase-3 and has approximately 57% sequence similarity to caspase-3 to promote apoptotic morphology (Boucher *et al*., 2012; Gee *et al*.,2002). Another study found that caspase-7 also deactivates ICAD allowing nuclear apoptosis (Wolf *et al*., 1999). Similarly, other studies reported that MCF-7 cells null of caspase-3 had undergone membrane blebbing and additional apoptotic morphology after cytotoxic treatment (Chen *et al*., 2004; Jänicke, 2008; Wang *et al*., 2008). Therefore, it is expected that UJ3 would activate caspase-7 activity in MCF-7 cells to bring about the nuclear apoptotic morphology (Figure 3.23 (E)) and Figure 3.17 (E)) previously

discussed. Western blot analysis revealed that UJ3 resulted in the presence of the active cleaved form of caspase-7 (20 kDa) at the IC_{50} treatment (Figure 3.20A (D)).

PARP functions in DNA stability, repair and replication. PARP is also involved in maintaining energy balance in apoptosis and prevents necrosis. PARP proteolysis inhibits PARP activity, which is a considerable apoptotic hallmark. Many studies reported that caspase-7 is responsible for PARP cleavage in apoptosis, especially in cells that are null of caspase-3 (Boucher *et al*., 2012; Los *et al*., 2002; Oliver *et al*., 1998). A study reported that caspase-7 displayed higher efficiency in cleaving PARP than caspase-3. Caspase-7 binding and proteolytic efficiency against PARP were aided by critical lysine residues in the N-terminal domain of caspase-7 (Boucher *et al*., 2012). In the present study, western blot analysis revealed PARP cleavage at the same UJ3 (IC_{50}) concentration that displayed caspase-7 cleavage (Figure 3.20A (D)). These findings infer that cytochrome *c* expulsion at the UJ3 IC_{50} concentration indirectly activated caspase-7 (based on the order of events studied it is assumed that this was aided by caspase-9 activation and apoptosome formation), cleaving PARP and promoting the nuclear apoptosis morphology.

Many studies reported that the cell type, intensity or concentration of the drug, variety of drug stimuli and exposure time are factors that influence apoptotic events, including caspase activity (Sundquis *et al*., 2006). Mooney *et al*. (2002), reported that STS treated MCF-7 (caspase-3 null) and T47D (caspase-3 present) cells resulted in earlier apoptotic events in the MCF-7 than the T47D cells. A time-dependent decrease in $\Delta\Psi m$ was observed after STS treatment and cytochrome *c* was expelled 2 hrs post-treatment in the MCF-7 and 4 hrs post-treatment in the T47D, determined via western blots. PARP underwent proteolysis 3 hrs after STS treatment in the MCF-7 and T47D underwent partial PARP fragmentation at 24 hrs and 48 hrs. Optimum apoptosis was observed 24 hrs after STS treatment in the MCF-7 and 48 hrs in the T47D (Mooney *et al*., 2002). Masquelier *et al*. (2004), reported that higher dosages of daunorubicin in leukemia cells resulted in quicker apoptosis induction in HL60 cells and acute myelogenous leukemia. These observations were made by quicker caspase-3 activation (using an *in vitro* caspase assay) and significant apoptotic DNA fragmentation (using flow cytometry and PI staining) at higher drug dosages compared to lower dosages (Masquelier *et al*., 2004).

In the present study, western blot analysis revealed that at high UJ3 concentrations (20 µM), no cleaved caspase-7 or PARP fragments were detected after 24 hr exposures. These findings may be due to the higher concentration of UJ3, resulting in a quicker procession of the apoptosis pathway. As a result, cytochrome *c* may have been expelled earlier than 24 hrs and the time point may have already been missed (Figure 3.17 (E)). The earlier release of

cytochrome *c* would result in earlier proteolysis of caspase-7 and PARP that could not be detected after 24 hr treatments. Moreover, if apoptosis proceeded quicker at the UJ3 (20 µM) treatment, it would be expected that Hoechst 33258 staining would have already revealed nuclear DNA fragmentation at this concentration since this is an end morphological effect of apoptosis. Such a finding was observed (Figure 3.23 (E)) and the lower concentration of UJ3 IC_{50} (Figure 3.17 (D) and Figure 3.17 (D)) did not show any DNA fragmentation yet. Furthermore, Light micrographs at the higher UJ3 (20 µM) concentration revealed late apoptotic bodies (Figure 3.6 (G)). Similarly, the high CDDP concentration effect on caspase activity may not be detected at 24 hr exposures but at earlier time intervals. Therefore, to possibly determine caspase-7 and PARP cleaved fragments at high UJ3 concentrations such as 20 µM, shorter exposure intervals of UJ3 should be included in addition to the 24 hr exposure period. Furthermore, the full-length PARP at UJ3 (20 µM) treatment (Figure 3.20A (C)) is of low intensity; this may be due to much of the full-length PARP undergoing cleavage of which the fragments were not detected in the 24 hr study. However, in addition to caspase-7, caspase-9 cleaves PARP substrate (Mooney *et al*., 2002); therefore, this may explain the low intensity of the full-length PARP.

Caspase-8 is not only an initiator of the extrinsic death-receptor ligation pathway but is also associated with cross-talk in the intrinsic pathway via cleavage of Bid to form truncated Bid (tBid), which regulates pro-apoptotic effector proteins such as Bax and Bak to permeabilize the mitochondrial membrane. The resultant MOMP facilitates the release of pro-apoptotic proteins that expedite the activation of executioner caspase-3 and caspase-7 (Elmore, 2007). In the present study, $\Delta\Psi m$ was reduced and to determine if caspase-8 contributed to MOMP and the release of cytochrome *c*, western blot analysis was carried out. Ferreira *et al*. (2015), reported that Ag (I) phosphine complexes activated both intrinsic and extrinsic pathways. Interestingly, in the present study, no caspase-8 activity was detected at the high UJ3 (20 µM) concentration (Figure 3.20B (C)) and the IC_{50} treatment (Figure 3.20B (D)). The reduced $\Delta\Psi m$ and proceeding apoptotic events were managed through the classical intrinsic apoptosis pathway.

Engelbrecht *et al*. (2018), reported that UJ3 activated caspase-9 and PARP activity in SNO oesophageal cells at a low concentration of 10 µM over a 24 hr exposure. Ferreira *et al*. (2015), tested a panel of Ag (I) phosphine complexes over 24 hr exposure treatments and reported that some of these complexes activated caspase-7, caspase-9 and caspase-8 activity at 10 µM treatment. In agreement with the present study, UJ3 at the low IC_{50} concentration (14.1 µM) activated caspase-7 and cleaved PARP.

4.4 UJ3 conducts CICD via AIF expulsion in MDA-MB-231

AIF is a bifunctional flavoprotein that resides in the mitochondrial intermembrane space. AIF functions in redox metabolism (possibly as a ROS scavenger) and regulation of oxidative phosphorylation (Sevrioukova, 2011). When mitochondria encounter apoptotic stimuli MOMP activation promotes AIF proteolysis and migration into the cytosol, interacting directly with nuclei to conduct CICD (Barbosa *et al*., 2016; Loane *et al*., 2015). AIF executes many apoptotic characteristics (Figure 4.2). Biochemical and morphological analysis post-UJ3 treatment corresponded to apoptotic features induced by AIF activity in MDA-MB-231. Features included extensive DNA fragmentation (Figure 3.19 (D)), chromatin condensation (Figure 3.19 (C)), nuclear shrinkage (Figure 3.25 (E)), PS exposure independent of caspase activity (Figure 3.11 (C)), a swift loss in $\Delta\Psi m$, ((Figure 3.13 (D) and Figure 3.19 (C - E)) and increased ROS production (Figure 3.15).

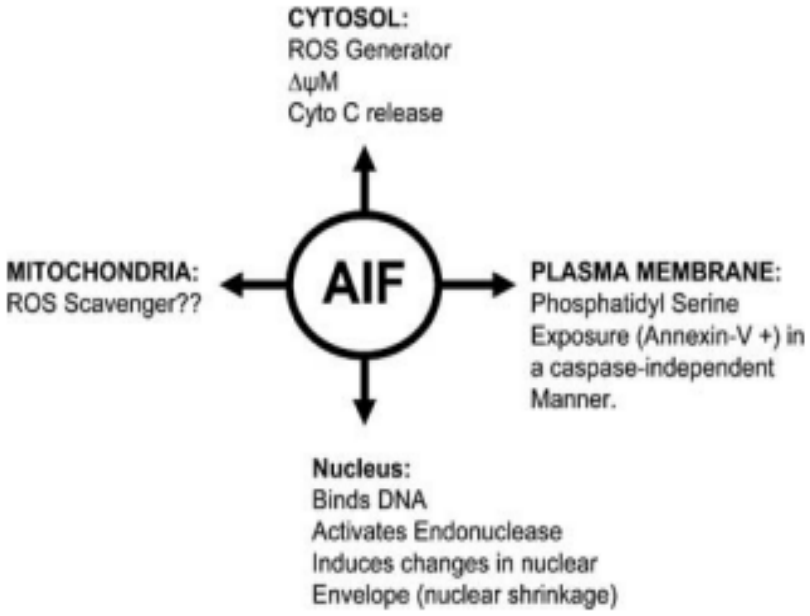

Figure 4.2: Biochemical and morphological characteristics linked to AIF activation. UJ3 treated MDA-MB-231 cells displayed PS exposure, absence of caspase activity, loss of $\Delta\Psi m$, ROS production, changes in nuclear shape, chromatin condensation and DNA fragmentation (Adapted from Cregan *et al*., 2004).

Nearly all AIF-mediated apoptotic features were present, except for cytochrome *c* release post-UJ3 treatment. As a result, AIF was fluorescently tracked for migration from the mitochondrial intermembrane space with Alexa-488 tagged anti-AIF antibody. UJ3 treatment (Figure 3.25 (D - E)) resulted in prominent AIF leakage corresponding to the area of the nuclei space (marked by white arrows). As the UJ3 concentration increased, so did AIF fluorescence (Figure 3.25 (D - E)). These findings suggest that UJ3 promoted AIF translocation to the nuclei, resulting in the apoptotic nuclear morphology detected. CICD pathways are derived from common MOMP activation in response to apoptotic ques (Tait and Green, 2008).

AIF may be expelled from the mitochondria via four common MOMP-dependent pathways (Cregan *et al*., 2004). AIF expulsion may occur due to MOMP via the conventional intrinsic apoptosis pathway (1) (Figure 4.3), resulting in cytochrome *c* release, AIF release and a caspase cascade (Cregan *et al*., 2004). In the present study, cytochrome *c* (Figure 3.19 (C – E), caspase-3 (Figure 3.21A (A)), caspase-7 (Figure 3.21B (C)) and caspase-8 activity (Figure 3.21B (D)) were not detected at both UJ3 IC_{50} and UJ3 (20 µM) concentrations and since apoptotic features were present regardless of caspase activity this is indicative of CICD. However, future studies may include a pan-caspase inhibitor such as z-VAD-fmk to confirm these findings. In the next MOMP-dependent pathway (2) (Figure 4.3), AIF could be released via PARP-mediated AIF expulsion. This pathway relies on Bax and mitochondrial depolarization. When energy levels drop to an extreme low, an excitotoxic response will result in secondary PARP signaling, which activates AIF release without caspase activity (Cregan *et al*., 2004). The next MOMP-dependent pathway (3) (Figure 4.3) relies on high cytosolic calcium levels due to ER stress that activates Bax activity via calpain-mediated MOMP, which facilitates the release of AIF (Cregan *et al*., 2004). The present study did not monitor calpain activity and this could be proposed as a future study to determine any interactions with AIF release post-UJ3 treatment. Some studies have found that calpains mediate AIF activation via proteolysis and aid in detachment from the mitochondrial membrane (Łopatniuk and Witkowski, 2011). An alternative MOMP-dependent pathway (4) (Figure 4.3) relies on stimuli or oxidants that promote the release of cathepsins from lysosomes. Cathepsins then cleave substrates, including Bid to promote MOMP. Cathepsins cleave similar caspase substrates, including PARP (Jäättelä and Tschopp, 2003). However, PARP was not cleaved by UJ3 treatment in this study (Figure 3.21A (B)). Therefore, various stimuli, including ER stress, may facilitate AIF release via Bax/BH3-dependent MOMP (Figure 1.8) post-UJ3 treatment.

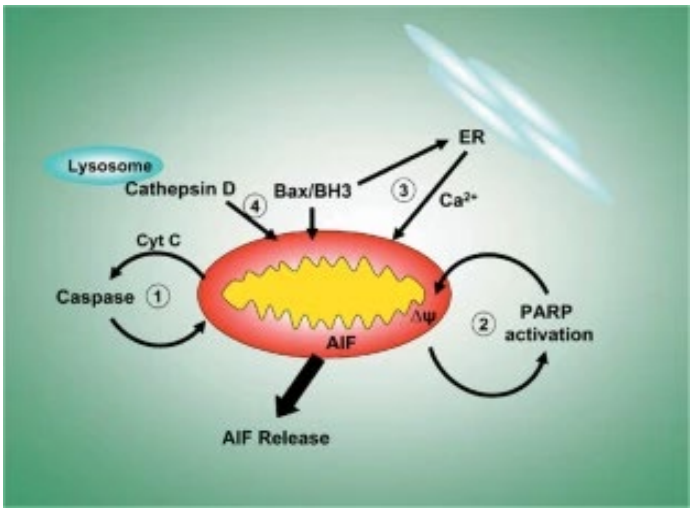

Figure 4.3: The many MOMP-dependent pathways that assist AIF expulsion from the mitochondrial intermembrane space to the cytosol (Adapted from Cregan *et al*., 2004).

Baysan *et al*. (2007), reported that arsenic trioxide induced mitochondrial-mediated apoptosis in B cells (BCL-2 null) via increased ROS, decreased ΔΨm, cytochrome *c* release, AIF release, caspase activity and increased expression of Bax and Bim proteins (Baysan *et al*., 2007). One study reported that Ag (I)-NHC complexes targeted the mitochondria of HL60 leukemia cells. The silver complex reduced ΔΨm and resulted in AIF and caspase-12 migration to the nucleus, which prompted DNA fragmentation and apoptosis. Caspase-12 was activated in response to ER stress and cell death was independent of caspase-3 activity, cell-cycle arrest and ROS (Eloy *et al*., 2012). In contrast, Sunilkumar *et al*. (2020), reported that Oxyresveratrol triggers AIF-mediated CICD via increased ROS levels and PARP cleavage. The increase in ROS after treatment was responsible for reducing ΔΨm, aiding AIF expulsion. Elevated ROS due to DNA impairment may result in PARP cleavage, which precedes AIF migration from the intermembrane space. Subsequently, resulting in additional AIF features, including DNA fragmentation and PS exposure. Apoptosis was confirmed as caspase-independent by the addition of a pan-caspase inhibitor (QVD-OBH) (Sunilkumar *et al*., 2020).

Literature on the capability of metal complexes to activate AIF-mediated apoptosis is limited. Anti-cancer drugs that promote AIF-mediated CICD can be used in combination with drugs that promote classical caspase-dependent apoptosis to improve clinical outcomes by enhancing treatment efficacy (Feng *et al*., 2012). Based on the findings in this study, MOMP may have been stimulated via disrupted bioenergetics or oxidative stress. The reduced ΔΨm facilitated the release of AIF to the cytosol, followed by migration to the nucleus. In the nucleus, the endonuclease activity of AIF promoted DNA condensation and fragmentation, which resulted in MDA-MB-231 apoptotic death.

4.5 Summary of the proposed UJ3 mechanism in MCF7- and MDA-MB-231

UJ3 targeted the mitochondria of both MCF-7 and MDA-MB-231, which corresponded to reduced $\Delta\Psi m$. Apoptotic UJ3 stimuli may encompass oxidative stress or DNA damage. Other triggers not investigated in this study include genetic stress, oncogene expression, up-regulation of pro-apoptotic proteins and down-regulation of anti-apoptotic proteins, excessive calcium influx and ER stress (Cregan *et al*., 2004, Saraste and Pulkki, 2000; Wong, 2011). The apoptotic stimuli would have led to the activation of BH-3-only proteins permitting oligomerization of effector Bax and Bak to initiate MOMP via the opening of the mitochondrial permeability transition pore. The MCF-7 cell line followed the intrinsic apoptosis pathway (left) and the MDA-MB-231 followed the AIF-mediated CICD apoptosis pathway (right) (Figure 4.4). UJ3 promoted cytochrome *c* expulsion, which activated caspase-7 (in caspase-3 absent cells), activating downstream proteins essential to DNA and cytoskeletal integrity. End effects of apoptosis included membrane blebbing, apoptotic bodies, cell shrinkage and PS exposure. In this study, PARP cleavage prevented DNA repair facilitating nuclear apoptosis. These findings were based on nuclear pyknosis, DNA fragmentation and DNA condensation. In the MDA-MB-231, MOMP expelled AIF from the mitochondrial intermembrane space to the cytosol. Thereafter, AIF translocated to the nucleus and its endonuclease activity resulted in DNA fragmentation, chromatin condensation and nuclear pyknosis (Figure 4.4).

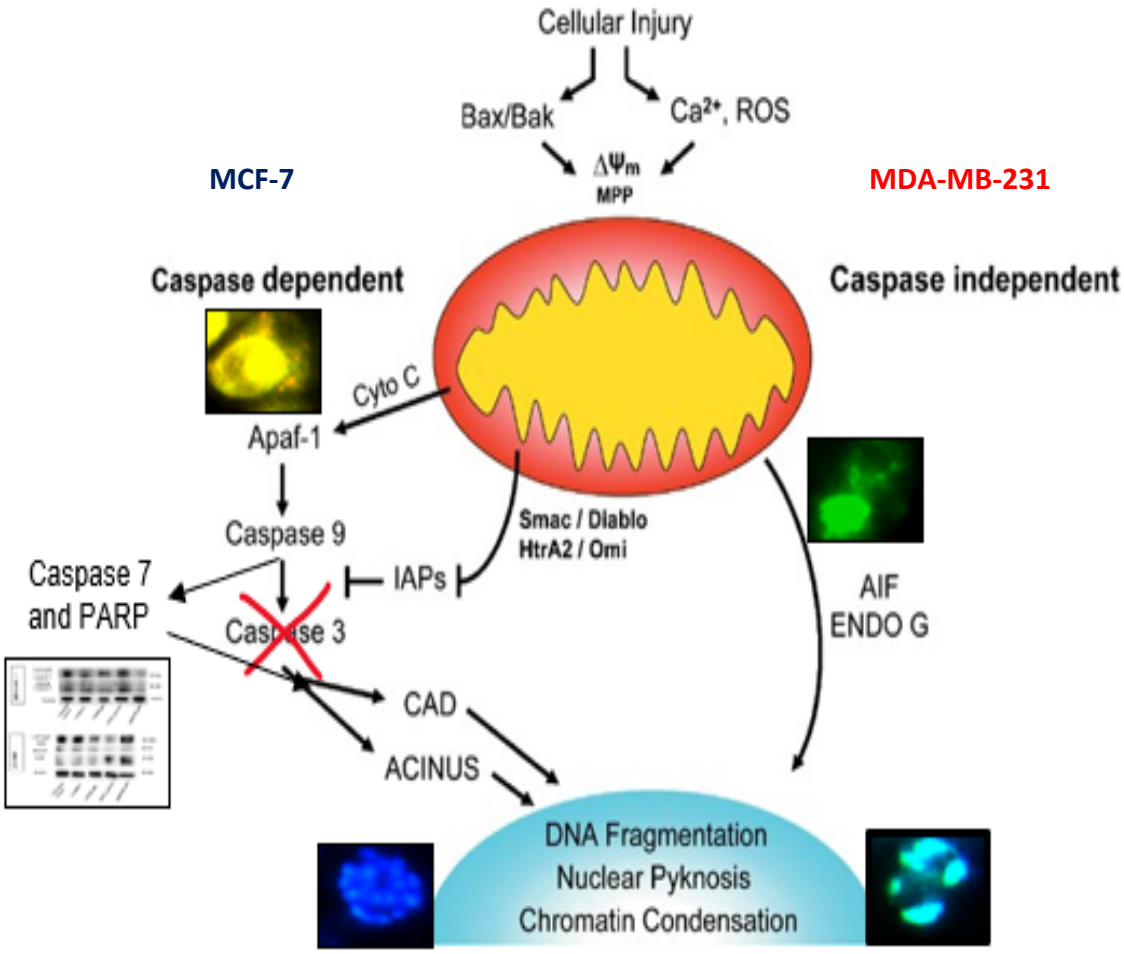

Figure 4.4: The mechanistic action of UJ3 inducing mitochondrial-mediated apoptosis in malignant breast cell lines. UJ3 targeted the mitochondria to elicit apoptosis. More specifically, the intrinsic apoptosis pathway in **MCF-7** (left) and the AIF-mediated CICD apoptosis pathway in **MDA-MB-231** (right). The intrinsic pathway relied on cytochrome *c* release, followed by caspase-7 and PARP cleavage to generate the end morphological apoptotic effects. The caspase-independent pathway relied on AIF migration directly to the nucleus to elicit apoptotic nuclear morphology (Adapted from Cregan *et al*., 2004 and modified to the present study).

Chapter 5: Conclusion

The alamar blue® proliferation assay, CellTiter-Glo® Luminescent viability assay and light micrographs were studied to evaluate the pharmacological properties of UJ3. In support of the study hypothesis, UJ3 exhibited pharmacological properties determined by the complex's malignant selectivity, cytotoxicity and sustained potency in the MCF-7 cell line. Similarly, UJ3 proved selective and cytotoxic to the MDA-MB-231. However, its pharmacodynamic profile was impeded via cell recovery, which could result from many recovery mechanisms, such as the p-glycoprotein efflux pump that is highly expressed in this cell line. The selectivity of UJ3 may be attributed to a favorable hydro-lipophilicity balance that permits access to the mitochondria, and the high transmembrane potentials of malignant cells may further guide selectivity. The detection of limited ATP production in both malignant cell lines post-treatment infer disrupted bioenergetics and possible impairment of the electron transport chain. The severity of disrupted bioenergetics may be attributed to the metabolic preference between the two malignant cell lines.

Light microscopy, Hoechst 33258 labeling, Annexin V and 7-AAD assay, MitoPotential assay, MitoTracker Orange labeling and oxidative stress were studied to determine the cell death modality. In support of the hypothesis, UJ3 induced apoptosis cell death via mitochondrial targeting, which was determined via reduced mitochondrial membrane potential that coincided with disrupted bioenergetic studies and possible accumulation of UJ3 in the mitochondria. The nuclear apoptotic morphology (chromatin condensation, DNA fragmentation and nuclear pyknosis), phosphatidylserine externalization and late apoptotic morphology post-treatment in both cell lines are indicative of the apoptosis modality. Oxidative stress was higher in the MDA-MB-231 than the MCF-7. The increased ROS levels in the MDA-MB-231 may be attributed to the inhibition of TrxR by UJ3. The high basal level of ROS in this cell line may have enhanced susceptibility to oxidative stress. Oxidative stress may have been a stimulus for apoptosis in this study that promoted depolarization of the mitochondrial membrane in the MDA-MB-231 cell line.

UJ3 induced the intrinsic apoptosis pathway in the MCF-7 cell line via cytochrome *c* expulsion, activated caspase-7 activity and PARP cleavage, which facilitated the end morphological effects of apoptosis. Higher concentrations of UJ3 may have resulted in an earlier procession of the apoptosis pathway compared to lower dosages. This may describe the lack of cleaved caspase-7 and PARP at UJ3 (20 μM) compared to the bands observed at UJ3 IC_{50} (14.1 μM). Caspase-8 activity did not influence the mitochondrial membrane potential, as the active form was not detected at high and low UJ3 dosages. As a result, this confirms that UJ3 induces the intrinsic apoptosis pathway in the MCF-7 cell line. In the MDA-MB-231, UJ3 did not activate caspase-3, caspase-7, caspase-8 and did not promote PARP cleavage. However, this cell

line's biochemical and morphological characteristics were linked to AIF activation. AIF was fluorescently tracked for migration from the mitochondrial intermembrane space with Alexa-488 tagged anti-AIF antibody. UJ3 resulted in prominent AIF leakage into the nuclei area, which explains the nuclear apoptotic morphology. These findings suggest that UJ3 induces AIF-mediated apoptosis in MDA-MB-231. Therefore, UJ3 executes the intrinsic apoptosis pathway in MCF-7 cells and AIF-mediated apoptosis in MDA-MB-231 via mitochondrial targeting. To further clarify the mechanism of action, many future studies are required.

5.1 Future studies

- To confirm whether UJ3 influenced the electron transport chain of malignant cells. The electron transport rate between complex I and III in MCF-7 and MDA-MB-231 mitochondrial extracts can be measured spectrophotometrically, as detailed by Gazzano *et al*. (2018).
- To determine whether UJ3 inhibits thioredoxin reductase to promote oxidative stress, especially in MDA-MB-231, a TrxR assay should be employed. The TrxR protocol is detailed by Quintana *et al*. (2022). The results of the TrxR assay should be compared to ROS levels, electron transport rate activity and mitochondrial activity to confirm disrupted bioenergetics post-UJ3 treatment.
- Western blots should be performed for the MCF-7 cell line with shorter treatment exposure times in addition to the 24 hr study. This will confirm changes in caspase-7, caspase-8 and PARP activity in response to treatment. This is especially important for high UJ3 concentrations, such as 20 µM, as cells may have undergone apoptosis at earlier time points compared to lower dosages (Masquelier *et al*., 2004).
- In the MCF-7 cell line, UJ3 initiated the intrinsic apoptosis pathway, and it is expected that caspase-9 activated pro-caspase-7. To confirm whether caspase-9 was activated, a western blot should be conducted at many time points in addition to 24 hr studies (Masquelier *et al*., 2004).
- To confirm whether UJ3 initiates a caspase-independent apoptosis pathway in the MDA-MB-231 cells, a pan-caspase inhibitor such as z-VAD-fmk should be included. If UJ3-treated cells undergo AIF-mediated apoptosis in the presence of a z-VAD-fmk caspase inhibitor, this will confirm that UJ3 induces CICD in this cell line. The z-VAD-fmk protocol is detailed by van der Walt *et al*. (2016). Furthermore, the activity of AIF can be determined via western blot analysis. Since AIF is known to result in 50 kb DNA fragmentation, AIF nuclear involvement can be confirmed via gel electrophoresis detailed in Sevrioukova (2011). The role of calcium ions, calpains and cathepsins should be investigated post-UJ3 treatment to aid in

developing the mechanism of action regarding CICD and reduced ΔΨm. Cathepsin and calpain activity can be quantified via cleavage of calpain or cathepsin substrates linked to a fluorophore that emits fluorescence upon cleavage (Knopp *et al*., 2021). Endoplasmic reticulum stress and the requirement of calcium ions to promote CICD can be studied via calcium blockers such as BAPTA-AM (Fu *et al*., 2019) in UJ3-treated cells.

- The involvement of the BCL-2 family should be determined post-UJ3 treatment in both cell lines. For instance, the up-regulation or activity of the effector Bax and Bak proteins via western blot analysis can explain the depolarisation of the mitochondrial membrane (Adams *et al*., 2019) post-UJ3 treatment and confirm UJ3 association with mitochondrial targeting.
- Flow cytometry cell-cycle analysis can determine at which cell cycle phase UJ3 initiates cell cycle arrest. This will aid in determining a more precise apoptotic mechanism. To examine whether UJ3 targets DNA, the UV vis absorption of UJ3 should be studied, or DNA thermal studies may be conducted. DNA thermal studies involve the denaturation of duplex DNA. If UJ3 stabilizes the DNA duplex after the denaturation to ssDNA, then UJ3 interacts with DNA. Isothermal titration calorimetry is a technique that may be employed to determine how and whether UJ3 binds DNA by titrating UJ3 in DNA extracts and monitoring various DNA binding parameters such as entropy, enthalpy and binding stoichiometry (Palchaudhuri and Hergenrother, 2007).

Chapter 6: Reference list

Abul Haj, M., Aakeröy, C. and Desper, J., 2013. Silver(i) coordination chemistry: from 1-D chains to molecular rectangles. *New J. Chem.*, 37(1), pp.204-211.

Adams, C., Clark-Garvey, S., Porcu, P. and Eischen, C., 2019. Targeting the Bcl-2 Family in B Cell Lymphoma. *Frontiers in Oncology*, 8.

Alkabban, F. and Ferguson, T., 2022. *Breast cancer*. [ebook] StatPearls. Available at: <https://www.ncbi.nlm.nih.gov/books/NBK482286/> [Accessed 7 June 2022].

Amin, M., Greene, F., Edge, S., Compton, C., Gershenwald, J., Brookland, R., Meyer, L., Gress, D., Byrd, D. and Winchester, D., 2017. The Eighth Edition AJCC Cancer Staging Manual: Continuing to build a bridge from a population-based to a more "personalized" approach to cancer staging. *CA: A Cancer Journal for Clinicians*, 67(2), pp.93-99.

Anstey, E., Shoemaker, M., Barrera, C., O'Neil, M., Verma, A. and Holman, D., 2017. Breastfeeding and Breast Cancer Risk Reduction: Implications for Black Mothers. *American Journal of Preventive Medicine*, 53(3), pp.S40-S46.

Ashton, T., McKenna, W., Kunz-Schughart, L. and Higgins, G., 2018. Oxidative Phosphorylation as an Emerging Target in Cancer Therapy. *Clinical Cancer Research*, 24(11), pp.2482-2490.

Astolfi, L., Ghiselli, S., Guaran, V., Chicca, M., Simoni, E., Olivetto, E., Lelli, G. and Martini, A., 2013. Correlation of adverse effects of cisplatin administration in patients affected by solid tumours: A retrospective evaluation. *Oncology Reports*, 29(4), pp.1285-1292.

Azubuike, S., Muirhead, C., Hayes, L. and McNally, R. (2018). Rising global burden of breast cancer: the case of sub-Saharan Africa (with emphasis on Nigeria) and implications for regional development: a review. *World Journal of Surgical Oncology*, 16(1).

Bagowski, C., 1999. Cell-type specific phosphorylation of threonines T654 and T669 by PKD defines the signal capacity of the EGF receptor. *The EMBO Journal*, 18(20), pp.5567-5576.

Bahcecioglu, G., Basara, G., Ellis, B., Ren, X. and Zorlutuna, P., 2020. Breast cancer models: Engineering the tumor microenvironment. *Acta Biomaterialia*, 106, pp.1-21.

Banti, C. and Hadjikakou, S., 2013. Anti-proliferative and anti-tumor activity of silver(i) compounds. *Metallomics*, 5(6), pp.569.

Barbosa, D., Capela, J., de Lourdes Bastos, M. and Carvalho, F., 2016. Mitochondrial Trails in the Neurotoxic Mechanisms of MDMA. *Neuropathology of Drug Addictions and Substance Misuse*, 2, pp.431-444.

Barillo, D. and Marx, D., 2014. Silver in medicine: A brief history BC 335 to present. *Burns*, 40, pp.S3-S8.

Baudino, T., 2015. Targeted Cancer Therapy: The Next Generation of Cancer Treatment. *Current Drug Discovery Technologies*, 12(1), pp.3-20.

Berners-Price, S. and Sadler, P., 1988. Phosphines and metal phosphine complexes: Relationship of chemistry to anticancer and other biological activity. *Structure and Bonding*, 70, pp.27-102.

Berners-Price, S. and Sadler, P., 1996. Coordination chemistry of metallodrugs: insights into biological speciation from NMR spectroscopy. *Coordination Chemistry Reviews*, 151, pp.1-40.

Bhardwaj, P., Au, C., Benito-Martin, A., Ladumor, H., Oshchepkova, S., Moges, R. and Brown, K., 2019. Estrogens and breast cancer: Mechanisms involved in obesity-related development, growth and progression. *The Journal of Steroid Biochemistry and Molecular Biology*, 189, pp.161-170.

Bhatia, M., McGrath, K., Di Trapani, G., Charoentong, P., Shah, F., King, M., Clarke, F. and Tonissen, K., 2016. The thioredoxin system in breast cancer cell invasion and migration. *Redox Biology*, 8, pp.68-78.

Biersack, B., Ahmad, A., H. Sarkar, F. and Schobert, R., 2012. Coinage Metal Complexes Against Breast Cancer. *Current Medicinal Chemistry*, 19(23), pp.3949-3956.

Boeckler, F., Joerger, A., Jaggi, G., Rutherford, T., Veprintsev, D. and Fersht, A., 2008. Targeted rescue of a destabilized mutant of p53 by an in silico screened drug. *Proceedings of the National Academy of Sciences*, 105(30), pp.10360-10365.

Bosch, A., Eroles, P., Zaragoza, R., Viña, J. and Lluch, A., 2010. Triple-negative breast cancer: Molecular features, pathogenesis, treatment and current lines of research. *Cancer Treatment Reviews*, 36(3), pp.206-215.

Boucher, D., Blais, V. and Denault, J., 2012. Caspase-7 uses an exosite to promote poly(ADP ribose) polymerase 1 proteolysis. *Proceedings of the National Academy of Sciences*, 109(15), pp.5669-5674.

Bucevičius, J., Lukinavičius, G. and Gerasimaitė, R., 2018. The Use of Hoechst Dyes for DNA Staining and beyond. *Chemosensors*, 6(2), pp.18.

Burkard, M. and Jallepalli, P., 2015. Genomic instability and carcinogenesis. *Systems Biology of Cancer*, pp.93-112.

Canudo-Barreras, G., Ortego, L., Izaga, A., Marzo, I., Herrera, R. and Gimeno, M., 2021. Synthesis of New Thiourea-Metal Complexes with Promising Anticancer Properties. *Molecules*, 26(22), p.6891.

Chatelut, E., Delord, J. and Canal, P., 2003. Toxicity Patterns of Cytotoxic Drugs. *Investigational New Drugs*, 21(2), pp.141-148.

Chen, J., Konopleva, M., Andreeff, M., Multani, A., Pathak, S. and Mehta, K., 2004. Drug-resistant breast carcinoma (MCF-7) cells are paradoxically sensitive to apoptosis. *Journal of Cellular Physiology*, 200(2), pp.223-234.

Chen, J., Lu, L., feng, Y., Wang, H., Dai, L., li, Y. and Zhang, P., 2011. PKD2 mediates multi-drug resistance in breast cancer cells through modulation of P-glycoprotein expression. *Cancer Letters*, 300(1), pp.48-56.

Chen, Y., McMillan-Ward, E., Kong, J., Israels, S. and Gibson, S., 2007. Oxidative stress induces autophagic cell death independent of apoptosis in transformed and cancer cells. *Cell Death & Differentiation*, 15(1), pp.171-182.

Cohen, G., 1997. Caspases: the executioners of apoptosis. *Biochemical Journal*, 326(1), pp.1-16.

Compton, C., 2021. *Cancer: The Enemy from Within*. 1st ed. Switzerland: Springer Nature, pp.26-40.

Dai, Y., Lawrence, T. and Xu, L., 2009. Overcoming cancer therapy resistance by targeting inhibitors of apoptosis proteins and nuclear factor-kappa B. *Am J Tranl Res*, 1(1), pp.1-15.

Dammak, K., Porchia, M., De Franco, M., Zancato, M., Naïli, H., Gandin, V. and Marzano, C., 2020. Antiproliferative Homoleptic and Heteroleptic Phosphino Silver(I) Complexes: Effect of Ligand Combination on Their Biological Mechanism of Action. *Molecules*, 25(22), p.5484.

Dasari, S. and Bernard Tchounwou, P., 2014. Cisplatin in cancer therapy: Molecular mechanisms of action. *European Journal of Pharmacology*, 740, pp.364-378.

Denton, D. and Kumar, S., 2018. Autophagy-dependent cell death. *Cell Death & Differentiation*, 26(4), pp.605-616.

Dong, H., Holth, A., Kleinberg, L., Ruud, M., Elstrand, M., Tropé, C., Davidson, B. and Risberg, B., 2009. Evaluation of Cell Surface Expression of Phosphatidylserine in Ovarian Carcinoma Effusions Using the Annexin-V/7-AAD Assay. *American Journal of Clinical Pathology*, 132(5), pp.756-762.

Dong, L., Gopalan, V., Holland, O. and Neuzil, J., 2020. Mitocans Revisited: Mitochondrial Targeting as Efficient Anticancer Therapy. *International Journal of Molecular Sciences*, 21(21), p.7941.

Edge, S. and Compton, C., 2010. The American Joint Committee on Cancer: the 7th Edition of the AJCC Cancer Staging Manual and the Future of TNM. *Annals of Surgical Oncology*, 17(6), pp.1471-1474.

Elmore, S. (2007). Apoptosis: A Review of Programmed Cell Death. Toxicologic Pathology, 35(4), pp.495-516.

Eloy, L., Jarrousse, A., Teyssot, M., Gautier, A., Morel, L., Jolivalt, C., Cresteil, T. and Roland, S., 2012. Anticancer Activity of Silver-N-Heterocyclic Carbene Complexes: Caspase-Independent Induction of Apoptosis via Mitochondrial Apoptosis-Inducing Factor (AIF). *ChemMedChem*, 7(5), pp.805-814.

Engelbrecht, Z., Meijboom, R. and Cronjé, M., 2018. The ability of silver(I) thiocyanate 4-methoxyphenyl phosphine to induce apoptotic cell death in esophageal cancer cells is correlated to mitochondrial perturbations. *BioMetals*, 31(2), pp.189-202.

Fadok, V., Bratton, D., Frasch, S., Warner, M. and Henson, P., 1998. The role of phosphatidylserine in recognition of apoptotic cells by phagocytes. *Cell Death & Differentiation*, 5(7), pp.551-562.

Farzaneh, S. and Zarghi, A., 2016. Estrogen Receptor Ligands: A Review (2013–2015). *Scientia Pharmaceutica*, 84(3), pp.409-427.

Feng, X. and Koh, D., 2013. Roles of Poly(ADP-Ribose) Glycohydrolase in DNA Damage and Apoptosis. *International Review of Cell and Molecular Biology*, 304, pp.227-281.

Feng, Y., Spezia, M., Huang, S., Yuan, C., Zeng, Z., Zhang, L., Ji, X., Liu, W., Huang, B., Luo, W., Liu, B., Lei, Y., Du, S., Vuppalapati, A., Luu, H., Haydon, R., He, T. and Ren, G., 2018. Breast cancer development and progression: Risk factors, cancer stem cells, signaling pathways, genomics, and molecular pathogenesis. *Genes & Diseases*, 5(2), pp.77-106.

Ferreira, E., Munyaneza, A., Omondi, B., Meijboom, R. and Cronjé, M., 2015. The effect of 1:2 Ag(I) thiocyanate complexes in MCF-7 breast cancer cells. *BioMetals*, 28(4), pp.765-781.

Figueroa, J., Gray, E., Pashayan, N., Deandrea, S., Karch, A., Vale, D., Elder, K., Procopio, P., van Ravesteyn, N., Mutabi, M., Canfell, K. and Nickson, C., 2021. The impact of the Covid-19 pandemic on breast cancer early detection and screening. *Preventive Medicine*, 151, p.106585.

Franz, K. and Metzler-Nolte, N., 2019. Introduction: Metals in Medicine. *Chemical Reviews*, 119(2), pp.727-729.

Frezza, M., Hindo, S., Chen, D., Davenport, A., Schmitt, S., Tomco, D. and Ping Dou, Q., 2010. Novel Metals and Metal Complexes as Platforms for Cancer Therapy. *Current Pharmaceutical Design*, 16(16), pp.1813-1825.

Fu, Z., Fan, Q., Zhou, Y., Zhao, Y. and He, Z., 2019. Elimination of Intracellular Calcium Overload by BAPTA-AM-Loaded Liposomes: A Promising Therapeutic Agent for Acute Liver Failure. *ACS Applied Materials & Interfaces*, 11(43), pp.39574-39585.

Furchner, J., Richmond, C. and Drake, G., 1971. Comparative Metabolism of Radionuclides in Mammals - V. Retention of 192Ir in the Mouse, Rat, Monkey and Dog. *Health Physics*, 20(4), pp.375-382.

Gałczyńska, K., Drulis-Kawa, Z. and Arabski, M., 2020. Antitumor Activity of Pt(II), Ru(III) and Cu(II) Complexes. *Molecules*, 25(15), pp.3492.

Galluzzi, L., Maiuri, M., Vitale, I., Zischka, H., Castedo, M., Zitvogel, L. and Kroemer, G., 2007. Cell death modalities: classification and pathophysiological implications. *Cell Death & Differentiation*, 14(7), pp.1237-1243.

Gandin, V. and Fernandes, A., 2015. Metal- and Semimetal-Containing Inhibitors of Thioredoxin Reductase as Anticancer Agents. *Molecules*, 20(7), pp.12732-12756.

Gandin, V., Fernandes, A., Rigobello, M., Dani, B., Sorrentino, F., Tisato, F., Björnstedt, M., Bindoli, A., Sturaro, A., Rella, R. and Marzano, C., 2010. Cancer cell death induced by phosphine gold(I) compounds targeting thioredoxin reductase. *Biochemical Pharmacology*, 79(2), pp.90-101.

Gazzano, E., Lazzarato, L., Rolando, B., Kopecka, J., Guglielmo, S., Costamagna, C., Chegaev, K. and Riganti, C., 2018. Mitochondrial Delivery of Phenol Substructure Triggers Mitochondrial Depolarization and Apoptosis of Cancer Cells. *Frontiers in Pharmacology*, 9(580).

Ghosh, S., 2019. Cisplatin: The first metal based anticancer drug. *Bioorganic Chemistry*, (88), pp. 102925

Gianferrara, T., Bratsos, I. and Alessio, E., 2009. A categorization of metal anticancer compounds based on their mode of action. *Dalton Transactions*, (37), pp.7588.

Giuliano, A., Connolly, J., Edge, S., Mittendorf, E., Rugo, H., Solin, L., Weaver, D., Winchester, D. and Hortobagyi, G., 2017. Breast Cancer-Major changes in the American Joint Committee

on Cancer eighth edition cancer staging manual. *CA: A Cancer Journal for Clinicians*, 67(4), pp.290-303.

Goldberg, M., 2019. Morphologic and Biochemical Criteria of Cell Death: Apoptosis and Necrosis. *Journal of Cancer Science & Treatment*, 1(1), pp.17-24.

Golstein, P. and Kroemer, G., 2007. Cell death by necrosis: towards a molecular definition. *Trends in Biochemical Sciences*, 32(1), pp.37-43.

Guerin, M., Mckernan, D., O'brien, C. and Cotter, T., 2006. Retinal ganglion cells: dying to survive. *The International Journal of Developmental Biology*, 50(8), pp.665-674.

Gutiérrez, L., Stepien, G., Gutiérrez, L., Pérez-Hernández, M., Pardo, J., Pardo, J., Grazú, V. and de la Fuente, J., 2017. Nanotechnology in Drug Discovery and Development. *Comprehensive Medicinal Chemistry III*, pp.264-295.

Habib, A., V., M., Iqbal, M., Bhatti, H., Ahmed, M. and Majid, A., 2019. Unsymmetrically substituted benzimidazolium based Silver(I)-N-heterocyclic carbene complexes: Synthesis, characterization and in vitro anticancer study against human breast and colon cancer. *Journal of Saudi Chemical Society*, 23(7), pp.795-808.

Han, J., Han, M. and Tung, C., 2013. A non-toxic fluorogenic dye for mitochondria labeling. *Biochimica et Biophysica Acta (BBA) - General Subjects*, 1830(11), pp.5130-5135.

Hanahan, D. and Weinberg, R., 2000. The Hallmarks of Cancer. *Cell*, 100(1), pp.57-70.

Hanahan, D. and Weinberg, R., 2011. Hallmarks of Cancer: The Next Generation. *Cell*, 144(5), pp.646-674.

Hanahan, D., 2022. Hallmarks of Cancer: New Dimensions. *Cancer Discovery*, 12(1), pp.31-46.

Hannah, R., Riss, T. and Moravec, R., 2001. CellTiter-Glo™ luminescent cell viability assay: A sensitive and rapid method for determining cell viability. *Promega cell notes*, (2).

Harbeck, N., Penault-Llorca, F., Cortes, J., Gnant, M., Houssami, N., Poortmans, P., Ruddy, K., Tsang, J. and Cardoso, F., 2019. Breast cancer. *Nature Reviews Disease Primers*, 5(1), pp.1-31.

Harker, C., Tielink, E. and Whitehouse, M., 1991. Studies on the interaction of gold(I) phosphines with 2-thiouracil. Related studies with silver(I) phosphines. *Inorganica Chimica Acta*, 181(1), pp.23-30.

Harurluoglu, B., Altay, A., Caglar, S., Kubra Kagan Yeniceri, E., Caglar, B. and Sibel Şahin, Z., 2021. Binuclear silver(I) complexes with the non-steroidal anti-inflammatory drug tolfenamic acid: Synthesis, characterization, cytotoxic activity and evaluation of cellular mechanism of action. *Polyhedron*, 202, p.115189.

Harvey, N. and Kumar, S., 1998. The role of caspases in apoptosis. *Adv Biochem Eng Biotechnol*, 62, pp.107-128.

Henry-Mowatt, J., Dive, C., Martinou, J. and James, D., 2004. Role of mitochondrial membrane permeabilization in apoptosis and cancer. *Oncogene*, 23(16), pp.2850-2860.

Hirsch, T., Marchetti, P., Susin, S., Dallaporta, B., Zamzami, N., Marzo, I., Geuskens, M. and Kroemer, G., 1997. The apoptosis-necrosis paradox. Apoptogenic proteases activated after mitochondrial permeability transition determine the mode of cell death. *Oncogene*, 15(13), pp.1573-1581.

Hofmann, J., 2004. Protein Kinase C Isozymes as Potential Targets for Anticancer Therapy. *Current Cancer Drug Targets*, 4(2), pp.125-146.

Human-Engelbrecht, Z., Meijboom, R. and Cronjé, M., 2017. Apoptosis-inducing ability of silver(I) cyanide-phosphines useful for anti-cancer studies. *Cytotechnology*, 69(4), pp.591-600.

Iacopetta, D., Mariconda, A., Saturnino, C., Caruso, A., Palma, G., Ceramella, J., Muià, N., Perri, M., Sinicropi, M., Caroleo, M. and Longo, P., 2017. Novel Gold and Silver Carbene Complexes Exert Antitumor Effects Triggering the Reactive Oxygen Species Dependent Intrinsic Apoptotic Pathway. *ChemMedChem*, 12(24), pp.2054-2065.

Jäättelä, M. and Tschopp, J., 2003. Caspase-independent cell death in T lymphocytes. *Nature Immunology*, 4(5), pp.416-423.

Jafarzadeh, E., Montazeri, V., Aliebrahimi, S., Sezavar, A., Ghahremani, M. and Ostad, S., 2022. Combined regimens of cisplatin and metformin in cancer therapy: A systematic review and meta-analysis. *Life Sciences*, 304, p.120680.

Jänicke, R., 2008. MCF-7 breast carcinoma cells do not express caspase-3. *Breast Cancer Research and Treatment*, 117(1), pp.219-221.

Jiang, X., Stockwell, B. and Conrad, M., 2021. Ferroptosis: mechanisms, biology and role in disease. *Nature Reviews Molecular Cell Biology*, 22(4), pp.266-282.

Juan, M., Wenzel, U., Ruiz-Gutierrez, V., Daniel, H. and Planas, J., 2006. Olive Fruit Extracts Inhibit Proliferation and Induce Apoptosis in HT-29 Human Colon Cancer Cells. *The Journal of Nutrition*, 136(10), pp.2553-2557.

Jungwirth, U., Kowol, C., Keppler, B., Hartinger, C., Berger, W. and Heffeter, P., 2011. Anticancer Activity of Metal Complexes: Involvement of Redox Processes. *Antioxidants & Redox Signaling*, 15(4), pp.1085-1127.

Kamiloglu, S., Sari, G., Ozdal, T. and Capanoglu, E., 2020. Guidelines for cell viability assays. *Food Frontiers*, 1(3), pp.332-349.

Kannan, K. and Jain, S., 2000. Oxidative stress and apoptosis. *Pathophysiology*, 7(3), pp.153-163.

Karakosta, A., Golias, C., Charalabopoulos, A., Peschos, D., Batistatou, A. and Charalabopoulos, K., 2005. Genetic models of human cancer as a multistep process. Paradigm models of colorectal cancer, breast cancer, and chronic myelogenous and acute lymphoblastic leukaemia. *Journal of Experimental & Clinical Cancer Research*, 24(4), pp.505-14.

Kawahara, A., Ohsawa, Y., Matsumura, H., Uchiyama, Y. and Nagata, S., 1998. Caspase-independent Cell Killing by Fas-associated Protein with Death Domain. *Journal of Cell Biology*, 143(5), pp.1353-1360.

Kehoe, R., Cholak, J. and Story, R., 1940. A Spectrochemical Study of the Normal Ranges of Concentration of Certain Trace Metals in Biological Materials. *The Journal of Nutrition*, 19(6), pp.579-592.

Kerr, J., Wyllie, A. and Currie, A., 1972. Apoptosis: A Basic Biological Phenomenon with Wideranging Implications in Tissue Kinetics. *British Journal of Cancer*, 26(4), pp.239-257.

Kholmukhamedov, A., Schwartz, J. and Lemasters, J., 2013. Mitotracker probes and mitochondrial membrane potential. *Shock*, 39(6), pp.543.

Klaunig, J., 2020. Carcinogenesis. *An Introduction to Interdisciplinary Toxicology*, pp.97-110.

Knopp, R., Jastaniah, A., Dubrovskyi, O., Gaisina, I., Tai, L. and Thatcher, G., 2021. Extending the Calpain–Cathepsin Hypothesis to the Neurovasculature: Protection of Brain Endothelial Cells and Mice from Neurotrauma. *ACS Pharmacology & Translational Science*, 4(1), pp.372-385.

Koh, J. and Kim, M., 2019. Introduction of a New Staging System of Breast Cancer for Radiologists: An Emphasis on the Prognostic Stage. *Korean Journal of Radiology*, 20(1), pp.69.

Koh, M., Ho, W., Yeap, S., Ali, N., Boo, L. and Alitheen, N., 2021. Regulation of Cellular and Cancer Stem Cell-Related Putative Gene Expression of Parental and CD44+CD24− Sorted MDA-MB-231 Cells by Cisplatin. *Pharmaceuticals*, 14(5), p.391.

Koren, E. and Fuchs, Y., 2021. Modes of Regulated Cell Death in Cancer. *Cancer Discovery*, 11(2), pp.245-265.

Kriel, F. and Coates, J., 2012. Synthesis and Antitumour Activity of Gold(I) and Silver(I) Complexes of Hydrazine-Bridged Diphosphine Ligands. *Sabinet African Journals*, 65, pp.271-279.

Kroemer, G. and Martin, S., 2005. Caspase-independent cell death. *Nature Medicine*, 11(7), pp.725-730.

Lambert, M., Mendenhall, E., Kim, A., Cubasch, H., Joffe, M. and Norris, S., 2020. Health system experiences of breast cancer survivors in urban South Africa. *Women's Health*, 16, p.174550652094941.

Lansdown, A., 2006. Silver in Health Care: Antimicrobial Effects and Safety in Use. *Biofunctional Textiles and the Skin*, 33, pp.17-34.

Lara, H., Ayala-Nuñez, N., Ixtepan-Turrent, L. and Rodriguez-Padilla, C., 2010. Mode of antiviral action of silver nanoparticles against HIV-1. *Journal of Nanobiotechnology*, 8(1), pp.1.

Leclerc, A., Jerusalem, G., Devos, M., Crielaard, J. and Maquet, D., 2016. Multidisciplinary management of breast cancer. *Archives of Public Health*, 74(1).

Lee, E. and Muller, W., 2010. Oncogenes and Tumor Suppressor Genes. *Cold Spring Harbor Perspectives in Biology*, 2(10), pp.a003236-a003236.

Lee, J., Kim, D., Kim, J. and Kim, P., 2000. In vitro cytotoxicity tests on cultured human skin fibroblasts to predict skin irritation potential of surfactants. *Toxicology in Vitro*, 14(4), pp.345-349.

Lee, Y., Lin, P., Rahmawati, E., Ma, Y., Chan, C. and Tzeng, C., 2019. Mitochondria Research in Human Reproduction. *The Ovary*, pp.327-335.

Li, J. and Yuan, J., 2008. Caspases in apoptosis and beyond. *Oncogene*, 27(48), pp.6194-6206.

Li, X., Wang, Y., Li, M., Wang, H. and Dong, X., 2021. Metal Complexes or Chelators with ROS Regulation Capacity: Promising Candidates for Cancer Treatment. *Molecules*, 27(1), p.148.

Lin, Y., Boone, M., Meuris, L., Lemmens, I., Van Roy, N., Soete, A., Reumers, J., Moisse, M., Plaisance, S., Drmanac, R., Chen, J., Speleman, F., Lambrechts, D., Van de Peer, Y., Tavernier, J. and Callewaert, N., 2014. Genome dynamics of the human embryonic kidney 293 lineage in response to cell biology manipulations. *Nature Communications*, 5(1).

Loane, D., Stoica, B. and Faden, A., 2015. Neuroprotection for traumatic brain injury. *Handbook of Clinical Neurology*, 127, pp.343-366.

Lopez, J. and Tait, S., 2015. Mitochondrial apoptosis: killing cancer using the enemy within. *British Journal of Cancer*, 112(6), pp.957-962.

Los, M., Mozoluk, M., Ferrari, D., Stepczynska, A., Stroh, C., Renz, A., Herceg, Z., Wang, Z. and Schulze-Osthoff, K., 2002. Activation and Caspase-mediated Inhibition of PARP: A Molecular Switch between Fibroblast Necrosis and Apoptosis in Death Receptor Signaling. *Molecular Biology of the Cell*, 13(3), pp.978-988.

Łukasiewicz, S., Czeczelewski, M., Forma, A., Baj, J., Sitarz, R. and Stanisławek, A., 2021. Breast Cancer—Epidemiology, Risk Factors, Classification, Prognostic Markers, and Current Treatment Strategies—An Updated Review. *Cancers*, 13(17), pp.4287.

Luqmani, Y., 2005. Mechanisms of Drug Resistance in Cancer Chemotherapy. *Medical Principles and Practice*, 14(Suppl. 1), pp.35-48.

Ly, J., Grubb, D. and Lawen, A., 2003. The mitochondrial membrane potential (Δψm) in apoptosis; An update. *APOPTOSIS*, 8(2), pp.115-128.

Mahepal, S., Bowen, R., Mamo, M., Layh, M. and Jansen van Rensburg, C., 2008. The In Vitro Antitumour Activity of Novel, Mitochondrial-Interactive, Gold-Based Lipophilic Cations. *Metal-Based Drugs*, 2008, pp.1-5.

Maltese, W. and Overmeyer, J., 2014. Methuosis. *The American Journal of Pathology*, 184(6), pp.1630-1642.

Mansoori, B., Mohammadi, A., Davudian, S., Shirjang, S. and Baradaran, B., 2017. The Different Mechanisms of Cancer Drug Resistance: A Brief Review. *Advanced Pharmaceutical Bulletin*, 7(3), pp.339-348.

Martin, S., O'Brien, G., Nishioka, W., McGahon, A., Mahboubi, A., Saido, T. and Green, D., 1995. Proteolysis of Fodrin (Non-erythroid Spectrin) during Apoptosis. *Journal of Biological Chemistry*, 270(12), pp.6425-6428.

Martínez-Jiménez, F., Muiños, F., Sentís, I., Deu-Pons, J., Reyes-Salazar, I., Arnedo-Pac, C., Mularoni, L., Pich, O., Bonet, J., Kranas, H., Gonzalez-Perez, A. and Lopez-Bigas, N., 2020. A compendium of mutational cancer driver genes. *Nature Reviews Cancer*, 20(10), pp.555-572.

Masquelier, M., Zhou, Q., Gruber, A. and Vitols, S., 2004. Relationship between daunorubicin concentration and apoptosis induction in leukemic cells. *Biochemical Pharmacology*, 67(6), pp.1047-1056.

Mc Gee, M., Hyland, E., Campiani, G., Ramunno, A., Nacci, V. and Zisterer, D., 2002. Caspase-3 is not essential for DNA fragmentation in MCF-7 cells during apoptosis induced by the pyrrolo-1,5-benzoxazepine, PBOX-6. *FEBS Letters*, 515(1-3), pp.66-70.

McIlwain, D., Berger, T. and Mak, T., 2013. Caspase Functions in Cell Death and Disease. *Cold Spring Harbor Perspectives in Biology*, 5(4), pp.a008656-a008656.

McKeage, M., Berners-Price, S., Galettis, P., Bowen, R., Brouwer, W., Ding, L., Zhuang, L. and Baguley, B., 2000. Role of lipophilicity in determining cellular uptake and antitumour activity of gold phosphine complexes. *Cancer Chemotherapy and Pharmacology*, 46(5), pp.343-350.

McKeage, M., Maharaj, L. and Berners-Price, S., 2002. Mechanisms of cytotoxicity and antitumor activity of gold(I) phosphine complexes: the possible role of mitochondria. *Coordination Chemistry Reviews*, 232(1-2), pp.127-135.

McKinnell, R., Parchment, R., Perantoni, A., Pierce, G. and Damjanov, I., 2006. Carcinogenesis. *The Biological Basis of Cancer*, pp.80-125.

Meattini, I., Livi, L., Lorito, N., Becherini, C., Bacci, M., Visani, L., Fozza, A., Belgioia, L., Loi, M., Mangoni, M., Lambertini, M. and Morandi, A., 2022. Integrating radiation therapy with targeted treatments for breast cancer: From bench to bedside. *Cancer Treatment Reviews*, 108, pp.102417.

Medici, S., Peana, M., Crisponi, G., Nurchi, V., Lachowicz, J., Remelli, M. and Zoroddu, M., 2016. Silver coordination compounds: A new horizon in medicine. *Coordination Chemistry Reviews*, 327–328, pp.349-359.

Medici, S., Peana, M., Nurchi, V. and Zoroddu, M., 2019. Medical Uses of Silver: History, Myths, and Scientific Evidence. *Journal of Medicinal Chemistry*, 62, pp.5923-5943.

Medici, S., Peana, M., Nurchi, V., Lachowicz, J., Crisponi, G. and Zoroddu, M., 2015. Noble metals in medicine: Latest advances. *Coordination Chemistry Reviews*, 284, pp.329-350.

Medvetz, D., Hindi, K., Panzner, M., Ditto, A., Yun, Y. and Youngs, W., 2008. Anticancer Activity of Ag(I) N-Heterocyclic Carbene Complexes Derived from 4,5-Dichloro-1H-Imidazole. *Metal-Based Drugs*, 2008, pp.1-7.

Meijboom, R., Bowen, R. and Berners-Price, S., 2009. Coordination complexes of silver(I) with tertiary phosphine and related ligands. *Coordination Chemistry Reviews*, 253(3-4), pp.325-342.

Melaiye, A. and Youngs, W., 2005. Silver and its application as an antimicrobial agent. *Expert Opinion on Therapeutic Patents*, 15(2), pp.125-130.

Mohd Sofyan, N., Nordin, F., Mohd Abd Razak, M., Abdul Halim, S., Mohd Khir, N., Muhammad, A., Rajab, N. and Sarip, R., 2018. New Silver Complexes with Mixed Thiazolidine and Phosphine Ligands as Highly Potent Antimalarial and Anticancer Agents. *Journal of Chemistry*, 2018, pp.1-10.

Molinaro, C., Martoriati, A., Pelinski, L. and Cailliau, K., 2020. Copper Complexes as Anticancer Agents Targeting Topoisomerases I and II. *Cancers*, 12(10), p.2863.

Mooney, L., Al-Sakkaf, K., Brown, B. and Dobson, P., 2002. Apoptotic mechanisms in T47D and MCF-7 human breast cancer cells. *British Journal of Cancer*, 87(8), pp.909-917.

Muhammad, T., Chidharla, A. and Kasi, A., 2022. *Cancer Chemotherapy*. [ebook] StatPearls Publishing. Available at: <https://www.ncbi.nlm.nih.gov/books/NBK564367/> [Accessed 7 June 2022].

Okuno, S., Shimizu, S., Ito, T., Nomura, M., Hamada, E., Tsujimoto, Y. and Matsuda, H., 1998. Bcl-2 Prevents Caspase-independent Cell Death. *Journal of Biological Chemistry*, 273(51), pp.34272-34277.

Olelewe, C., Kim, J., Ofori, S., Mertens, R., Gukathasan, S. and Awuah, S., 2022. Gold(III)-P-chirogenic complex induces mitochondrial dysfunction in triple-negative breast cancer. *iScience*, 25(5), p.104340.

Oliveira, P., Colaço, A., Chaves, R., Guedes-Pinto, H., De-La-Cruz P., L. and Lopes, C., 2007. Chemical carcinogenesis. *Anais da Academia Brasileira de Ciências*, 79(4), pp.593-616.

Oliver, F., de la Rubia, G., Rolli, V., Ruiz-Ruiz, M., de Murcia, G. and Murcia, J., 1998. Importance of Poly(ADP-ribose) Polymerase and Its Cleavage in Apoptosis. *Journal of Biological Chemistry*, 273(50), pp.33533-33539.

Ota, A., Tajima, M., Mori, K., Sugiyama, E., Sato, V. and Sato, H., 2021. The selective cytotoxicity of silver thiosulfate, a silver complex, on MCF-7 breast cancer cells through ROS-induced cell death. *Pharmacological Reports*, 73(3), pp.847-857.

Ow, Y., Green, D., Hao, Z. and Mak, T., 2008. Cytochrome c: functions beyond respiration. *Nature Reviews Molecular Cell Biology*, 9(7), pp.532-542.

Palchaudhuri, R. and Hergenrother, P., 2007. DNA as a target for anticancer compounds: methods to determine the mode of binding and the mechanism of action. *Current Opinion in Biotechnology*, 18(6), pp.497-503.

Panchuk-Voloshina, N., Haugland, R., Bishop-Stewart, J., Bhalgat, M., Millard, P., Mao, F., Leung, W. and Haugland, R., 1999. Alexa Dyes, a Series of New Fluorescent Dyes that Yield Exceptionally Bright, Photostable Conjugates. *Journal of Histochemistry & Cytochemistry*, 47(9), pp.1179-1188.

Patwardhan, G., Marczyk, M., Wali, V., Stern, D., Pusztai, L. and Hatzis, C., 2021. Treatment scheduling effects on the evolution of drug resistance in heterogeneous cancer cell populations. *npj Breast Cancer*, 7(1).

Pedrosa, P., Carvalho, A., V. Baptista, P. and R. Fernandes, A., 2018. Inorganic Coordination Chemistry: Where We Stand in Cancer Treatment?. *Basic Concepts Viewed from Frontier in Inorganic Coordination Chemistry*, pp.38-39.

Perry, S., Norman, J., Barbieri, J., Brown, E. and Gelbard, H., 2011. Mitochondrial membrane potential probes and the proton gradient: a practical usage guide. *BioTechniques*, 50(2), pp.98-115.

Pettinari, C., Marchetti, F., Lupidi, G., Quassinti, L., Bramucci, M., Petrelli, D., Vitali, L., Guedes da Silva, M., Martins, L., Smoleński, P. and Pombeiro, A., 2011. Synthesis, Antimicrobial, and Antiproliferative Activity of Novel Silver(I) Tris(pyrazolyl)methanesulfonate and 1,3,5-Triaza-7-phosphadamantane Complexes. *Inorganic Chemistry*, 50(21), pp.11173-11183.

Politano, A., Campbell, K., Rosenberger, L. and Sawyer, R., 2013. Use of Silver in the Prevention and Treatment of Infections: Silver Review. *Surgical Infections*, 14(1), pp.8-20.

Porter, A. and Jänicke, R., 1999. Emerging roles of caspase-3 in apoptosis. *Cell Death & Differentiation*, 6(2), pp.99-104.

Potgieter, K., Cronjé, M. and Meijboom, R., 2016. Synthesis of silver(I) p-substituted phenyl diphenyl phosphine complexes with the evaluation of the toxicity on a SNO cancer cell line. *Inorganica Chimica Acta*, 453, pp.443-451.

Potgieter, K., Engelbrecht, Z., Naganagowda, G., Cronjé, M. and Meijboom, R., 2017. Anticancer activity of silver(I) cyclohexyldiphenylphosphine complexes toward SNO cancer cells. *Journal of Coordination Chemistry*, 70(15), pp.2644-2658.

Quintana, M., Rodriguez-Rius, A., Vellé, A., Vives, S., Sanz Miguel, P. and Triola, G., 2022. Dinuclear silver and gold bisNHC complexes as drug candidates for cancer therapy. *Bioorganic & Medicinal Chemistry*, 67, p.116814.

Rafique, S., Idrees, M., Nasim, A., Akbar, H. and Athar, A., 2010. Transition metal complexes as potential therapeutic agents. *Biotechnology and Molecular Biology Reviews*, 5(2), pp.38-45.

Raju, S., Kumar, S., Sekar, P., Murugesan, M. and Karthikeyan, M., 2022. Silver Complexes as Anticancer Agents: A Perspective Review. *German Journal of Pharmaceuticals and Biomaterials*, 1(1), pp.06-28.

Rampersad, S., 2012. Multiple Applications of Alamar Blue as an Indicator of Metabolic Function and Cellular Health in Cell Viability Bioassays. *Sensors*, 12(9), pp.12347-12360.

Raninga, P., Di Trapani, G., Vuckovic, S., Bhatia, M. and Tonissen, K., 2015. Inhibition of thioredoxin 1 leads to apoptosis in drug-resistant multiple myeloma. *Oncotarget*, 6(17), pp.15410-15424.

Ricci, M. and Zong, W., 2006. Chemotherapeutic Approaches for Targeting Cell Death Pathways. *The Oncologist*, 11(4), pp.342-357.

Rock, K. and Kono, H., 2008. The Inflammatory Response to Cell Death. *Annual Review of Pathology: Mechanisms of Disease*, 3(1), pp.99-126.

Rohn, J. and Noteborn, M., 2004. The viral death effector Apoptin reveals tumor-specific processes. *Apoptosis*, 9(3), pp.315-322.

Rubartelli, A., Bajetto, A., Allavena, G., Wollman, E. and Sitia, R., 1992. Secretion of thioredoxin by normal and neoplastic cells through a leaderless secretory pathway. *Journal of Biological Chemistry*, 267(34), pp.24161-24164.

Sakagami, H., Shimada, J., Hashimoto, K. and Okamura, M., 2004. Apoptosis-inducing Activity of Cisplatin (CDDP) against Human Hepatoma and Oral Squamous Cell Carcinoma Cell Lines. *Anticancer Research*, 24, pp.655-662.

Saraste, A. and Pulkki, A., 2000. Morphologic and biochemical hallmarks of apoptosis. *Cardiovascular Research*, 45(3), pp.528-537.

Sarmiento-Salinas, F., Delgado-Magallón, A., Montes-Alvarado, J., Ramírez-Ramírez, D., Flores-Alonso, J., Cortés-Hernández, P., Reyes-Leyva, J., Herrera-Camacho, I., Anaya-Ruiz, M., Pelayo, R., Millán-Pérez-Peña, L. and Maycotte, P., 2019. Breast Cancer Subtypes Present a Differential Production of Reactive Oxygen Species (ROS) and Susceptibility to Antioxidant Treatment. *Frontiers in Oncology*, 9.

Serra, M., Columbano, A., Ammarah, U., Mazzone, M. and Menga, A., 2020. Understanding Metal Dynamics Between Cancer Cells and Macrophages: Competition or Synergism?. *Frontiers in Oncology*, 10.

Sevrioukova, I., 2011. Apoptosis-Inducing Factor: Structure, Function, and Redox Regulation. *Antioxidants & Redox Signaling*, 14(12), pp.2545-2579.

Sharma, G., Dave, R., Sanadya, J., Sharma, P. and Sharma, k. (2010). Various types and management of breast cancer overview. Journal of advanced pharmaceutical technology & research, 1(2), pp.109- 126.

Shehat, M. and Tigno-Aranjuez, J., 2019. Flow Cytometric Measurement Of ROS Production In Macrophages In Response To FcγR Cross-linking. *Journal of Visualized Experiments*, (145).

Siddiqui, I., Sanna, V., Ahmad, N., Sechi, M. and Mukhtar, H., 2015. Resveratrol nanoformulation for cancer prevention and therapy. *Annals of the New York Academy of Sciences*, 1348(1), pp.20-31.

Silva, D., Becceneri, A., Santiago, J., Gomes Neto, J., Ellena, J., Cominetti, M., Pereira, J., Hannon, M. and Netto, A., 2020. Silver(i) complexes of 3-methoxy-4-hydroxybenzaldehyde thiosemicarbazones and triphenylphosphine: structural, cytotoxicity, and apoptotic studies. *Dalton Transactions*, 49(45), pp.16474-16487.

Sim, W., Barnard, R., Blaskovich, M. and Ziora, Z., 2018. Antimicrobial Silver in Medicinal and Consumer Applications: A Patent Review of the Past Decade (2007–2017). *Antibiotics*, 7(4), pp.93.

Skowron, M., Oing, C., Bremmer, F., Ströbel, P., Murray, M., Coleman, N., Amatruda, J., Honecker, F., Bokemeyer, C., Albers, P. and Nettersheim, D., 2021. The developmental origin of cancers defines basic principles of cisplatin resistance. *Cancer Letters*, 519, pp.199-210.

Smoot, B., Wampler, M. and Topp, K. (2009). Breast Cancer Treatments and Complications: Implications for Rehabilitation. Rehabilitation Oncology, 27(3), pp.16-26.

Sodhi, R. and Paul, S., 2019. Metal Complexes in Medicine: An Overview and Update from Drug Design Perspective. *Cancer Therapy & Oncology International Journal*, 14(1).

Stratton, M., Campbell, P. and Futreal, P., 2009. The cancer genome. *Nature*, 458(7239), pp.719-724.

Stryjska, K., Radko, L., Chęcińska, L., Kusz, J., Posyniak, A. and Ochocki, J., 2020. Synthesis, Spectroscopy, Light Stability, Single-Crystal Analysis, and In Vitro Cytotoxic Activity on HepG2 Liver Cancer of Two Novel Silver(I) Complexes of Miconazole. *International Journal of Molecular Sciences*, 21(10), p.3629.

Sundquis, T., Moravec, R., Niles, A., O'Brien, M. and Riss, T., 2006. *Timing your apoptosis assays*. PROMEGA, pp.18-21.

Sung, H., Ferlay, J., Siegel, R., Laversanne, M., Soerjomataram, I., Jemal, A. and Bray, F., 2021. Global Cancer Statistics 2020: GLOBOCAN Estimates of Incidence and Mortality Worldwide for 36 Cancers in 185 Countries. *CA: A Cancer Journal for Clinicians*, 71(3), pp.209-249.

Sutter, S., Slinker, A., Balumuka, D. and Mitchell, K., 2016. Surgical Management of Breast Cancer in Africa: A Continent-Wide Review of Intervention Practices, Barriers to Care, and Adjuvant Therapy. *Journal of Global Oncology*, 3(2), pp.162-168.

Tait, S. and Green, D., 2008. Caspase-independent cell death: leaving the set without the final cut. *Oncogene*, 27(50), pp.6452-6461.

Tait, S. and Green, D., 2013. Mitochondrial Regulation of Cell Death. *Cold Spring Harbor Perspectives in Biology*, 5(9), pp.a008706-a008706.

Tait, S., Ichim, G. and Green, D., 2014. Die another way – non-apoptotic mechanisms of cell death. *Journal of Cell Science*, 127(10), pp.2135-2144.

Tan, C., Lu, Y., Ji, L. and Mao, Z., 2014. Metallomics insights into the programmed cell death induced by metal-based anticancer compounds. *Metallomics*, 6(5), pp.978.

Theodossiou, T., Ali, M., Grigalavicius, M., Grallert, B., Dillard, P., Schink, K., Olsen, C., Wälchli, S., Inderberg, E., Kubin, A., Peng, Q. and Berg, K., 2019. Simultaneous defeat of

MCF7 and MDA-MB-231 resistances by a hypericin PDT–tamoxifen hybrid therapy. *npj Breast Cancer*, 5(1).

Trudu, F., Amato, F., Vaňhara, P., Pivetta, T., Peña-Méndez, E. and Havel, J., 2015. Coordination compounds in cancer: Past, present and perspectives. *Journal of Applied Biomedicine*, 13(2), pp.79-103.

van der Walt, N., Zakeri, Z. and Cronjé, M., 2016. The Induction of Apoptosis in A375 Malignant Melanoma Cells by Sutherlandia frutescens. *Evidence-Based Complementary and Alternative Medicine*, 2, pp.1-14.

Van Lint, J., Rykx, A., Maeda, Y., Vantus, T., Sturany, S., Malhotra, V., Vandenheede, J. and Seufferlein, T., 2002. Protein kinase D: an intracellular traffic regulator on the move. *Trends in Cell Biology*, 12(4), pp.193-200.

Vanderpuye, V., Grover, S., Hammad, N., PoojaPrabhakar, Simonds, H., Olopade, F. and Stefan, D., 2017. An update on the management of breast cancer in Africa. *Infectious Agents and Cancer*, 12(1).

Vanneman, M. and Dranoff, G., 2012. Combining immunotherapy and targeted therapies in cancer treatment. *Nature Reviews Cancer*, 12(4), pp.237-251.

Vénéreau, E., Ceriotti, C. and Bianchi, M., 2015. DAMPs from Cell Death to New Life. *Frontiers in Immunology*, 6, pp.422.

Vorobjeva, N. and Chernyak, B., 2020. NETosis: Molecular Mechanisms, Role in Physiology and Pathology. *Biochemistry (Moscow)*, 85(10), pp.1178-1190.

Wang, C., Shih, W., Chang, H., Kuo, Y., Hung, W., Ong, T. and Li, W., 2011. Preparation and Characterization of Amino-Linked Heterocyclic Carbene Palladium, Gold, and Silver Complexes and Their Use as Anticancer Agents That Act by Triggering Apoptotic Cell Death. *Journal of Medicinal Chemistry*, 54(14), pp.5245-5249.

Wang, R., Wang, X., Li, B., Lin, F., Dong, K., Gao, P. and Zhang, H., 2008. Tumor-specific adenovirus-mediated PUMA gene transfer using the survivin promoter enhances radiosensitivity of breast cancer cells in vitro and in vivo. *Breast Cancer Research and Treatment*, 117(1), pp.45-54.

Weinstein, I., Gattoni-Celli, S., Kirschmeier, P., Lambert, M., Hsiao, W., Backer, J. and Jeffrey, A., 1984. Multistage carcinogenesis involves multiple genes and multiple mechanisms. *Journal of Cellular Physiology*, 121(3), pp.127-137.

Weiss, A., Chavez-MacGregor, M., Lichtensztajn, D., Yi, M., Tadros, A., Hortobagyi, G., Giordano, S., Hunt, K. and Mittendorf, E., 2018. Validation Study of the American Joint Committee on Cancer Eighth Edition Prognostic Stage Compared With the Anatomic Stage in Breast Cancer. *JAMA Oncology*, 4(2), pp.203.

Who. 2022. *Cancer*. [online] Available at: <https://www.who.int/news-room/fact-sheets/detail/cancer> [Accessed 19 July 2022].

Winter, E., Chiaradia, L., Silva, A., Nunes, R., Yunes, R. and Creczynski-Pasa, T., 2014. Involvement of extrinsic and intrinsic apoptotic pathways together with endoplasmic reticulum stress in cell death induced by naphthylchalcones in a leukemic cell line: Advantages of multi-target action. *Toxicology in Vitro*, 28(5), pp.769-777.

Wolf, B., Schuler, M., Echeverri, F. and Green, D., 1999. Caspase-3 Is the Primary Activator of Apoptotic DNA Fragmentation via DNA Fragmentation Factor-45/Inhibitor of Caspase-activated DNase Inactivation. *Journal of Biological Chemistry*, 274(43), pp.30651-30656.

Wong, R. (2011). Apoptosis in cancer: from pathogenesis to treatment. Journal of Experimental & Clinical Cancer Research, 30(1).

Xu, L., Wang, Y., Huang, J., Chen, C., Wang, Z. and Xie, H., 2020. Silver nanoparticles: Synthesis, medical applications and biosafety. *Theranostics*, 10(20), pp.8996-9031.

Yan, G., Elbadawi, M. and Efferth, T., 2020. Multiple cell death modalities and their key features (Review). *World Academy of Sciences Journal*, 2(2), pp.39-48.

Yilmaz, V., Icsel, C., Batur, J., Aydinlik, S., Sahinturk, P. and Aygun, M., 2017. Structures and biochemical evaluation of silver(I) 5,5-diethylbarbiturate complexes with bis(diphenylphosphino)alkanes as potential antimicrobial and anticancer agents. *European Journal of Medicinal Chemistry*, 139, pp.901-916.

Zartilas, S., Hadjikakou, S., Hadjiliadis, N., Kourkoumelis, N., Kyros, L., Kubicki, M., Baril, M., Butler, I., Karkabounas, S. and Balzarini, J., 2009. Tetrameric 1:1 and monomeric 1:3 complexes of silver(I) halides with tri(p-tolyl)-phosphine: A structural and biological study. *Inorganica Chimica Acta*, 362(3), pp.1003-1010.

Zeng, L., Gupta, P., Chen, Y., Wang, E., Ji, L., Chao, H. and Chen, Z., 2017. The development of anticancer ruthenium(ii) complexes: from single molecule compounds to nanomaterials. *Chemical Society Reviews*, 46(19), pp.5771-5804.

Zhang, Z., Zhou, L., Xie, N., Nice, E., Zhang, T., Cui, Y. and Huang, C., 2020. Overcoming cancer therapeutic bottleneck by drug repurposing. *Signal Transduction and Targeted Therapy*, 5(1).

Zhu, H. and Doğan, B., 2021. American Joint Committee on Cancer's Staging System for Breast Cancer, Eighth Edition: Summary for Clinicians. *European Journal of Breast Health*, 17(3), pp.234-238.

Zielonka, J., Joseph, J., Sikora, A., Hardy, M., Ouari, O., Vasquez-Vivar, J., Cheng, G., Lopez, M. and Kalyanaraman, B., 2017. Mitochondria-Targeted Triphenylphosphonium-Based Compounds: Syntheses, Mechanisms of Action, and Therapeutic and Diagnostic Applications. *Chemical Reviews*, 117(15), pp.10043-10120.

Zimmermann, M. and Meyer, N., 2011. Annexin V/7-AAD Staining in Keratinocytes. *Methods in Molecular Biology*, 740, pp.57-63.

TurnItIn Report

turnitin

Digital Receipt

This receipt acknowledges that Turnitin received your paper. Below you will find the receipt information regarding your submission.

The first page of your submissions is displayed below.

Submission author:	Alisha Badal
Assignment title:	Thesis submission.
Submission title:	Badal_1102823_MSc Dissertation-2.docx
File name:	Badal_1102823_MSc_Dissertation.docx
File size:	7.99M
Page count:	116
Word count:	32,769
Character count:	185,901
Submission date:	28-Jul-2022 03:53PM (UTC+0200)
Submission ID:	1876188311